CENTRO INTERNACIONAL DE ESTUDOS
DE DOUTORAMENTO E AVANZADOS
DA USC (CIEDUS)

TESE DOUTORAL

UNCONVENTIONAL MARKERS OF ALZHEIMER DISEASE

Alexis Moscoso Rial

ESCOLA DE DOUTORAMENTO INTERNACIONAL

PROGRAMA DE DOUTORAMENTO EN INVESTIGACIÓN CLÍNICA EN MEDICINA

SANTIAGO DE COMPOSTELA

2019

USC
UNIVERSIDADE
DE SANTIAGO
DE COMPOSTELA

DECLARACIÓN DO AUTOR DA TESE

Unconventional markers of Alzheimer Disease

D. Alexis Moscoso Rial

Presento a miña tese, seguindo o procedemento axeitado ao Regulamento, e declaro que:

1) A tese abarca os resultados da elaboración do meu traballo.
2) De selo caso, na tese faise referencia ás colaboracións que tivo este traballo.
3) A tese é a versión definitiva presentada para a súa defensa e coincide coa versión enviada en formato electrónico.
4) Confirmo que a tese non incorre en ningún tipo de plaxio doutros autores nin de traballos presentados por min para a obtención doutros títulos.
5) O doutorando declara non ter ningún conflito de interese en relación coa tese de doutoramento.

En Santiago de Compostela, 29 de novembro de 2019

Asdo. Alexis Moscoso

USC
UNIVERSIDADE
DE SANTIAGO
DE COMPOSTELA

AUTORIZACIÓN DO DIRECTOR / TITOR DA TESE

Unconventional markers of Alzheimer Disease

D. Pablo Aguiar Fernández.

D. Juan Pardo Montero.

D. Álvaro Ruibal Morell.

INFORMAN:

Que a presente tese, correspóndese co traballo realizado por D. Alexis Moscoso Rial, baixo a nosa dirección, e autorizamos a súa presentación, considerando que reúne os requisitos esixidos no Regulamento de Estudos de Doutoramento da USC, e que como director desta non incorre nas causas de abstención establecidas na Lei 40/2015.

En Santiago de Compostela, 29 de novembro de 2019

Asdo. Pablo Aguiar Asdo. Juan Pardo Asdo. Álvaro Ruibal

USC
UNIVERSIDADE
DE SANTIAGO
DE COMPOSTELA

AGRADECIMIENTOS

No podría empezar estos agradecimientos sin dar primero las gracias a mi madre, a mi padre y a mi hermano por todos sus sacrificios y su apoyo incondicional durante tantos años, aún cuando en ocasiones pudiera no merecerlo. Sin ellos jamás habría llegado hasta aquí.

Gracias a Irene por todo el cariño, las sonrisas y por ayudarme cuando las cosas se ponían difíciles. Gracias por hacer de mí una persona mejor.

Gracias a mi tutor Álvaro Ruibal por todo el apoyo, la confianza y el cariño que siempre me hizo sentir.

Gracias a mis directores Pablo Aguiar y Juan Pardo por guiarme y ayudarme durante estos años.

Gracias a mis compañeros Jesús, Noemí, David, Anxo, Manuel, Lara y Cristina por hacer del laboratorio un lugar tan agradable para trabajar.

Gracias a todos los médicos, enfermeros y demás personal del servicio de Medicina Nuclear por toda su amabilidad y ganas de colaborar en la investigación que llevamos a cabo.

USC
UNIVERSIDADE
DE SANTIAGO
DE COMPOSTELA

RESUMEN EXTENSO

Neuropatológicamente, la enfermedad de Alzheimer se caracteriza por una acumulación anormal de proteína amiloide, en forma de placas extracelulares, y de proteína tau, en forma de ovillos dentro las neuronas, en el cortex cerebral. A pesar de que este "paradigma cortical" ha sido siempre el predominante a la hora de entender la enfermedad de Alzheimer, recientes estudios neuropatológicos y de neuroimagen muestran que otras estructuras cerebrales juegan un papel crucial en el origen y progresión de esta devastadora enfermedad. Es por ello que, en esta tesis, exploramos nuevos biomarcadores de la enfermedad de Alzheimer, es decir, marcadores que van más allá de los clásicos indicadores corticales de amiloide, tau y neurodegeneración. En particular, los biomarcadores explorados en esta tesis se centran en el rol de la patología en sustancia blanca y de los deterioros sutiles en la cognición en la progresión y patogénesis de la enfermedad de Alzheimer. Para ello hemos utilizado datos provenientes de uno de los mayores estudios observacionales de la enfermedad Alzheimer, el Alzheimer's Disease Neuroimaging Initiative (ADNI), en el que múltiples biomarcadores neuroquímicos y de neuroimagen son estudiados a lo largo del tiempo en las fases preclínica, prodrómica y de demencia de la enfermedad de Alzheimer. Esta tesis se estructura en tres estudios principales, cuyo objetivo radica en responder a las siguientes cuestiones: 1) ¿Están las lesiones en sustancia blanca relacionadas con la acumulación patológica de proteína amiloide? 2) ¿Está la desmielinización, medida con tomografía por emisión de positrones de amiloide, relacionada con la progresión de la enfermedad de Alzheimer? 3) ¿Es la memoria episódica un buen marcador de la progresión sintomática de la enfermedad de Alzheimer? ¿Provee valor predictivo a los biomarcadores de amiloide, tau y neurodegeneración? Entre otras pruebas, la Alzheimer's Disease Neuroimaging Initiative proporciona datos de tomografía por emisión de positrones de amiloide, así como datos de resonancia magnética nuclear y de líquido cefalorraquídeo, lo que permite poner a prueba las anteriores hipótesis en una cohorte única en términos de tamaño y de seguimiento longitudinal. Para contestar la primera de las anteriores cuestiones, se midieron las lesiones en sustancia blanca a través de las hiperintensidades medidas por resonancia magnética nuclear con atenuación de fluidos. Las hiperintensidades en sustancia blanca son hallazgos radiológicos comunes en el cerebro envejecido, e inicialmente se creía que estos hallazgos estaban asociados exclusivamente a enfermedades cerebrovasculares isquémicas. Sin embargo, más y más evidencia apunta a que las hiperintensidades en sustancia blanca emergen al mismo tiempo que los cambios patológicos característicos de la enfermedad de Alzheimer. En este sentido, varios estudios han hallado que las hiperintensidades se asociaban con la severidad de la taupatía y la neurodegeneración en pacientes con enfermedad de Alzheimer, siendo la degeneración Walleriana el mecanismo hipotetizado como responsable de esta alteración de la sustancia blanca. Esta hipótesis implicaría que la degeneración neuronal sería pues responsable del daño en sustancia en blanca, y por tanto estas hiperintensidades no serían un marcador temprano de la enfermedad. No obstante, estudios más recientes en enfermedad de Alzheimer de origen genético apuntan que las hiperintensidades en áreas posteriores del cerebro emergen simultáneamente con los primeros cambios patológicos en los niveles de amiloide y tau en líquido cefalorraquídeo, lo que sugiere que las hiperintensidades en sustancia blanca son una de las características patológicas más tempranas de la enfermedad de Alzheimer, desafiando entonces la hipótesis de la degeneración walleriana. Estos hallazgos fueron respaldados por dos estudios recientes que muestran que las hiperintensidades localizadas en regiones parietales y frontales se asocian únicamente con amiloide, pero no con tau, en ancianos

cognitivamente intactos. Debido a la naturaleza no longitudinal de estos estudios, no está todavía claro si las hiperintensidades relacionadas con el amiloide son detectables antes de que lo haga el amiloide en una imagen de amiloide por tomografía por emisión de positrones. De ser así, las hiperintensidades en sustancia blanca podrían ayudar a identificar a los llamados "acumuladores" de amiloide con niveles subclínicos de la enfermedad de Alzheimer. Estos sujetos podrían ser los candidatos óptimos para las terapias anti-amiloide. Para testear esta hipótesis, estudiamos las asociaciones entre la carga global y los patrones regionales de hiperintensidades, y la acumulación de amiloide a lo largo del tiempo en participantes cognitivamente normales con bajo carga de amiloide en el cortex en ADNI. Se examinaron ciento cincuenta y nueve participantes cognitivamente normales de ADNI con baja carga de amiloide, medida con tomografía por emisión de positrones de amiloide, al inicio del estudio. Todos los participantes fueron escaneados en una resonancia magnética de 3T, con secuencias T1 y FLAIR para la medida de las lesiones en sustancia en blanca. Todos los participantes tienen una imagen de tomografía por emisión de positrones de amiloide al inicio del estudio, y al menos otra tomografía más de seguimiento, adquiridas en intervalos de 2 años hasta los 8 años. El volumen de las hiperintensidades se midió usando un método automático. Se aplicó corrección de volumen parcial para la cuantificación objetiva de los escáneres de amiloide. La asociación entre la carga de hiperintensidades global y regional, y la acumulación de amiloide se estudió utilizando modelos lineales mixtos ajustados por datos demográficos y carga de amiloide al inicio del estudio. Los resultados indican que no hubo correlaciones significativas entre las hiperintensidades y la captación amiloide cortical al inicio del estudio. Sin embargo, en el análisis longitudinal, el aumento de la captación cortical de amiloide basal y el aumento de las hiperintensidades basales globales, frontales y parietales se asociaron con una acumulación de amiloide más rápida. La acumulación de amiloide relacionada con hiperintensidades se produjo en las regiones corticales parietales, frontales y, en menor medida, cinguladas. Estos resultados permanecieron inalterados después de un análisis de sensibilidad que excluyó a los participantes con las captaciones de amiloide cortical más altas. Nuestros hallazgos son consistentes con estudios anteriores que analizan simultáneamente el papel de amiloide y tau en la aparición de lesiones en sustancia blanca. La relación entre las hiperintensidades en sustancia blanca y el amiloide, independiente de tau, particularmente con hiperintensidades parietales, fue también hallada en estudios transversales en enfermedad de Alzheimer autosómica y en dos estudios recientes en ancianos no dementes. Los resultados de este trabajo suman a estos hallazgos transversales previos, observando longitudinalmente que un patrón similar de hiperintensidades es detectable a niveles subclínicos de patología de amiloide, lo que respalda parcialmente la hipótesis de que las lesiones en sustancia blanca son secundarias al depósito de amiloide. Aunque el vínculo entre el depósito temprano de amiloide y el daño a la sustancia blanca todavía no está claro, la relación podría explicarse por a través de varios mecanismos como la desmielinización debida a la disfunción de los oligodendrocitos producida por oligómeros de amiloide, así como la degeneración axonal secundaria a la activación de la microglía por la acumulación de amiloide. Sin embargo, los hallazgos del presente estudio no excluyen la posibilidad de que los patrones observados de hiperintensidades tengan una etiología vascular, posiblemente a través de un vínculo causal o interactivo entre la patología cerebrovascular y el depósito de amiloide, como sugieren estudios previos. La disfunción endotelial o una disfunción más amplia de la barrera hematoencefálica pueden ser los vínculos clave, ya que pueden conducir tanto a la formación de hiperintensidades como a la alteración del aclaramiento de amiloide, favoreciendo así la acumulación de amiloide cerebral. Se necesitan más estudios neuropatológicos y de imagen para comprender completamente la relación entre la acumulación temprana de amiloide, las

alteraciones en sustancia blanca y la patología vascular. Este es el primer estudio que identifica una distribución espacial específica de hiperintensidades que es predictiva de la acumulación futura de amiloide entre ancianos cognitivamente normales sin patología de amiloide detectable mediante tomografía por emisión de positrones. Estos hallazgos podrían tener implicaciones importantes para la identificación temprana de la acumulación de amiloide en la enfermedad de Alzheimer y para ensayos clínicos de prevención de esta enfermedad. Para contestar a la pregunta número 2 anteriormente expuesta, analizamos como la desmielinización de la sustancia blanca, medida mediante tomografía por emisión de positrones de amiloide, se relaciona con los biomarcadores de la enfermedad de Alzheimer y con su progresión cognitiva y neurodegenerativa. Apoyado por investigaciones recientes en esclerosis múltiple, la imagen de tomografía por emisión de positrones de amiloide se ha postulado como un marcador de degeneración de la sustancia blanca. Aunque el mecanismo de ligado del trazador a la sustancia blanca todavía no se entiende completamente, se ha sugerido que los trazadores de amiloide podrían unirse a la estructura de la lámina beta de la proteína de mielina, reflejando así la integridad de la mielina incluso en sustancia blanca de apariencia radiológica normal. A pesar de la evidencia anteriormente mencionada, la asociación de la desmielinización reflejada por la tomografía por emisión de positrones de amiloide con la progresión de enfermedad de Alzheimer todavía no se ha investigado. En este estudio, planteamos la hipótesis de que una captación baja de trazador de tomografía por emisión de positrones de amiloide en la sustancia blanca refleja la desmielinización de esta región, y que este cambio patológico está asociado con la progresión de la enfermedad de Alzheimer. Para probar estas hipótesis, se examinaron las asociaciones entre la captación de Florbetapir, un trazador fluorinado de amiloide, en la sustancia blanca cerebral, y los biomarcadores de la enfermedad de Alzheimer, la cognición, y los cambios clínicos y neurodegenerativos longitudinales. Además, también se exploraron las asociaciones entre la captación de Florbetapir en el tronco encefálico y los marcadores anteriormente mencionados para explorar si la patología desmielinizante de la sustancia blanca se extiende a regiones alejadas de la corteza cerebral. Para ello, se incluyeron todos los participantes de ADNI con imágenes de resonancia magnética, tomografía por emisión de positrones de amiloide (Florbetapir) y punciones lumbares realizadas al inicio del estudio (n = 745). Primeramente, se evaluaron las asociaciones transversales entre la captación de Florbetapir en la sustancia blanca y tronco encefálico, y los biomarcadores de cognición, de imagen y de líquido cefalorraquídeo. En los análisis longitudinales, investigamos si la captación basal de Florbetapir en la sustancia blanca y en el tronco encefálico se asociaron con un deterioro cognitivo más rápido, una mayor acumulación de hiperintensidades en la sustancia blanca y unos volúmenes del hipocampo más bajos. Los análisis transversales mostraron que la baja captación de Florbetapir en sustancia blanca y tronco encefálico, independientemente de la captación cortical, las hiperintensidades en sustancia blanca y el diagnóstico clínico, se asociaron con niveles más bajos de amiloide en líquido cefalorraquídeo. En pacientes con deterioro cognitivo ligero con amiloide cortical elevado (A+), la baja captación de Florbetapir en sustancia blanca y en tronco encefálico también se asociaron con niveles más altos de tau en líquido cefalorraquídeo y con cognición global más deteriorada. Longitudinalmente, la baja captación de Florbetapir tanto en sustancia blanca como en tronco encefálico se asociaron con un deterioro cognitivo más rápido, mayor acumulación longitudinal de hiperintensidades en sustancia blanca y mayores tasas de atrofia del hipocampo entre los participantes A+ cognitivamente normales y con deterioro cognitivo ligero. Tomados en conjunto, nuestros hallazgos se suman a los estudios recientes que vinculan las lesiones en sustancia blanca con una reducción de la captación del trazador de amiloide en envejecimiento normal y en

esclerosis múltiple, y sugieren que la degeneración de la sustancia blanca, medida mediante tomografía por emisión de positrones con trazadores de amiloide, es relevante para la progresión cognitiva y patológica de la enfermedad de Alzheimer preclínica y prodrómica. Los mecanismos detrás de la disminución global en la captación de Florbetapir en la sustancia blanca observada en sujetos con amiloide cortical elevado no están claros. Un estudio reciente sugiere que las lesiones parietales en sustancia blanca son específicas de la enfermedad de Alzheimer, hipotetizando que estas se deben a la degeneración Walleriana secundaria a la degeneración neuronal. Aunque este efecto podría explicar nuestras observaciones, particularmente las relacionadas con tau y neurodegeneración, no está claro cómo las regiones alejadas del cortex, como la sustancia blanca profunda o el tronco encefálico, podrían verse afectadas por este proceso. Otro posible mecanismo de degeneración de la sustancia blanca relacionada con la enfermedad de Alzheimer es la acumulación anormal de amiloide soluble, la forma más tóxica de amiloide, en estas áreas. De acuerdo con un estudio neuropatológico, los oligómeros de amiloide, particularmente aquellos formados de Aβ-42, estaban anormalmente elevados en la sustancia blanca de los pacientes con la enfermedad de Alzheimer, independientemente de la gravedad de la patología cortical. La desmielinización asociada a estos oligómeros explicaría la fuerte correlación entre los niveles bajos de Aβ-42 en líquido cefalorraquídeo y la baja captación de Florbetapir en la sustancia blanca y tronco encefálico. Además, esta observación podría ayudar a comprender mejor por qué los niveles de Aβ-42 en líquido cefalorraquídeo se vuelven anormales antes que la tomografía por emisión de positrones de amiloide, lo que sugiere que las anomalías en la sustancia pueden preceder a las placas corticales detectables por neuroimagen. Es necesario explorar en futuros estudios si esta degeneración es el efecto desencadenante que conduce al depósito de amiloide cortical o simplemente una patología asociada a la edad que interacciona con la enfermedad de Alzheimer. En conclusión, nuestros hallazgos sugieren que la tomografía por emisión de positrones con trazadores de amiloide se puede usar como un marcador temprano de degeneración de la sustancia blanca, y que contribuye a la progresión de la enfermedad de Alzheimer. Se necesitan más estudios para comprender completamente el origen de la degeneración de la sustancia blanca en la enfermedad de Alzheimer, los cambios neuropatológicos asociados con una baja retención de trazador de amiloide en la sustancia blanca y las propiedades dinámicas de la retención del trazador de amiloide en la sustancia blanca. Finalmente, para responder a la tercera pregunta investigamos si la estadificación de los síntomas clínicos basada en la memoria episódica es capaz de describir la evolución secuencial de los síntomas cognitivos en pacientes con deterioro cognitivo ligero y con evidencia de cambios patológicos indicativos de la enfermedad de Alzheimer. El diseño de este estudio permite, al mismo tiempo, evaluar si este sistema de estadiaje proporciona un valor predictivo extra a los biomarcadores convencionales de amiloide, tau y neurodegeneración. Trescientos ochenta y siete sujetos con deterioro cognitivo ligero y con marcador de amiloide anormal fueron incluidos y reclasificados cognitivamente como deterioro "temprano" o "tardío" en función del deterioro episódico de la memoria. Se realizaron comparaciones transversales y longitudinales entre estos dos grupos para cada perfil de amiloide, tau y neurodegeneración. Los análisis transversales indican que el deterioro cognitivo ligero "temprano" representa una fase de transición entre la cognición normal y el deterioro cognitivo ligero "tardío" en términos de biomarcadores de la enfermedad de Alzheimer. Después de ajustar por factores de confusión y niveles de amiloide, tau y neurodegeneración, el deterioro cognitivo ligero “tardío” progresó significativamente más rápido que el deterioro cognitivo ligero “temprano” solo en los perfiles con marcadores anormales de amiloide y tau. La estadificación de la memoria episódica es útil para describir

los síntomas en la enfermedad de Alzheimer prodrómica y complementa los perfiles de biomarcadores de amiloide, tau y neurodegeneración. Aunque estudios previos habían comparado los deterioros cognitivos ligeros “tempranos” y “tardíos”, el alto número de falsos positivos en el grupo de deterioro cognitivo ligero “temprano” podría haber sesgado las comparaciones usadas en estos estudios, lo que plantea serias dudas sobre la eficacia de la estadificación basada en memoria episódica para monitorizar la cognición en la enfermedad de Alzheimer prodrómica. En este estudio se optó por hacer uso de los biomarcadores para resolver este dilema, de forma que los sujetos con deterioro cognitivo ligero “temprano” realmente se encuentran con cambios neuropatológicos de la enfermedad de Alzheimer. Entre estos pacientes, la estadificación basada en la memoria episódica resulta ser útil para detectar los cambios cognitivos más sutiles asociados a la enfermedad de Alzheimer, lo que abre una potencial ventana terapéutica que podría beneficiar a estos pacientes. Además, se demostró que el estadiaje basado en memoria episódica es un predictor independente del deterioro cognitivo futuro y de la progresión a demencia, más allá de los biomarcadores de amiloide, tau y neurodegeneración. Este resultado apoya la noción de que aunque estos marcadores convencionales describen gran parte del deterioro clínico observado, otros factores asociados a la enfermedad de Alzheimer, es decir, nuevos biomarcadores, deben ser explorados y analizados para llegar a comprender en profundidad las causas del deterioro cognitivo. Por ejemplo, estos hallazgos podrían reflejar, en vez de un método más preciso para monitorizar cambios cognitivos, pacientes con una reserva cognitiva superior. Estos pacientes serían por tanto más resistentes frente a la misma cantidad de cambios neuropatológicos, lo que abre la puerta a su estudio más detallado para identificar cuáles son realmente dichos mecanismos de resistencia a la patología. Estudios futuros analizarán las causas por las cuales unos pacientes resisten peor que otros los cambios neuropatológicos. Dado que en el nuevo marco de investigación del Instituto Nacional sobre el Envejecimiento y la Asociación de Alzheimer solo se considera un solo estadio cognitivo para todo el espectro del deterioro cognitivo ligero, estos hallazgos pueden tener implicaciones importantes para el esquema de estadificación clínica numérica de dicho marco, así como para futuros ensayos clínicos basados en perfiles de biomarcadores para pacientes con deterioro cognitivo ligero. Los resultados globales de esta tesis respaldan la hipótesis de que otros biomarcadores no convencionales, que van más allá de los clásicos marcadores de amiloide, tau y neurodegeneración, están asociados con la patogénesis y la progresión de la enfermedad de Alzheimer. Específicamente, esta tesis proporciona las siguientes conclusiones: 1) Las hiperintensidades en sustancia blanca están asociadas con una acumulación más rápida de amiloide cortical en sujetos cognitivamente normales sin evidencia de amiloidosis cortical, medida mediante tomografía por emisión de positrones con trazador de amiloide. 2) La retención del trazador de tomografía por emisión de positrones de amiloide sustancia blanca es sensible a la patología desmielinizante en la sustancia blanca. Esta desmielinización predice la progresión en la enfermedad de Alzheimer preclínica y prodrómica. 3) La memoria episódica es útil para monitorizar el espectro cognitivo prodrómico y proporciona información pronóstica complementaria a los biomarcadores de amiloide, tau y neurodegeneración.

USC
UNIVERSIDADE
DE SANTIAGO
DE COMPOSTELA

PUBLICACIONES DERIVADAS DE ESTA TESIS

- **Moscoso A**, et al. Association of white matter lesions with subthreshold amyloid accumulation, 2019, en revisión en Annals of Neurology, *IF: 9.496, Q1 (D1).*
- **Moscoso A**, et al. Association between amyloid PET tracer uptake in white matter and Alzheimer Disease progression, 2019, en revisión en Neurology, *IF: 8.689, Q1 (D1).*
- López-González FJ, **Moscoso A**, et al. Spill-in counts in the quantification of 18F-florbetapir on Aβ-negative subjects: the effect of including white matter in the reference region. 2019, EJNMMI Physics, en prensa. *IF: 3.475, Q1.*
- **Moscoso A**, et al. Staging the cognitive continuum in prodromal Alzheimer's Disease with episodic memory, Neurobiol Aging, 2019 Jul 30;84:1-8. *IF: 4.398, Q1.*
- **Moscoso A,** et al. Prediction of Alzheimer's disease dementia with MRI beyond the short-term: Implications for the design of predictive models. Neuroimage Clin. 2019;23:101837. *IF: 3.943, Q1.*
- **Moscoso A,** et al. Texture analysis of high-resolution dedicated breast 18 F-FDG PET images correlates with immunohistochemical factors and subtype of breast cancer. Eur J Nucl Med Mol Imaging. 2018 Feb;45(2):196-206. *IF: 7.182, Q1 (D1).*
- Fernández-Ferreiro A, j , **Moscoso A**, et al. Positron Emission Tomography for the Development and Characterization of Corneal Permanence of Ophthalmic Pharmaceutical Formulations. Invest Ophthalmol Vis Sci. 2017 Feb 1;58(2):772-780. *IF: 3.812, Q1.*
- Fernández-Ferreiro A, j , **Moscoso A**, et al. In vivo eye surface residence determination by high-resolution scintigraphy of a novel ion-sensitive hydrogel based on gellan gum and kappa-carrageenan. Eur J Pharm Biopharm. 2017 May;114:317-323. *IF: 4.708, Q1.*

USC
UNIVERSIDADE
DE SANTIAGO
DE COMPOSTELA

ABSTRACT

Although typically conceptualized as a cortical disease, recent neuropathological and neuroimaging investigations on Alzheimer Disease suggest that other brain structures play an important role in the pathogenesis and progression of this devastating condition. In this thesis, we explored novel markers of Alzheimer Disease beyond the classical cortical pathology measures of amyloid, tau, and neurodegeneration. We focused on the role of white matter abnormalities, assessed with magnetic resonance imaging but also with amyloid positron emission tomography, in predicting early pathologic changes and disease progression, as well as on the added value of cognition to amyloid, tau, and neurodegeneration biomarkers. Overall, we found that these unconventional markers provide useful information to detect the earliest pathological changes of the disease, providing a better understanding of the mechanisms that lead to amyloid deposition and cognitive decline.

USC
UNIVERSIDADE
DE SANTIAGO
DE COMPOSTELA

LIST OF ABBREVIATIONS

A = Amyloid status

Aβ = Amyloid beta

Aβ42 = 42 amino acid isoform of β-amyloid

AD = Alzheimer Disease

ADAS-Cog-13 = Alzheimer's Disease Assessment Scale—Cognitive 13-Item

ADNI = Alzheimer's Disease Neuroimaging Initiative

aHV = adjusted Hippocampal Volume

APOE = Apolipoprotein E gene

CDR-SB = Clinical Dementia Rating—Sum of Boxes

CN = Cognitively Normal

CSF = Cerebrospinal Fluid

DTI = Diffusion tensor imaging

EMCI = Early MCI

ErWM = Eroded WM mask

FDR = False Discovery Rate

FLAIR = Fluid-Attenuated Inversion Recovery

LMCI = Late MCI

LST = Lesion Segmentation Toolbox

MCI = Mild Cognitive Impairment

MMSE = Mini-Mental State Examination

MRI = Magnetic Resonance Imaging

(N) = Neurodegeneration status

NC = Numeric Clinical

NIA-AA = National Institute on Aging – Alzheimer's Association

PET = Positron Emission Tomography

PiB = (11C)-labeled Pittsburgh Compound B

PSF = Point Spread Function

p-tau = Phosphorylated tau

PVE = Partial volume effects

ROI = Region of interest

SD = Standard deviation

SGTM = Symmetric Geometric Transfer Matrix

SMC = Subjective Memory Complaints

SUVR = Standardized Uptake Value Ratio

T = Tau status

TIV = Total intracranial volume

t-tau = Total tau

VBM = Voxel-based morphometry

WM = White matter

WMH = White matter hyperintensities

USC
UNIVERSIDADE
DE SANTIAGO
DE COMPOSTELA

CONTENTS

1 INTRODUCTION 1

1.1 ALZHEIMER DISEASE 2

1.2 CONVENTIONAL ALZHEIMER DISEASE BIOMARKERS 4

1.2.1 CSF biomarkers 4

1.2.2 Imaging biomarkers 4

1.3 UNCONVENTION ALZHEIMER DISEASE BIOMARKERS 10

1.3.1 White matter hyperintensities 10

1.3.2 Amyloid PET as a marker of myelin integrity 12

1.3.3 Episodic Memory 13

1.4 WHY WE NEED UNCONVENTIONAL BIOMARKERS 14

2 OBJECTIVES 15

2.1 HYPOTHESES 16

2.2 SPECIFIC OBJECTIVES 16

3 METHODS 17

3.1 THE ALZHEIMER'S DISEASE NEUROIMAGING INITIATIVE 18

3.2 ADNI PARTICIPANTS 19

3.3 CSF ANALYSIS IN ADNI 20

3.4 NEUROIMAGING PROTOCOLS IN ADNI 20

3.4.1 MRI 20

3.4.2 Amyloid PET imaging 21

3.5 NEUROIMAGING ANALYSIS 23

3.5.1 T1 MRI analysis 23

3.5.2 FLAIR MRI analysis 25

3.5.3 Amyloid PET analysis 26

3.6 ETHICAL ASPECTS AND INFORMED CONSENTS 26

4 RESULTS 27

4.1 ASSOCIATION OF WHITE MATTER HYPERINTENSITIES WITH SUBTHRESHOLD AMYLOID ACCUMULATION 28

4.1.1 Specific Methods 28

4.1.2 Findings 30

4.1.3 Discussion 37

4.2 ASSOCIATION BETWEEN AMYLOID PET TRACER UPTAKE IN WHITE MATTER AND ALZHEIMER DISEASE PROGRESSION 40

4.2.1 Specific Methods 40

4.2.2 Findings 42

4.2.3 Discussion 50

4.3 STAGING THE COGNITIVE CONTINUUM IN PRODROMAL ALZHEIMER DISEASE WITH EPISODIC MEMORY 52

4.3.1 Specific Methods 52

4.3.2 Findings 55

4.3.3 Discussion 59

5 CONCLUSIONS 63

6 BIBLIOGRAPHY 65

7 APPENDICES 79

USC
UNIVERSIDADE
DE SANTIAGO
DE COMPOSTELA

INTRODUCTION

1 INTRODUCTION

1.1 ALZHEIMER DISEASE

Alzheimer disease (AD) is a progressive neurodegenerative disease that courses with a wide variety of cognitive, functional, and behavioral alterations [1]. The disease can be classified according to the age of onset into early-onset AD and late-onset AD. Early onset AD accounts for about 1% to 6% of all cases and emerges roughly between 30 and 60 years. Late onset AD, characterized by an age at onset superior to 60 years, accounts for around 95% of cases. Recent estimations indicate that, by 2050, one in every 85 people will develop AD dementia [2]. The costs associated to AD in the USA will increase from its current annual $259 billion US dollars to more than $1 trillion USD by 2050 [3]. This financial burden is currently superior to that of cancer or cardiovascular disease [4]. The median survival times after a clinical diagnosis of AD range from 3 to 8 years depending on the age of diagnosis [5]. As of today, no effective treatment exists to cure or halter AD.

Neuropathologically, AD displays an abnormal deposition of insoluble forms of amyloid β in the form of plaques in extracellular spaces, as well as in blood vessels, and aggregation of the microtubule protein tau in neurofibrillary tangles in neurons [6]. The abnormal accumulation of these two proteins is believed to be responsible for neurodegeneration, in the form of synaptic loss and selective neuronal death, and cognitive decline in AD [7]. The most accepted hypothesis states that amyloid accumulate first, triggering the accumulation of tau and the subsequent neurodegeneration and cognitive decline, as depicted in Figure 1.

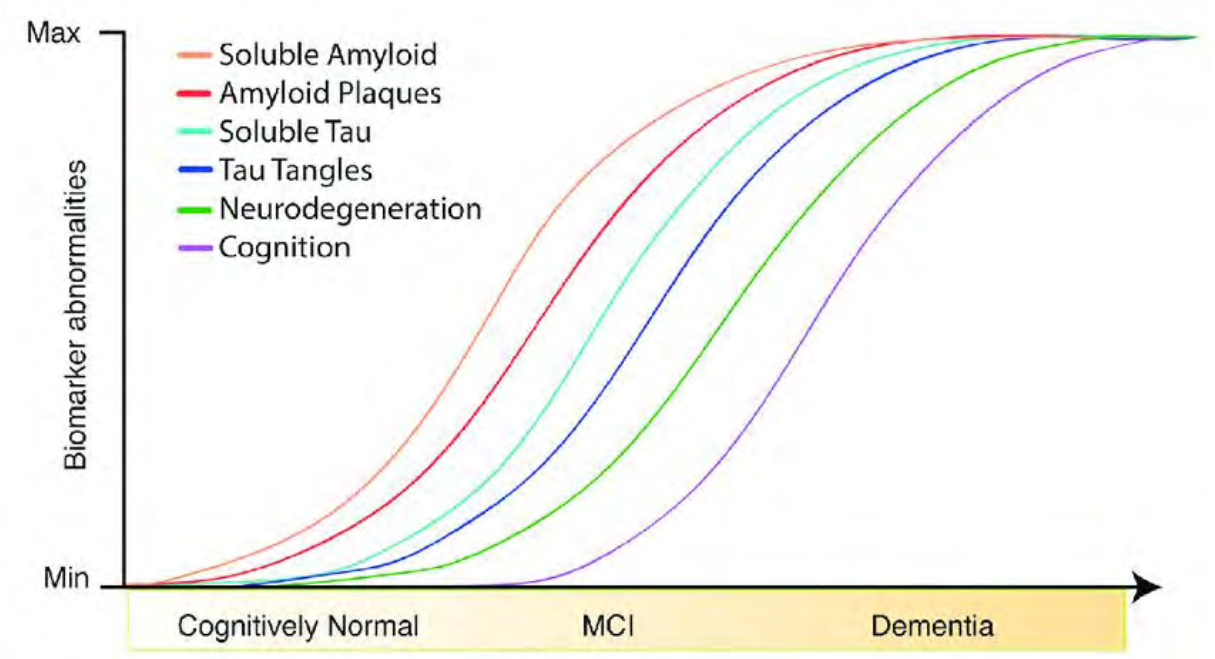

Figure 1 - Hypothetical model of the dynamics of AD neuropathologic changes. Adapted from [8].

From a clinical perspective, AD cognitive changes progress over a long-time frame. Memory loss is the most common symptom and one of the earliest to be impaired. These memory deficits affect the ability to learn and recall new material, resulting in multiple daily-life problems such as forgetting of names and appointments or misplacement of belongings. Other non-amnestic symptoms are also common in AD: impaired language and visuospatial skills, such as problems with words or recognizing faces, and executive dysfunction, which involves difficulties for reasoning and solving simple problems. At least one of these cognitive deficits must be present for the clinical diagnosis of AD. Also, an evident cognitive decline must be evident over a substantial time period, as evidenced by a history of worsening by someone close to the patient or by clinical assessments by a qualified dementia physician [9]. When these cognitive deficits are sufficiently severe to significantly interfere with patient's activities of daily life, a diagnosis of AD dementia is usually made.

It is also possible to diagnose the early cognitive changes associated with AD by using a clinical entity known as mild cognitive impairment (MCI). The clinical criteria for MCI, as defined by Petersen et al [10], include: (1) memory impairment, (2) objective memory deficit, (3) absence of other cognitive disorders or repercussions on daily life, (4) normal general cognitive function and (5) absence of dementia. The absence of cognitive deterioration in a non-memory domain is also required. The concept of MCI was very successful in identifying a group of patients at a high risk of progression to dementia, particularly AD dementia, representing the first effective effort towards an early diagnosis of AD.

However, clinical diagnosis of AD solely based on cognitive symptoms has severe limitations. It is now well known that the classical multidomain amnestic dementia phenotype used to define probable AD [9] does not imply AD pathologic change at autopsy [11-13]. About 10% to 30% of individuals clinically diagnosed as AD dementia by experts do not display AD neuropathologic changes at autopsy [11]. Conversely, the absence of clinical symptoms does not exclude the presence of AD pathologic change: 30% to 40% of cognitively normal (CN) elderly people have AD neuropathologic changes at autopsy [13-14].

The fact that a significant proportion of CN elderly display AD neuropathologic changes has led to the definition of preclinical AD [15]. This stage, that may last several years or even decades before the onset of symptoms, is characterized by the abnormal accumulation of amyloid and tau proteins in the brain without evident cognitive impairment. Recent studies indicate that preclinical AD patients, diagnosed *in vivo* by using imaging techniques to measure the presence of amyloid plaques and tau tangles, experience significantly faster rates of cognitive decline [16], evidencing the relevance of pathological changes even in the absence of significant cognitive impairment.

The precise definition of AD is currently under debate. Based on the aforementioned neuropathological findings in CN older people, the latest update of the National Institute on Aging – Alzheimer's Association (NIA-AA) research framework in 2018 propose the diagnosis of AD solely based on the *in vivo* assessment of the two pathological hallmarks of AD, amyloid plaques and tau neurofibrillary tangles [17]. This implies that the diagnosis of AD, under this new paradigm, would no longer require the presence of clinical symptoms, radically changing the traditional conceptualization of AD as a clinicopathological entity [18]. Clinical symptoms and neurodegeneration are relegated as markers of disease progression. Thus, the focus is now placed on the tools that allow us to identify AD-related pathological changes *in vivo*, i.e., on the so-called AD biomarkers.

1.2 CONVENTIONAL ALZHEIMER DISEASE BIOMARKERS

The term biomarker, i.e., biological marker, refers to a broad spectrum of objective indications of a medical state that are observed from outside the patient and that can be measured accurately and reproducibly [19]. Biomarkers stand in contrast to clinical symptoms, which are limited by the perception of symptoms by the patients. In AD, the most commonly used biomarkers are the ones that track the progression of the two pathological hallmarks of AD, i.e., amyloid and tau, as well as cortical biomarkers of neurodegeneration. These biomarkers play a central role in the 2018 NIA-AA research framework [17] for defining AD, as well as have been proven useful to predict clinically relevant outcomes among demented, MCI, and preclinical AD patients [20-22]. Biomarkers can be used to track both AD-specific pathologic changes, i.e., amyloid and tau, and cortical neurodegeneration, which is non-specific for AD. Two main groups of *conventional* biomarkers, which provide largely overlapping information about the disease, are currently accepted in the NIA-AA research framework: 1) Cerebrospinal Fluid (CSF) and 2) Imaging biomarkers [17]. In the following paragraphs, we review the AD biomarkers that are relevant for this thesis. More information about the AD biomarkers not reviewed here, i.e., metabolism and tau Positron Emission Tomography (PET), can be found in [23-24].

1.2.1 CSF biomarkers

CSF is a clear fluid produced by the choroid plexus and found in the ventricular system and subarachnoid spaces surrounding the brain and spinal cord. CSF analysis is an invasive technique that requires a lumbar puncture. The use of CSF analyses for aiding in AD diagnosis was therefore difficult since lumbar puncture may be refused by the patients, but also by the clinicians due to fear of complications in the form of post lumbar puncture headache. Over the past years, however, it has been shown that the incidence of post lumbar puncture headache among elderly is low [25]. The use of small gauge needles has also reduced the risk of this complication.

The theoretical background for CSF biomarkers relies on the fact that molecular changes in the brain extracellular and interstitial environments are reflected in CSF, since the single-cell layer epithelium separating the brain and the CSF facilitates the exchange of molecules between these two compartments.

The core CSF biomarkers for AD include the 42 amino acid isoform (Aβ42) of β-amyloid, phosphorylated tau (p-tau), and total tau (t-tau). These analytes capture key aspects of disease progression such as aggregation and deposition of the Aβ42 peptide into plaques, phosphorylation of tau and tangle formation, and neuronal and axonal degeneration. Core AD CSF biomarkers have been extensively validated as a valuable diagnostic and prognostic tool in AD at the preclinical, MCI, and dementia stages [26-28]. However, a potential limitation is the large variability in measurements between different laboratories, as well as over time for different batches of reagents [29]. In this regard, recent investigations indicate that automated arrays may help reduce variability across laboratories and that robust cut-points can be derived [30].

1.2.2 Imaging biomarkers

Structural and molecular imaging allow us to “see” how the brain looks and works in life. Being able to examine the processes occurring in the brain in a non-invasive way, and to inspect the different brain dynamics in response to disease and intervention, has had an enormous impact on clinical practice and research in AD. Over the past 20 years, an

increasing number of sophisticated neuroimaging techniques has become widely available, allowing specific pathological features of the disease to be investigated in detail. Now, we can assess histopathological hallmarks of disease, but also brain activity, microstructure, perfusion, connectivity, metabolism—*in vivo*. In the field of AD, neuroimaging techniques allowed us to better understand the progression of the pathological cascade and how it relates with cognitive symptoms [31], although we do not have yet a full understanding of the dynamics of AD [32]. In this thesis, we made use of the two most studied and validated imaging techniques in AD: structural MRI and amyloid PET.

1.2.2.1 Structural Magnetic Resonance Imaging

Magnetic Resonance Imaging (MRI) is a powerful, non-invasive diagnostic imaging technique widely used to obtain detailed information about the anatomical properties of different organs, both healthy and diseased. MRI scanners use strong magnetic fields and magnetic field gradients to generate high-quality images of the organs in the body. MRI does not involve the use of ionizing radiation, which distinguishes it from PET and CT.

In the AD field, structural MRI is regarded as an important and useful diagnostic and prognostic tool for AD. The most common sequence is the T1-weighted, which allows us to evaluate the morphology of the brain with millimetric resolution and assess subtle atrophic changes. MRI-based measures of atrophy are considered appropriate markers of neurodegeneration [17] and are useful to track and predict disease progression [33]. Atrophy appears to be an inexorable process that accompanies neurodegeneration. The patterns of brain atrophy correlate well with cognitive deficits in both cross-sectional and longitudinal studies [34]. Brain atrophy patterns resemble those of tau deposition [35]. The earliest topography of tau deposition and associated MRI-detectable atrophic changes typically involve the perforant (polysynaptic) hippocampal pathway (entorhinal cortex, hippocampus and posterior cingulate cortex), which is consistent with the early memory deficits observed in mild AD [36]. As the disease progresses, atrophic changes in temporal, parietal and frontal cortices are correlated with neuronal loss, as well as with praxic, visuospatial and behavioral impairments [37]. The validity of MRI as a marker of progression was confirmed longitudinally by several studies. Rates of change in several structural measures, including whole-brain [38], entorhinal cortex [39], hippocampus [40], and also ventricular enlargement [41], were found to occur in tandem with changes in cognition. A representative case of normal aging and AD atrophic changes can be seen in Figure 2.

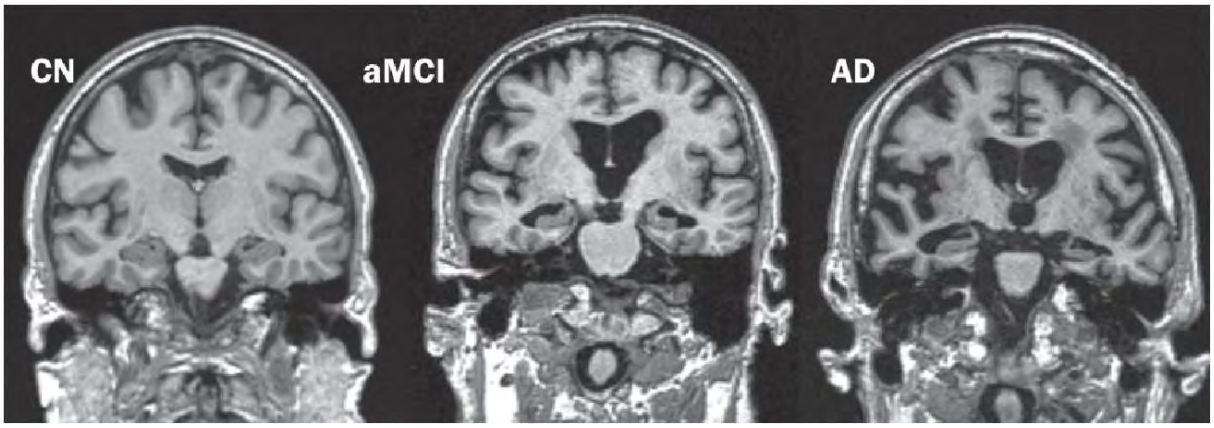

Figure 2 - Examples of T1 MRI scans from a cognitively normal subject (left), an amnestic MCI (middle), and an AD demented patient (right). Adapted from [42].

The following quantification methods are commonly used when atrophic changes in different individuals need to be compared:

- **Visual assessment:**

  Often, visual assessment of the severity of atrophy in the medial temporal lobe is regarded as a measure of disease progression [43]. Visual assessment is a fast and practical way to assess MRI scans but it is not sensitive to subtle atrophic changes and suffers from inter and intra rater variability.

- **Quantitative volumetric techniques:**

  Volumetric measurements are the most commonly used quantitative metric in AD. Traditionally, volumes of interest were manually traced. However, the increase in computational resources has allowed the use of automated methods.

  1. *Manual tracing*: Manual delineation and quantification of the volume of medial temporal lobe structures such as the hippocampus or entorhinal cortex have been commonly used in AD and provide an objective quantitative measure of the degree of atrophy [44]. The main drawback is that manual segmentations can be tedious and time-consuming.
  2. *Automated and semi-automated techniques*: Over the recent years, a variety of different methods have been developed to automatically parcellate gray matter and cortical surfaces into volumes of interest. Cortical surfaces are used to compute global and regional cortical thickness. Since automated and semi-automated methods do not require important manual edits, they are tremendously useful for large-scale studies.

  An advantage of volumetric approaches, such as measuring hippocampal volume, is that these metrics describe an a priori known anatomical structure that is closely related to the pathological features of the disease and functionally related to clinical symptoms – episodic memory impairment. The disadvantage of using a priori regions of interest is that the information obtained is spatially limited and does not exploit all the available information in a T1 scan.

- **Quantitative voxel-based method:**

  This methodology allows us to assess atrophy without any a priori assumption about the volume of interest.

  1. *Voxel-based techniques*: Voxel-based morphometry (VBM) [45] provides a powerful way to test for a wide variety of hypothesis, including group and correlational analyses. Although VBM permits the visualization of the spatial patterns of neurodegeneration characteristic of the disease, these patterns are statistical averages over certain population, so this method cannot be aid in the diagnosis of AD.

2. *Automated individual subject diagnosis:* New automated approaches that take into account the multivariable nature of neuroimaging data have been developed over the last years. These novel methods learn the disease and health patterns from a large sample of diseased and control MRI scans, providing subject-specific continuous scores of the degree of pathologic changes, summarizing in a single metric all the information contained in the MRI scan [46].

1.2.2.2 Amyloid PET

PET is a technique that allows track physiological function by looking at metabolism, proteins, and radiolabelled drugs, among others. PET provides the opportunity to carry out both visual and quantitative analyses, allowing changes over time to be monitored as a disease progresses or in response to a specific treatment. The PET camera system detects coincident pairs of gamma rays emitted indirectly by a positron-emitting radioligand, most commonly fluorine-18. Radioligands are injected into the body on a biologically active molecule (radioactive tracer) that transport the radioligand to the target of interest. Different tracers and radioligands can be used depending on the purpose of the PET study. 3D images of tracer concentration throughout the body are then reconstructed using complex mathematical techniques. In modern PET machines, 3D tracer imaging is often accomplished with the help of a computed tomography X-ray scan acquired on the patient during the same session, in the PET camera. This X-ray scan improves the quality of the PET image, as well as helps the nuclear physician to better correlate PET findings with anatomical structures. Although recent advances have importantly increased image quality, current resolution of modern PET scanners is low compared to that of MRI (4-5 mm).

1.2.2.2.1 Amyloid PET tracers

PET with amyloid tracers has revolutionized neuroimaging in aging and AD over the past years by enabling the detection of amyloid plaques, one of the defining pathologic features of AD. The first specific tracer for amyloid-beta (Aβ) studied in humans was the carbon-11 (11C)-labeled Pittsburgh Compound B (PiB). PiB is an analogue of thioflavin-T that binds to fibrillar Aβ with high sensitivity and specificity [47]. PiB displays high affinity to both extra-cellular amyloid plaques (mainly composed of the Aβ 1-42 peptide) and vascular amyloid deposits (mainly composed of Aβ 1-40 peptides) [48]. PET with PiB has become an essential part of research studies on AD. However, the short half-life of 11C (20 minutes) limits its use to facilities equipped with a cyclotron, severely limiting its clinical applicability. Because of this, a new generation of amyloid tracers labeled with fluorine-18 (18F, 110-minute half-life) has been developed, allowing to produce and deliver amyloid tracers for widespread clinical use. Three 18F amyloid imaging agents are already available and have been prospectively validated in autopsy studies: flutemetamol, a 3'-fluoro analog of PIB [49]; florbetapir, a styrylpyridine derivative [50]; and florbetaben, a derivative of stilbene [51]. A Florbetapir scan of a cognitively normal subject without amyloid burden and an AD demented patient with elevated cortical amyloid can be seen in Figure 3. A significantly higher Florbetapir uptake in the frontal, parietal, and lateral temporal cortices and striatum is the commonly observed retention pattern in AD demented patients compared to CN subjects.

An interesting characteristic of amyloid tracers, as can be seen in Figure 3 as well, is the elevated uptake in both controls and AD patients in the white matter, brainstem, and pons. This tracer retention is considered to be non-specific since amyloid plaques in these

areas are unlikely in subjects without evident cortical pathology [52]. It is now well known that amyloid tracers bind to the myelin protein, and its use as marker of myelin integrity is currently under active investigation [53]. These findings are of uttermost importance for this thesis and will be discussed in detail later.

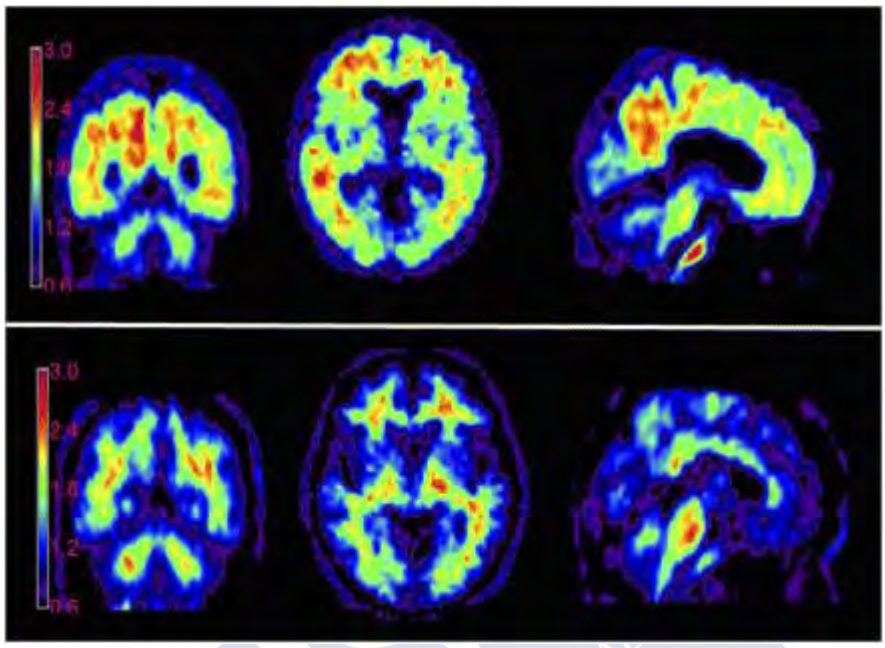

Figure 3 - Top: Example of an AD demented patient with elevated cortical amyloid. Bottom: Example of a CN subject with low cortical amyloid.

1.2.2.2.2 Quantification

Different methodologies have been employed for the quantification of amyloid PET scans. It has been shown that the highest accuracy can be achieved by using 90-min dynamic acquisitions and applying Logan [54] or reference tissue models [55]. However, 90-min acquisitions or arterial radioactivity sampling present practical difficulties, limiting its clinical applicability. A more practical approach that relatively preserved accuracy is to a start a 20-min imaging period 40 to 50 min after tracer injection. This time window was observed to be the one in which the tracer reaches a steady state equilibrium. Good test-retest variability (5–7%) can be obtained using this protocol [56], proving to be acceptable substitutes for more complicated dynamic studies. This precision is also kept longitudinally: in serial PiB imaging sessions, late uptake methods show a good intra-subject variability of 3% [57].

The definition of what constitutes an abnormal amyloid PET scan has been investigated in detail over the last years. As with MRI, amyloid PET scans can be evaluated visually. However, most research studies use a quantitative method in which radiotracer retention in a priori defined cortical regions of interest is measured, and then normalized to a reference value. In dynamic scans, the reference function can be an arterial input function but for most of the studies, which use late uptake acquisitions, the reference function is the measured retention in the cerebellar grey matter or the whole cerebellum. This quantity is known as Standardized Uptake Value Ratio (SUVR) [58]. For its calculation, one typically

uses one of the many available fully automated software packages to spatially register an anatomic parcellation of the cortex, usually obtained from a high resolution T1 MRI scan, to the amyloid PET scan. Then, uptake values are accurately extracted from selected regions of interest. With Florbetapir, the most commonly used cut-point for amyloid positivity is SUVR = 1.11, as defined using a cortical aggregate normalized to whole cerebellum uptake [58]. It must be noted that SUVR values are dependent on the specific amyloid ligand as well as on the image analysis used. The SUVR = 1.11 threshold was found to be the optimal in discriminating between demented and CN participants, however, lower thresholds are needed if one wants to capture the earliest stages of amyloid deposition [59]. Apart from the quantification in regions of interest, the same voxel-based techniques reviewed in Section 1.2.2.1 can be applied to amyloid PET scans.

As an effort to harmonize amyloid quantification across different protocols and amyloid ligands, the so-called Centiloid scale was proposed [60]. To define a centiloid scale in which express cortical amyloid retention, amyloid PET scans were performed in a group of typical AD patients to define the upper/pathological top of the scale (centiloid value = 100), and in a group of young CN individuals to define the low/healthy bottom of the scale (centiloid value = 0). Cortical SUVR values are then linearly scaled across this range, using the average values in these two groups.

1.2.2.2.3 Amyloid PET findings across the spectrum of AD

About 30% to 35% of CN and 50% to 60% MCI patients display elevated cortical tracer uptake [61-62], consistent with post-mortem studies [13-14,63]. In AD demented patients, about 85% to 90% present elevated cortical uptake in an amyloid PET scan [61]. Amyloid-negative patients diagnosed as AD dementia are widely regarded as patients who have been given an incorrect diagnosis [64]. Remarkably, cortical uptake strongly correlates with the most important genetic factor for late onset AD, the ε4 allele of the Apolipoprotein E (APOE) gene [65].

1.2.2.2.4 Amyloid PET and clinical outcomes

It is now well established that both CN elderly [16,20] and MCI subjects [66] with positive amyloid PET scans present faster rates of global cognitive deterioration. Amyloid-positivity is associated with more pathological markers of neurodegeneration across CN, MCI, and AD demented individuals [67]. Longitudinally, amyloid-positive subjects display faster rates of atrophy than amyloid-negative in CN and MCI [68-69].

1.2.2.2.5 Amyloid PET and clinical diagnosis

As noted by two recent reports, amyloid PET seems to be a valuable tool for the clinician: according to two recent reports, amyloid PET increases diagnostic certainty in the most complex cases of dementia [70] and significantly influences the clinical management of MCI and AD dementia patients [71]. However, one the major limitations for AD diagnosis at typical age of onset arises because 30% of CN individuals display elevated amyloid. This high age-associated prevalence implies that a positive amyloid PET cannot be regarded as causative of the observed clinical syndrome without taking into account the prior probability of positivity based solely on age. The dementia expert should therefore consider the possibility that concurrent, age-related amyloid positivity may not be relevant to the presenting symptoms. For this reason, amyloid PET is most commonly used as tool for ruling out AD as the cause of cognitive impairment [72]. Other measures of advanced brain

amyloidosis might help to make amyloid PET a diagnostic tool with a closer correlation to clinical symptoms [73].

1. 3 UNCONVENTIONAL ALZHEIMER DISEASE BIOMARKERS

Beside the aforementioned cortical biomarkers of amyloid, tau, and neurodegeneration, other markers that target different features of AD pathology, including imaging, fluid, and cognitive measures, are being actively investigated. Similar to cortical neurodegeneration markers, these new examinations probe non-specific features of AD that, however, might play an important role in the pathogenesis and progression of the disease. Many of these novel markers focus on pathologic changes in the cortex such as neuroinflammation, nevertheless, there is an increasing interest in how other structures such as the white matter (WM) [74] or the brainstem [75] contribute to AD pathology. This new paradigm challenges the traditional conception of AD as an exclusively cortical pathology, and points towards tight links between the earliest cortical pathologic changes in AD and WM abnormalities [76].

In this thesis, we continued this line of investigation and explored how WM abnormalities, assessed with both MRI and PET, contribute to AD pathological hallmarks and progression. Moreover, we also studied how a simple episodic memory assessment can aid in the prediction of progression among MCI participants with a complete biomarker description in terms of amyloid, tau, and neurodegeneration. In the following paragraphs we summarize the unconventional markers used in this work.

1.3.1 White matter hyperintensities

WM lesions, visualized as WM hyperintensities (WMH) in a Fluid-Attenuated Inversion Recovery (FLAIR) MRI scan, are commonly found in the aging brain. Initially thought to reflect normal-aging changes in WM tissue, WMH regions are now known to be histologically correlated with myelin pallor, tissue rarefaction associated with loss of myelin and axons, and mild gliosis [77]. Etiologically, WMH are commonly regarded as small vessel disease [78]. WMH also correlate with cognitive, functional, emotional, and motor abnormalities in elderly people [78]. Moreover, high WMH burden increases the risk of progression from MCI to AD dementia [79] and accelerates cognitive decline in CN older people [80], suggesting that these lesions might be etiologically linked to AD. Against this hypothesis, WMH are usually considered as a comorbidity rather than part of AD pathophysiology [81]. In the following, we review previously published evidence linking WMH and the two pathological hallmarks of AD, amyloid and tau.

1.3.1.1 White matter hyperintensities and amyloid

WMH burden is tightly linked to vascular risk factors and age, so determining the independent contributions to this burden from AD pathology is difficult and requires large populations. However, this limitation can be avoided by studying the temporal course of WMH in familial AD, given that age of onset is ~45 years and WMH related to vascular risk are unlikely at these ages. According to a recent study from the Dominantly Inherited Alzheimer Network in familial AD, WMH in posterior areas of the brain emerge 20 years before the onset of symptoms in familial AD, and in tandem with changes in CSF Aβ-42 and p-tau levels [76], suggesting that WMH are one of the earliest pathological features of AD. These findings in autosomal AD were later confirmed in two recent studies examining the associations between amyloid and tau among CN older individuals [82-83], finding a specific spatial association between WMH and global amyloid, but not tau. Since these studies are

cross-sectional, it is not possible to infer the causative pathway. However, several hypotheses have been proposed linking early amyloid deposition to WM damage, such as oligodendrocyte disfunction and demyelination induced by amyloid oligomers [74], or axonal degeneration secondary to amyloid-related microglial activation [84]. It is also possible that vascular pathology lead to amyloid deposition [85], though the mechanisms seem less clear. Further longitudinal studies are needed to understand the temporal ordering between WMH and amyloid deposition.

1.3.1.2 White matter hyperintensities and tau

Several neuropathological studies have previously found that WMH correlate with the severity of cortical tau pathology in AD dementia patients [86], particularly in parietal lobes [87]. The most accepted mechanism for this observation is Wallerian degeneration [88], in which axonal degeneration is subsequent to tau-mediated neuronal death. Neuroimaging studies have found no significant association, beyond that driven by amyloid, between WMH and tau in CN individuals [82-83], suggesting that Wallerian degeneration contributes to WMH only in late stages of the disease.

1.3.1.3 Quantification

At present, no unified criteria have been established for the measurement of WMH. Several methodologies exist to quantify the presence and severity of WMH burden on FLAIR, ranging from visual assessments to fully automated approaches. Visual scales are easy and reliable when employed by an experienced neuroradiologist, but they are not sensitive to subtle differences in WMH burden. Semi-automated and automated methods provide exact WMH volumes, allowing us to quantify WMH with a continuous variable, more sensitive to subtle associations. Commonly used visual rating scales include those proposed by Fazekas and Scheltens [89-90]. These scales have been successfully applied in cross-sectional studies since they display good intraobserver and interobserver variability for measuring WMH [91]. However, visual rating scales are time-consuming to apply, have ceiling effects and thus are not suitable for tracking WMH progression [92]. Although semiquantitative visual scales have been developed for tracking WMH change, automated WMH measurement methods provide the most accurate and fast quantification of WMH burden and progression [93]. An example of a FLAIR scan along with an automated segmentation of the WMH can be seen in Figure 4.

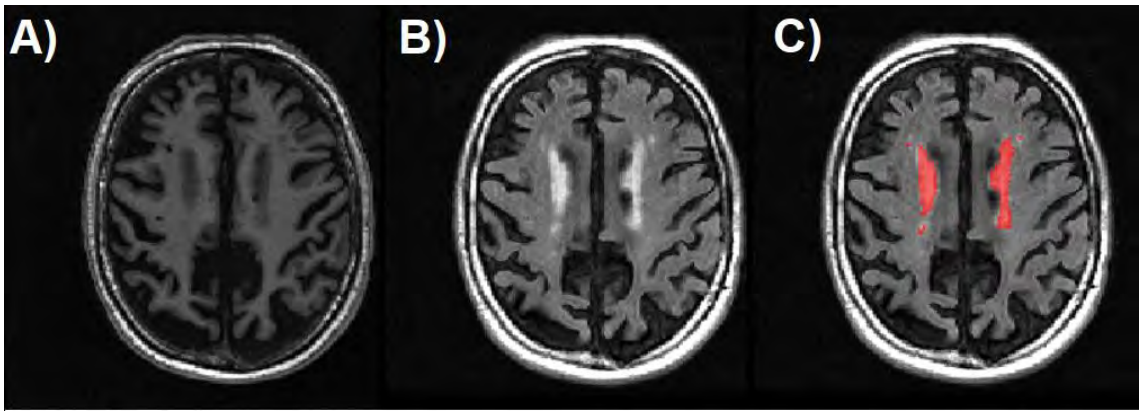

Figure 4 - Example of a A) T1 scan, B) FLAIR scan, and C) FLAIR scan along with the automated WMH segmentation in red.

1.3.2 Amyloid PET as marker of myelin integrity

In recent years, amyloid PET has been proposed as a potential marker of WM lesions in multiple sclerosis [94]. As already mentioned in Section 1.2.2.2.1, it is well known that all amyloid PET tracers show strong binding to the WM, independently of the presence of evident cortical amyloid burden. However, the mechanism of this binding is poorly understood. Although traditionally considered to be mainly driven by the non-displaceable and non-saturable characteristics of the ligands, this hypothesis seems to be inconsistent with longitudinal studies [95]. Based on the fact that some Congo Red derivatives used to derive amyloid PET ligands show high affinity for myelin, it has been suggested, as an alternative mechanism to explain WM binding, that the beta-sheet structure present in both amyloid plaques and in myelin binding proteins (which is the most abundant component of myelin) is a common target for amyloid PET tracers [94,96].

The hypothesis that amyloid PET ligands bind to myelin was initially investigated both *in vitro* and *ex vivo* by using PiB and autoradiography in human brain specimens [94], and subsequently in several studies in animal models and multiple sclerosis (see, for instance [97-98]). These studies showed that amyloid PET tracer retention in WM lesions is reduced, supporting the hypothesis that these tracers bind to myelin (Figure 5). PiB has been shown to display a stronger binding to normal-appearing WM than to perilesional tissue and WMH, in line with the well-known relative loss of myelin in these areas [97,99]. Importantly, longitudinal data support the hypothesized ability of PiB to track demyelination and remyelination profiles in single lesions over time [96,100]. All these findings strongly support the applicability of PiB in the evaluation of remyelination at the single-subject level, however, again, the short half-life of PiB severely restricts its use in clinical trials. For this reason, recent studies employed fluorinated tracers such as Florbetapir and Florbetaben to track demyelination *in vivo* in multiple sclerosis patients [98-99]. The use of fluorinated tracers would certainly increase the applicability of amyloid PET as a marker of the effectiveness of myelin repair therapies.

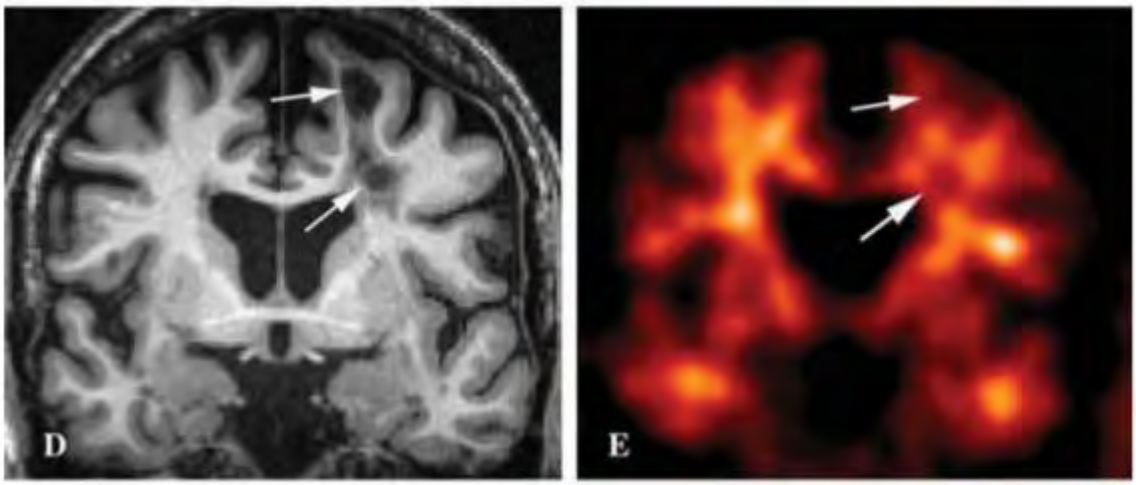

Figure 5 - Example of a multiple sclerosis patient displaying reduced PiB uptake in WM lesions. Adapted from [94].

Despite these promising results, several methodological questions regarding the optimal quantification of amyloid PET scans in multiple sclerosis remain unexplored. As of today, no

investigation has been conducted for determining the optimal acquisition protocols for myelin integrity imaging. Instead, all the studies used the same imaging protocols as for amyloid plaque imaging in AD. Also, there is no standard for the quantification of myelination processes, with most of the studies employing user-dependent methods and/or arbitrary ligand uptake cut-point values for defining de- and remyelination. Tracer kinetics in the WM of patients with multiple sclerosis need to be carefully explored as well. Partial volume effects might severely limit the applicability of this technique, since WM lesions in multiple sclerosis tend to be focal and relatively small, which make them prone to spill-in counts from the surrounding WM.

Coming back to the AD field, it is well known, as we have previously seen, that WM abnormalities, particularly demyelination, are characteristic features of the AD pathological progression. Apart from the already discussed WM lesions that also entail demyelination, myelin loss has been consistently observed in both neuropathology and imaging studies of AD brains [101-102]. Postmortem analyses of tissue of AD brains has revealed that the WM is chemically disrupted, compared with that of CN controls: the amounts of total protein, myelin basic protein, myelin proteolipid protein, cyclic nucleotide phosphohydrolase, and cholesterol are significantly decreased, clearly indicating a loss of myelin [103]. Moreover, demyelination correlated with the amount of amyloid peptides in the WM [103], suggesting a potential causal link between soluble amyloid oligomers, the most toxic form of amyloid, and demyelination [103]. In line with this hypothesis, a recent study has found that abnormal levels of CSF Aβ-42 and soluble amyloid precursor protein were associated with disrupted myelin in preclinical AD [104]. Despite the abundant evidence linking AD with myelin and amyloid PET tracer retention in the WM with myelin, no previous study has evaluated whether this uptake in the WM reflects progression and WM changes across the spectrum of AD.

1.3.3 Episodic memory

Episodic memory encodes our ability to learn, store, and retrieve information about particular personal experiences that occur in our lives. These memories commonly include information such as the time and place of an event, or more detailed characteristics of the event itself. Episodic memory impairment is one of the cognitive hallmarks of the early stages of AD, usually manifesting as an increased forgetting rate. Its neural substrate are the mesial temporal lobes, the diencephalon, and the basal forebrain, all of them severely affected by AD pathology. From a clinical perspective, standardized neuropsychological tests are commonly used to support the diagnosis of MCI or AD dementia and to measure the degree of severity of the patient's cognitive impairments [10,18]. They play an important role in the NIA-AA research framework for defining the MCI and dementia syndromal categories [17]. Commonly used tests for episodic memory include the Wechsler Memory Scale-Revised Logical Memory II (delayed recall), Visual Reproductions II (delayed recall), and the Auditory Verbal Learning Test (delayed recall) [105-106].

In an attempt to stage cognitive symptoms in MCI, the Alzheimer's Disease Neuroimaging Initiative and other studies proposed staging MCI patients into 'early' and 'late' substages, on the basis of episodic memory performance [107]. Several previous studies have demonstrated differences between these two substages, such as slower progression rates to AD dementia [108], different prevalence in the community in comparison to the clinic [108-109], and different clinicopathologic features [110-111], which support the idea of a sequential evolution between these two groups. However, recent evidence suggests that the

observed differences might be biased by the high prevalence of false positive MCI diagnoses in the early MCI substage [112-113], casting doubt on the usefulness of this staging scheme to track the cognitive continuum in prodromal AD. Moreover, it is also unclear whether this difference in episodic memory impairment is entirely driven by the amount of conventional pathology, i.e., amyloid, tau, and atrophy, or if, on the contrary, the different performance might be the reflection of other pathologic mechanisms in AD.

1.4 WHY WE NEED UNCONVENTIONAL BIOMARKERS

Based on the amyloid cascade hypothesis and the "Jack curves" [114-115], the AD scientific community has assumed over the past decades that the two pathological hallmarks of AD, i.e., amyloid plaques and tau neurofibrillary tangles, were the main driving forces in AD. While this "amyloid and tau" picture has provided enormous advances in our ability to identify the presence of abnormal changes and predict clinical outcomes of patients at every disease stage, recent studies suggest that this paradigm may not be sufficient to provide clinically relevant predictions. In the largest study to date predicting the memory outcomes of non-demented individuals over a median of 4.8 years, the predictive improvement when adding conventional imaging biomarkers of amyloid, tau, and neurodegeneration to accessible clinical variables was small enough to cast doubt on the usefulness and clinical relevance of these biomarkers [16]. This relatively disappointing result adds to the repetitive failures of many anti-amyloid immunotherapies and β-secretase inhibitor treatments, which have raised serious doubts about the importance of amyloid in AD pathogenesis, in spite of the rich evidence from genetics, neuropathology, and biomarker studies.

The key and early role of amyloid in AD pathogenesis has been supported by several genetic and biomarker studies in both familial and sporadic AD. Dominant mutations linked to the processing of the amyloid precursor protein lead to amyloid overproduction and cause familial AD [116]. Subjects with Down syndrome and APP gene triplication show higher amyloid production and develop early-onset dementia [117]. In contrast, other mutations known to reduce amyloid production, such as the Icelandic mutation, are associated with lower AD dementia risk. Thus, the hypothesis that the overproduction of amyloid or its impaired clearance are the triggers of AD pathogenesis has a solid support from genetic studies. However, the fact that amyloid is the initial triggering event in the AD pathological cascade does not imply that haltering amyloid overproduction would translate into a slowing down of disease progression. As noted in [118], amyloid overproduction might need to reach a certain threshold to cause harm or just be a simple trigger of other disease processes relevant for the clinical progression. Several different pathologic processes are now proposed as potential intervention targets, such as soluble amyloid oligomers [32] or neuroinflammatory processes [119].

It is therefore necessary to identify novel markers of AD-related pathology that will help us understand which are the important mechanisms that lead to the differing clinical outcomes observed in preclinical AD. This thesis is aimed at contributing to the identification of these novel markers of AD pathology, beyond the classical picture of cortical amyloid, tau, and neurodegeneration, and to explore their relationships with conventional measures of cortical pathology and clinical outcomes, with a focus in the preclinical stage of AD.

OBJECTIVES

2 OBJECTIVES

2.1 HYPOTHESES

Preclinical AD progression occurs over a long-time course of many years or even decades. To date, current models of preclinical and prodromal AD progression using conventional markers of amyloid, tau, and neurodegeneration have provided little to modest improvements to already accessible clinical data. Novel markers of AD pathology, more related with clinical progression, are needed in to better understand the AD physiopathological features that lead to cognitive decline in the earliest stages of AD. The study of non-cortical structures, such as the WM, and the added value of cognitive markers to the conventional markers of AD pathology will give us a better insight of other relevant pathologic processes in AD. This thesis formulates the following specific hypotheses:

- WMH are one of the earliest pathological features of AD. These WM lesions might become detectable even before amyloid does in a PET scan. WMH may thus predict future amyloid accumulation among CN elderly without evident cortical amyloid burden.
- WM demyelination is an early pathologic change in AD. Amyloid PET is sensitive to demyelination in the WM. Amyloid PET tracer uptake in the WM can be used as a marker of myelin integrity and therefore it is associated to abnormal CSF biomarkers and AD progression.
- Episodic memory provides complementary information on AD progression stage to conventional markers of amyloid, tau, and neurodegeneration.

2.2 SPECIFIC OBJECTIVES

The main goal of this thesis is the identification of novel, unconventional markers of AD pathology. The specific objectives are summarized in the following bullet-points:

- To investigate whether WMH are predictive of amyloid accumulation over time among CN individuals with no evident cortical amyloidosis as measured with amyloid PET.
- To explore whether demyelination, as measured with amyloid PET, is associated with abnormal AD CSF biomarkers and progression.
- To assess whether episodic memory is a useful marker of disease progression, and if it provides complementary prognostic information to conventional cortical markers of amyloid, tau, and neurodegeneration.

METHODS

3 METHODS

Although we have provided the specific methods used for each analysis in Section 4, here we summarize general methodological details applicable to all the analyses.

3.1 THE ALZHEIMER'S DISEASE NEUROIMAGING INITIATIVE

The Alzheimer's Disease Neuroimaging Initiative (ADNI) is a longitudinal multicenter study aimed at developing clinical, imaging, genetic, and biochemical markers for the early detection and tracking of AD. This collaborative study combines expertise and funding from both private and public sectors to study individuals with mild AD dementia, as well as those with MCI and elderly with no signs of cognitive impairment. Researchers at 63 participating sites in the US and Canada employ a variety of neuroimaging, biochemical, and genetic markers in order to track the pathological progression of AD in the human brain.

ADNI began in 2004 under the leadership of Dr. Michael W. Weiner, funded as a private-public partnership with $27 million contributed by 20 companies and two foundations through the Foundation for the National Institutes of Health and $40 million from the National Institute on Aging. The initial five-year study (ADNI-1) was extended by two years in 2009 by a Grand Opportunities grant (ADNI-GO), and in 2011 and 2016 by further competitive renewals of the ADNI-1 grant (ADNI-2, and ADNI-3, respectively). Details of each phase of the study are summarized in Figure 6.

STUDY CHARACTERISTICS	ADNI-1	ADNI-GO (Grand Opportunities)	ADNI-2	ADNI-3
Primary goal	Develop biomarkers as outcome measures for clinical trials	Examine biomarkers in earlier stages of disease	Develop biomarkers as predictors of cognitive decline, and as outcome measures	Study the use of tau PET and functional imaging techniques in clinical trials
Funding	$40 million federal (NIA), $27 million industry and foundation	$24 million American Recovery Act funds	$40 million federal (NIA), $27 million industry and foundation	$ 40 million federal (NIA), up to $20 million industry and foundation
Duration/start date	5 years/October 2004	2 years/September 2009	5 years/September 2011	5 years/September 2016
Cohort	200 elderly controls 400 MCI 200 AD	Existing ADNI-1 + 200 early MCI	Existing ADNI-1 and ADNI-GO + 150 elderly controls100 early MCI 150 late MCI 150 AD	Existing ADNI-1, ADNI-GO, ADNI-2 + 133 elderly controls 151 MCI 87 AD

Figure 6 - Summary of the different phases of the ADNI study.

A characteristic feature of ADNI from its inception was the resolve to make all data generated publicly available to researchers worldwide. This open data sharing had no precedent for NIH funded projects and required that the Informatics core provided a sophisticated infrastructure based at the Laboratory of Neuroimaging, currently at the University of Southern California, to allow the storage, curating and sharing of ADNI imaging, biomarker, clinical, and genetic data.

Without ADNI, a major limitation of multicenter studies was the development of standardized protocols that would allow the comparison of findings from multiple participating centers and scanners. A remarkable collaborative effort led to a set of protocols for PET and MRI, and the analysis of CSF biomarkers. These methods have proved crucial beyond the scope of ADNI. ADNI standardized protocols have been used in the vast majority of clinical trials run by

pharmaceutical companies developing disease modifying therapies for AD and most recently AD prevention trials.

3.2 ADNI PARTICIPANTS

To date, the ADNI has enrolled more than 1400 participants in the study. These participants are categorized in three main diagnostic cohorts, based on their clinical and cognitive status.

Enrolled participants were between 55 to 90 years old and were required to have a study partner in order to provide an external evaluation of functioning. Participants had to be fluent in either English or Spanish. All participants had to be willing to undergo all examinations, including neuroimaging and longitudinal follow-up studies. Subjects using psychoactive medications considered to potentially affect cognitive function were excluded.

The general inclusion and exclusion criteria for all the cohorts were as follows. All participants had to have a Hachinski Ischemic score [120] < 5; permitted medications should be stable over at least 4 weeks before screening; a Geriatric Depression Scale [121] score < 6; a study partner who spend more than 10 hours per week of contact either in person or on the telephone and who could escort the participant to the study clinical visits; visual and auditory acuity adequate for neuropsychological testing; good general health with no major diseases before enrollment; 6 grades of education or equivalent work history. Women were required to be sterile or 2 years past childbearing potential. Participants had to be in good condition so that they can complete a 3-year imaging study (2 years for participants with AD dementia). Participants allowed DNA extraction for APOE testing and banking, as well as for blood and urine examination for biomarkers. Subjects could not have any medical contraindications to MRI and could not be enrolled in other trials or studies concurrently.

Study participants were classified as CN, subjects with MCI, or subjects with mild AD dementia. The criteria for the classification of the participants were as follows. Regarding subjective memory complaints, the CN subjects were allowed to have memory complaints, while participants with MCI and AD dementia both had to have memory complaints. On the Mini-Mental State Examination (MMSE) [122], the range for CN and MCI participants was 24 to 30, while for AD dementia 20 to 26, all inclusive. The Clinical Dementia Rating [123] score for CN was 0, for participants with MCI was 0.5 with a requirement of the memory box score being at least 0.5, and for subjects with mild AD dementia was 0.5 or 1, with the same memory box requirement as in MCI. The memory criterion was determined using the delayed recall of 1 paragraph from the Logical Memory II subscale of the Wechsler Memory Scale–Revised [124], by using the following education-adjusted cut-points: CN: ≥9 for 16 years of education, ≥5 for 8 to 15 years of education, and ≥3 for 0 to 7 years of education. For subjects with MCI and mild AD dementia, these scores were ≤8 for 16 years of education, ≤4 for 8 to 15 years of education, and ≤2 for 0 to 7 years of education. Participants with MCI were required to keep largely preserved general cognition and functional performance and could not qualify by any means for the diagnosis of dementia [10]. Subjects with mild AD had to meet the National Institute of Neurological and Communicative Disorders and Stroke–Alzheimer's Disease and Related Disorders Association criteria for probable AD [9]. All subjects had to provide informed consent as compatible with the local participating institutions (Institutional Review Board regulations). All the participants provided written allowing for public dissemination of their anonymized data. Further details can be found at http://adni.loni.usc.edu/methods/documents/.

3.3 CSF ANALYSIS IN ADNI

CSF was acquired by lumbar puncture and stored at −80°C at the ADNI Biomarker Core laboratory at the University of Pennsylvania Medical Center. Aβ42, T-tau, and P-tau were measured by using the Elecsys β-Amyloid(1-42) CSF, and the Elecsys Phospho-Tau (181P) CSF, and Elecsys Total-Tau CSF immunoassays, according to preliminary kit vendor guidelines, as previously described [125]. The analyses were performed in a series of 36 runs, with each sample run one time for each of the three marker tests. Acceptance criteria as documented by the immunoassay vendor (Roche) was followed for these tests. Each of the 36 analytic runs was required to pass quality controls that ensure that measurements fulfill ADNI standards for precision and accuracy. The analyte measurement range were 200 to 1700 pg/ml for Aβ-42, 80 to 1300 pg/ml for Total-Tau, and 8 to 120 pg/ml for Phospho-Tau. Exploratory analyses on the values beyond Aβ-42 upper technical bound were performed using an extrapolation of the calibration curve. These extrapolated values were used in throughout this thesis. A remarkable feature of this kit is the strong correlation showed by Total-Tau and Phospho-Tau, which is represented in Figure 7 for 1215 ADNI participants.

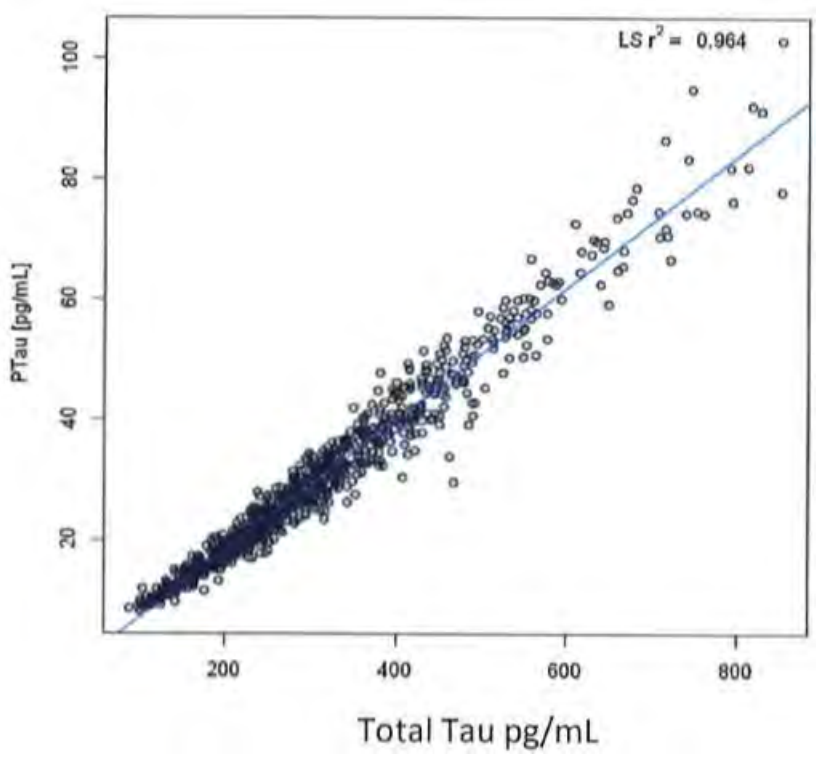

Figure 7 - Relation between Total-Tau and Phospho-Tau in the automated array Elecsys.

3.4 NEUROIMAGING PROTOCOLS IN ADNI

In the following paragraphs, neuroimaging protocols for the imaging techniques relevant for this thesis are summarized.

3.4.1 MRI

The ADNI MRI protocol has evolved over the 3 phases of the study. In ADNI1 (2004-2009), the protocol focused on consistent longitudinal structural imaging on 1.5T scanners using both T1- and dual echo T2-weighted sequences. 25% of ADNI1 participants were also scanned using basically the same protocol on 3T scanners. The protocol for ADNI-

GO/ADNI2 (2010-2016) was performed at 3T with T1-weighted imaging parameters similar to ADNI1. Dual echo T2-weighted scans from ADNI1 were replaced by 2D FLAIR and T2*-weighted scans in all participating sites. Both fully sampled and accelerated T1-weighted scans were acquired in each session. More advanced imaging techniques were included depending on scanner manufacturer: diffusion imaging on GE scanners, resting state functional MRI on Philips scanners and arterial spin labeling on Siemens scanners. ADNI3 imaging is currently done exclusively on 3T scanners. Nearly all the imaging sequences from ADNI2 have been updated for inclusion in ADNI 3, with a few important exceptions such as the protocols for FLAIR imaging. A summary of the acquisitions across the phases can be seen in Figure 8.

ADNI1 (1.5T Scanner)	ADNI GO/2 (3T Scanner)	ADNI 3
Participant Scan: 1. Localizer 2. MP-RAGE 3. MP-RAGE – REPEAT 4. B1 Calibration – Head Coil (if applicable) 5. B1 Calibration – Body Coil (if applicable) 6. T2 Dual Echo (Straight Axial – cover below cerebellum through top of head)	Participant Scan: 1. Localizer 1a. Calibration/Reference Scan (if applicable) 2. Sagittal MP-RAGE/IR-SPGR 3. Accelerated Sagittal MP-RAGE/IR-SPGR 4. Resting State fMRI (Philips Systems Only) – Subjects should have eyes OPEN. 5. Axial T2-FLAIR 6. Axial T2-Star 7. Axial ASL Perfusion (Siemens Systems Only) – Subjects should have eyes OPEN. 8. Axial DTI Scan (GE Systems)	Participant Scan: 1. 3 Plane Localizer 2. Accelerated Sagittal MPRAGE 3. Sagittal 3D FLAIR 4. Axial T2 STAR 5. Axial 3D PASL (Eyes Open) 6. Axial DTI 7. Field Mapping 8. Axial rsfMRI (Eyes Open) 9. HighResHippocampus
Phantom Scan: 1. Localizer 2. MP-RAGE (with slice thickness increased to cover phantom) 3. MP-RAGE – REPEAT (same as above) 4. B1 Calibration – Head Coil (if applicable) 5. B1 Calibration – Body Coil (if applicable) 6. T2 Dual Echo (Straight Axial – Through center of phantom) 7. MP-RAGE CORONAL (with slice thickness increased to cover phantom)	Phantom Scan: 1. Localizer 1a. Calibration/Reference Scan (if applicable) 2. QC Phantom MP-RAGE/IR-SPGR (Accelerated) 3. QC Phantom fMRI (Philips Systems)	Phantom Scan: 1. 3 Plane Localizer 2. QC Phantom MPRAGE

Figure 8 - Summary of the different MRI acquisitions across the different ADNI phases.

ADNI1 and ADNI-GO/2 MRI scans were preprocessed by the Mayo Clinic MRI core. This preprocessing provided intensity normalized and gradient unwarped TI image volumes for all ADNI1 and many ADNI-GO/2 scans. Over the last years, MR vendors started offering these corrections online as part of the reconstruction process, so ADNI stopped performing its own preprocessing and instead used the pipeline provided by the vendor of the product. Consequently, no offline TI image preprocessing is now needed in ADNI3.

Corrections applied to ADNI1 and ADNI-GO/2 T1 scans include Gradwarp, B1-correction, and N3. The application of these corrections depends on the manufacturer and system RF coil configuration. Philips Systems included a B1 correction with the reconstruction software at the time ADNI began. Moreover, Phillips gradients tend to be linear, so no gradwarping and no B1 correction was needed for these scanners. More details about MRI protocols can be found in http://adni.loni.usc.edu/methods/mri-tool/mri-analysis/.

3.4.2 Amyloid PET imaging

Amyloid PET imaging with Florbetapir began with ADNI-GO/2 after the pilot experience with PiB. The acquisition protocol consisted of 4 × 5 minute frames acquired at 50

to 70 minutes after ligand injection. In the following, quality control, standardization, and preprocessing are detailed.

3.4.2.1 Scan quality control

The quality control procedure consists of visual inspection, which includes the following steps: 1) qualitative assessment of head motion, 2) assessment of whether the entire brain was covered in the field-of-view, and 2) detection of artifacts arising from spatial mismatches between the transmission/CT and emission scans, or from detector and scanner normalization problems. Quality controlled scans were then preprocessed by aligning the 5-min frames to frame 1 employing an affine transformation with 6 degrees of freedom, using the NeuroStat "mcoreg" routine. The magnitude of motion between frames for the transformation parameters is checked and flagged when quality thresholds are exceeded. Correlation and root mean square error parameters are calculated between pairs of frames, both prior to and following co-registration. Both correlation and root mean square error matrices are inspected for frames that have low correlation values and/or high squared errors. Both visual inspection and quantitative measures are used to approve frames.

3.4.2.2 Scan standardization

After appropriate co-registration, all frames are averaged into a single "static" frame. To standardize averaged PET images, each subject's baseline averaged-FDG PET scan is aligned to the Talairach atlas using the NeuroStat "stereo" routine, in a grid of 160×160×96 isotropic voxels of 1.5 mm^3. This image is called now subject's "FDG Standard". The baseline averaged-Florbetapir scan is then co-registered to the "FDG Standard" using NeuroStat's "coreg" tool with a mutual-information cost-function. This co-registered scan becomes the "AV Standard". To process every follow-up scan in a similar manner, all frames of each follow-up amyloid PET scan are co-registered to the "AV Standard". Then, the individual frames of each scan are averaged. Averaged scans (both baseline and follow-up) are then intensity normalized. Florbetapir images are normalized using an atlas-based cerebellar gray matter reference region. With this procedure, all individual frames are registered using a single interpolation, yet yielding a common space for all the scans of each participant.

There are 20 different scanner models from three vendors in the 57 participating sites participating in ADNI-GO/2. Resolutions vary from ~4 to 8 mm. To better compare results across different centers, the ADNI PET core measured for each scan the specific in-plane and axial smoothing kernels needed to achieve an isotropic resolution of 8 mm. The smoothing kernels were calculated by comparing scans of the 3D-Hoffman brain phantom to a digital version of the phantom smoothed with an isotropic 8mm Gaussian filter. Each phantom image was smoothed using a grid search of in-plane and axial resolutions (0.5 mm increments) and then compared to the smoothed digital phantom. The kernel parameters that yielded the highest global correlation and lowest root mean squared error compared to the smoothed digital phantom was computed for each scan. The median value of each parameter across all scans of the same scanner model were chosen as the scanner's smoothing-kernel parameters. These parameters were used to smooth the previously pre-processed image for all scans of that model. Additional details on PET acquisition and processing can be found in http://adni.loni.usc.edu/methods/pet-analysis-method/pet-analysis/.

3.5 NEUROIMAGING ANALYSIS

In this section, an overview of the neuroimaging tools, including those for MRI and PET, used in this thesis is provided in the next paragraphs.

3.5.1 T1 MRI analysis

For the analysis of T1 MRI images we used two neuroimaging software packages, FreeSurfer [126] and SPM12 [127].

3.5.1.1 FreeSurfer

FreeSurfer is a suite of robust tools that allow automated analyses of relevant features in the human brain. Implemented analyses include volumetric segmentation of the common macroscopically visible structures, segmentation of hippocampal subfields, inter-subject registration based on cortical folding patterns, segmentation of white matter fascicles in diffusion MRI, parcellation of cortical folding patterns, estimation of architectonic boundaries from in vivo data, local mapping of the thickness of cortical gray matter, and the construction of surface models of the cerebral cortex.

For this thesis, FreeSurfer was primarily used for segmentation of subcortical and cortical structures.

- **Subcortical segmentation:** Subcortical segmentation comprised 5 stages. The first stage consists of an affine transformation with MNI305 space specifically designed to be robust against pathologic changes and to maximize the precision of the resulting segmentation. This is followed by an exploratory volumetric labeling. B1 bias field correction is then applied. Lastly, a high dimensional nonlinear volumetric registration to the MNI305 atlas is performed. After this preprocessing, the volume is labeled (see Figure 9). This volume-based pipeline only depends upon the skull stripping to create a mask of the brain in which the labeling of the structures is performed. The last stage, labelling the volume, is based on both a subject-independent probabilistic atlas and subject-specific measured values. The subject independent atlas is built using a training set of subjects whose brains have been segmented by hand. These labels are mapped into a common space MNI305 space so that a voxel-to-voxel correspondence can be established for all subjects. At each voxel in space, there exists the label that was assigned to each subject and the measured value (or values) for each subject. Three types of probability maps are then computed. First, the probability that the voxel belongs to each of the labeled structures. Second, the probability, computed from the training set, that a given voxel belongs to a label given the classification of its neighboring. Third, the probability distribution function of the voxel intensity value is estimated as a Gaussian distribution separately for each label at each voxel. The classification of each voxel in space is then achieved by iteratively finding the segmentation that maximizes the probability, estimated using the aforementioned probability maps, of input given the prior probabilities from the training set.

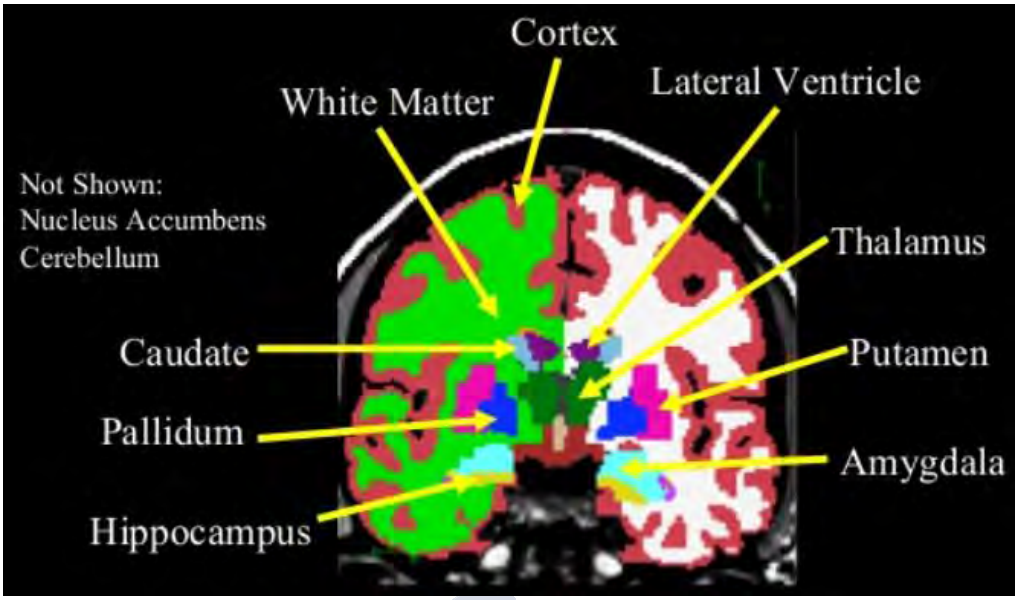

Figure 9 - FreeSurfer subcortical segmentation.

- **Cortical parcellation:** The surface-based procedure consists of several phases. First, the volume is affinely registered with the MNI305 atlas, allowing FreeSurfer to set seed points for later stages. The B1 bias field is estimated by measuring the variation in the white matter signal. The core of the WM is used to estimate the field across the whole volume. WM voxels with high likelihood of being WM are chosen based on the same three probability maps discussed for the subcortical segmentation. The intensity signal at each voxel is then divided by the estimated bias field at that location so as to remove the effect of the bias field. Then, the skull is stripped using a deformable template model and voxels are labelled as WM or non-WM based on intensity signal and neighbor probability maps. Separating planes are determined to separate the hemispheres from each other as well as to remove the cerebellum and brain stem. The position of the separating planes is computed with the expected MNI305 position of the corpus callosum and pons, as well as several rule-based algorithms that encode the expected shape of these structures. A primary surface is then initialized for each hemisphere by tiling the outside of the WM mass for that hemisphere. This initial surface is then refined to track the intensity gradients between the white and gray matter. This refined WM surface (white surface) is then nudged to follow the intensity gradients between the gray matter and CSF, generating the pial surface. The white and pial surfaces overlaid on the original T1-weighed image are shown in Figure 10. Atlas labelling is achieved following essentially the same procedure as with subcortical segmentation, but mapping the training set labels to an spherical space and using the curvature in each of the principal directions at a particular vertex instead of signal intensity.

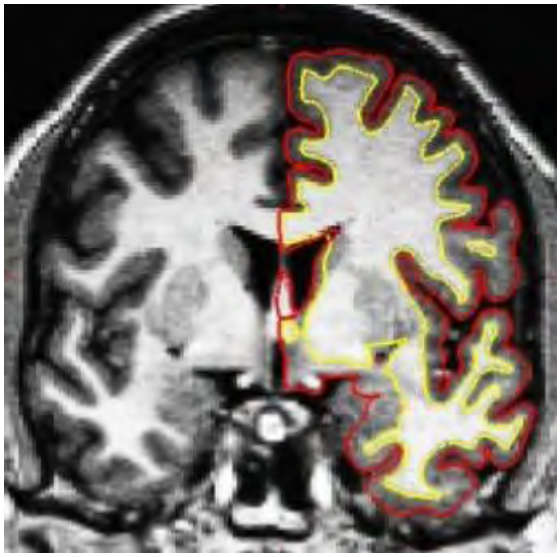

Figure 10 - Overlaid of both white and pial surfaces, generated by Freesurfer.

3.5.1.2 SPM12

SPM12 is the latest version of a software package (SPM) that has been designed for the analysis of brain imaging data sequences. The sequences can be a series of images from different cohorts, or time-series from the same subject. The present release is appropriate for the analysis of MRI and PET, among other techniques. SPM12 offers an almost unlimited variety of possibilities for the analysis of brain imaging data thanks to multiple available toolboxes. The T1 MRI analysis conducted with SPM12 in this thesis is restricted to the computation of the total intracranial volume, a variable commonly used to adjust for the confounding effect of differing head sizes. To this aim, we used the SPM12 tool "Tissue Volumes" [128]. Briefly, CSF, gray, and white matter probability are first generated by warping the T1 scan to analogous sets of tissue probability maps obtained after averaging segmentation of the IXI dataset http://www.brain-development.org/. These priors are used to define a total intracranial volume mask in standard space, and the total intracranial volume is then calculated by computing the totals of the modulated warped segmentations within this mask. This approach can potentially better model finer spatial detail than the regularized spatial registration. Moreover, this method showed to be more accurate than the FreeSurfer estimate when compared to manual segmentations [128].

3.5.2 FLAIR analysis

WMH volume were automatically calculated using the Lesion Segmentation Toolbox [129] of SPM12. This package determines the three tissue classes of gray matter, WM, and CSF from the T1-weighted scan, as done in the calculation of total intracranial volume. Then, the FLAIR intensity signal distribution from each tissue class is analyzed to detect extreme values, which are regarded as lesion beliefs. Next, conservative lesion beliefs are expanded toward liberal lesion beliefs by analyzing neighboring voxels and assigning them to lesions under specified criteria. This iterative process stops when no further voxels are assigned to lesions. Finally, the likelihood of belonging to WM or gray matter is weighted against the likelihood of belonging to lesions, yielding to lesion probability maps. Figure 2 C) shows an example of a segmentation of this toolbox.

3.5.3 Amyloid PET Analysis

Amyloid PET analysis was carried out using the FreeSurfer routine PETSurfer [130]. This pipeline allows, among other utilities, the quantification of mean regional uptake in both the aforementioned subcortical and cortical regions of interest derived from the FreeSurfer parcellation of the T1 scan. Also, this tool performs several types of partial volume corrections for PET data. For this thesis, we used the method known as Symmetric Geometric Transfer Matrix method [131]. Briefly, this model assumes that the observed PET signal in a voxel can be expressed as a linear combination of the true signals of all the regions of the brain:

$$y = X\beta$$

Where y is a vector with length equal to the number of voxels, X is a matrix of coefficients dependent on the scanner point-spread function and the anatomy, and β is the true signal we want to estimate. Thus, we only need to compute the matrix X and invert the linear system of equations.

The design matrix X was computed as follows. For each region of interest (ROI), an image was created in the PET space where the value in a voxel was the tissue fraction, as determined with a high-resolution MRI segmentation provided by Freesurfer [130], for that ROI in that voxel. This effectively accounts for the tissue fraction effect. The resulting image is sparse, so it is then smoothed by the point spread function of the scanner. The result, commonly known as the regional spread function, was then reshaped into a vector that becomes the column in X for that ROI. This was repeated for each ROI until X is fully defined.

3.6 ETHICAL ASPECTS AND INFORMED CONSENTS

All the data used in this thesis has been obtained from the Alzheimer's Disease Neuroimaging Initiative (ADNI), which provides anonymized study data for qualified researchers. All subjects had to provide informed consent as compatible with the local participating institutions (Institutional Review Board regulations) in ADNI. All the participants provided written allowing for public dissemination of their anonymized data. Therefore, no further approval of our Institutional Review Board is required for the analyses carried out in this thesis.

RESULTS

4 RESULTS

4.1 ASSOCIATION OF WHITE MATTER HYPERINTENSITIES WITH SUBTHRESHOLD AMYLOID ACCUMULATION

WMH, assessed with FLAIR MRI, are common radiological findings in the aging brain [132]. Although initially believed to be exclusively associated to small vessel cerebrovascular disease, an increasing body of literature suggests that the emergence of WMH is also secondary to AD pathologic changes [74,104,133-135]. In this regard, WMH were found to be associated with tau burden and neurodegeneration [87,136] in AD, being Wallerian degeneration [88] the most likely mechanism for this WM disruption. However, evidence from the Dominantly Inherited Alzheimer Network indicate that WMH in posterior areas of the brain emerge in tandem with changes in CSF Aβ-42 and p-tau levels [76], suggesting that WMH are one of the earliest pathological features of AD and challenging the Wallerian degeneration hypothesis. These findings were supported by a recent report showing that parietal and frontal WMH were associated with amyloid, but not with tau, among cognitively unimpaired elderly [82]. Similar findings were reported in [83]. It is not clear, however, whether amyloid-related WMH become detectable before amyloid does in a PET scan. If so, WMH might potentially help to identify amyloid "accumulators" with subclinical levels of pathology, who might be the optimal candidates for anti-amyloid therapies [137].

In the present study, we aimed at investigating whether measurable WMH precede PET-detectable amyloid deposition. For this, we studied the associations between baseline global and regional patterns of WMH and amyloid accumulation over time in cognitively normal participants with low baseline amyloid in ADNI.

4.1.1 Specific Methods

4.1.1.1 Study Design:

Data were downloaded from the LONI website in February 2019. Only ADNIGO-2 participants who were CN at baseline and underwent concurrent baseline T1-weighted, FLAIR, and amyloid (Florbetapir) PET scans were considered for this study. These participants were further classified into high or low amyloid burden using a prespecified cut-point for the Florbetapir PET SUVR in a cortical summary ROI normalized to whole cerebellum (SUVR = 1.11) [58]. This information was made publicly available by the ADNI PET core in http://adni.loni.usc.edu/data-samples/access-data/. For the purpose of this study, only participants with low amyloid burden (SUVR < 1.11, n = 190) were included. Detailed information about the eligibility criteria for the different diagnostic cohorts and imaging protocols can be found at http://adni.loni.usc.edu/methods/documents/.

4.1.1.2 Standard protocol approvals, registrations, and patient consents:

All participants provided written informed consent approved by the institutional review board of each ADNI participating institution.

4.1.1.3 Magnetic Resonance Imaging:

MRI was performed at 3T to obtain T1-weighted and FLAIR sequences. T1 scans were preprocessed by the ADNI MRI core to correct for image distortion, B1 non-uniformity, and residual inhomogeneity, as described previously [138]. FLAIR scans were obtained with a spatial resolution of 0.86 × 0.86 × 5 mm^3. Additional details of all MRI T1-weighted and FLAIR images can be found at http://adni.loni.usc.edu/methods/documents/mri-protocols/.

4.1.1.4 Amyloid PET

Florbetapir scans were acquired with a dynamic protocol of 4 frames of 5 minutes obtained at 50-70 minutes after injection. Frames were realigned, averaged, resliced to a common grid (1.5 mm^3), and smoothed to a resolution of 8 mm^3, corresponding to the lowest scanner resolution in ADNI. Follow-up amyloid PET scans were acquired at approximately 2-year intervals.

4.1.1.5 Image Analysis

4.1.1.5.1 MRI processing

Preprocessed T1 images were parcellated with FreeSurfer (v6.0) to derive cortical regions of interest for PET quantification. We inspected the resulting segmentations to ensure that no gross errors occurred. No further manual corrections of the parcellations were required.

Binary WMH maps were obtained using the Lesion Segmentation Toolbox (LST) in SPM12 [129,139] using a kappa value of 0.25 and a probability threshold of 1, as previously used with ADNI data [140]. We visually inspected and manually edited the WMH maps to remove non-WM voxels labelled as WMH (n = 25).

In order to measure WMH burden in WM lobes, we first filled lesions in the T1 scan using the LST toolbox [129,139] to avoid incorrect segmentations of WMH as CSF or grey matter. Then, filled T1 scans were spatially normalized using SPM12 'Normalize'. Using the inverse of this transformation, we brought back the Hammersmith atlas [141] to patient space and merged the regions that constitute the frontal, temporal, parietal, and occipital lobes in this atlas. Since WMH maps are by default generated in coregistration with T1 images, WMH voxels lying in these lobar regions were used to compute lobar WMH volumes. WMH volumes were normalized to total intracranial volume (TIV), as estimated with SPM12 by the 'Tissue Volumes' tool [128,142].

To conduct WMH voxel-wise analyses, we used the previously derived deformation field to normalize WMH maps with nearest neighbor interpolation and voxel size 1.5 × 1.5 × 1.5 mm^3. Binary normalized maps were then smoothed using an isotropic 8 mm gaussian filter and re-binarized so that only voxels with a probability > 0.15 of being WMH at this resolution were labelled as WMH.

4.1.1.5.2 Amyloid PET processing

Preprocessed Florbetapir images were coregistered to the FreeSurfer-parcellated T1 image that was closest in time using FreeSurfer's function mri_coreg. Results were visually inspected to ensure a correct coregistration. In a few cases, manual reorientation prior to run mri_coreg was necessary to achieve a correct registration. Coregistered images were corrected by partial volume effects (PVE) using the Symmetric Geometric Transfer Matrix

(SGTM) method [143] as implemented in PETSurfer [144]. Briefly, this pipeline creates a high-resolution segmentation of the T1 scan which, apart from the cortical and subcortical structures, also includes segmentations of the WM lobes, different CSF compartments, and extracerebral tissue. This segmentation is then used to account for the tissue fraction effect and to extract mean PET uptake values over these regions of interest. Finally, a linear system is solved to correct for spill-in and spill-out counts, yielding the PVE-corrected uptake values. A point spread function (PSF) of 8 mm was assumed for all the PET images, as previously done with ADNI data [145]. Since this study is focused on amyloid accumulation over time in low baseline amyloid participants, PVE correction is essential to avoid the confounding effect of spill-in counts from the WM, whose effect is more severe for higher contrasts between grey and WM [146-147]. Furthermore, SGTM was previously found to improve longitudinal amyloid PET measurements [145].

PVE-corrected global amyloid burden was calculated using the SUVR in the ADNI cortical summary region [58] normalized by the cerebellar grey matter. We did not use WM reference regions because of their reported associations with WM abnormalities potentially associated with AD [148-149]. Throughout this study, only cerebellar grey matter reference regions were used.

4.1.1.6 Statistical Analysis

Cross-sectional associations between baseline normalized WMH volumes (independent variable) and cortical SUVR (dependent variable) were assessed using linear regression, after covariate adjustment by age, sex, and APOE carriage. Linear Mixed models with subject-specific intercepts and time slopes were fitted to investigate whether baseline WMH were associated with longitudinal change in amyloid burden. We conducted these analyses for both the longitudinal SUVR in the ADNI cortical aggregate [58] as well as for each of the 19 ROIs (left and right averaged) that comprise this cortical aggregate. The models included age, sex, APOE status, baseline (cortical or regional) SUVR, and baseline normalized WMH volume, as well as their interaction with continuous time. Inspection of model residuals, QQ plots, and fitted vs residuals plots ascertained that no non-linear transformation of the variables was required.

To study the spatial WMH patterns associated with amyloid accrual, we performed similar mixed models at the WMH voxel level, replacing baseline normalized WMH volume by a binary variable indicating whether that voxel is a WMH (1) or normal appearing WM (0) in the normalized and smoothed WMH maps (Section 4.2.5.1). Only voxels with WMH in at least 6 participants (minimum number required to run the models) and with a probability of being WM > 0.90 were considered for the analysis.

A False Discovery Rate (FDR) [150] correction of $\alpha = 0.05$ was used to correct both the ROI and voxel-based analyses by multiple comparisons. As a sensitivity analysis, key findings were replicated using a more restrictive cut-point for amyloid negativity (5% lower, PVE uncorrected SUVR = 1.05). All the analyses were carried out in MATLAB 2017a.

4.1.2 Findings

4.1.2.1 Cohort Characteristics

Demographics of the subjects included in this study are shown in Table 1.

Table 1 - Demographics and imaging characteristics of the study participants. Results are displayed as mean (SD) for age and baseline cortical SUVR, and as median (range) for baseline white matter hyperintensity volume. Cortical SUVR change was estimated using both fixed and random effects of a linear mixed model with time as the only fixed effect and random intercepts and slopes per subject. Abbreviations: SUVR: Standardized uptake value ratio.

	(n = 190)
Age, years	73.1 (6.3)
Females (%)	46.8
APOE ε4 carriers (%)	20.0
Baseline white matter hyperintensity volume, cm^3	
Global	1.4 (0 to 41.4)
Frontal	0.6 (0 to 28.8)
Parietal	0.12 (0 to 21.8)
Occipital	0.10 (0 to 3.3)
Temporal	0.02 (0 to 2.7)
Baseline cortical SUVR	0.92 (0.13)
Cortical SUVR change, SUVR/year	0.022 (0.003)
Number of participants with follow-up amyloid PET scans	
N = 0	31
N = 1	43
N = 2	66
N = 3	48
N = 4	2

One hundred fifty-nine participants had at least one follow-up amyloid PET scan. Median amyloid PET follow-up was 4.4 years, range 1 to 8 years. The rate of cortical SUVR annual change, estimated as the fixed effect of a mixed model with time as the only fixed effect, was higher with PVE correction (0.022, 95% CI: 0.016 to 0.028, 2.4% compared to PVE corrected mean baseline cortical SUVR) than without (0.006, 95% CI: 0.003 to 0.009, 0.5% compared to PVE uncorrected mean baseline cortical SUVR). Accumulation trajectories are depicted in Figure 11.

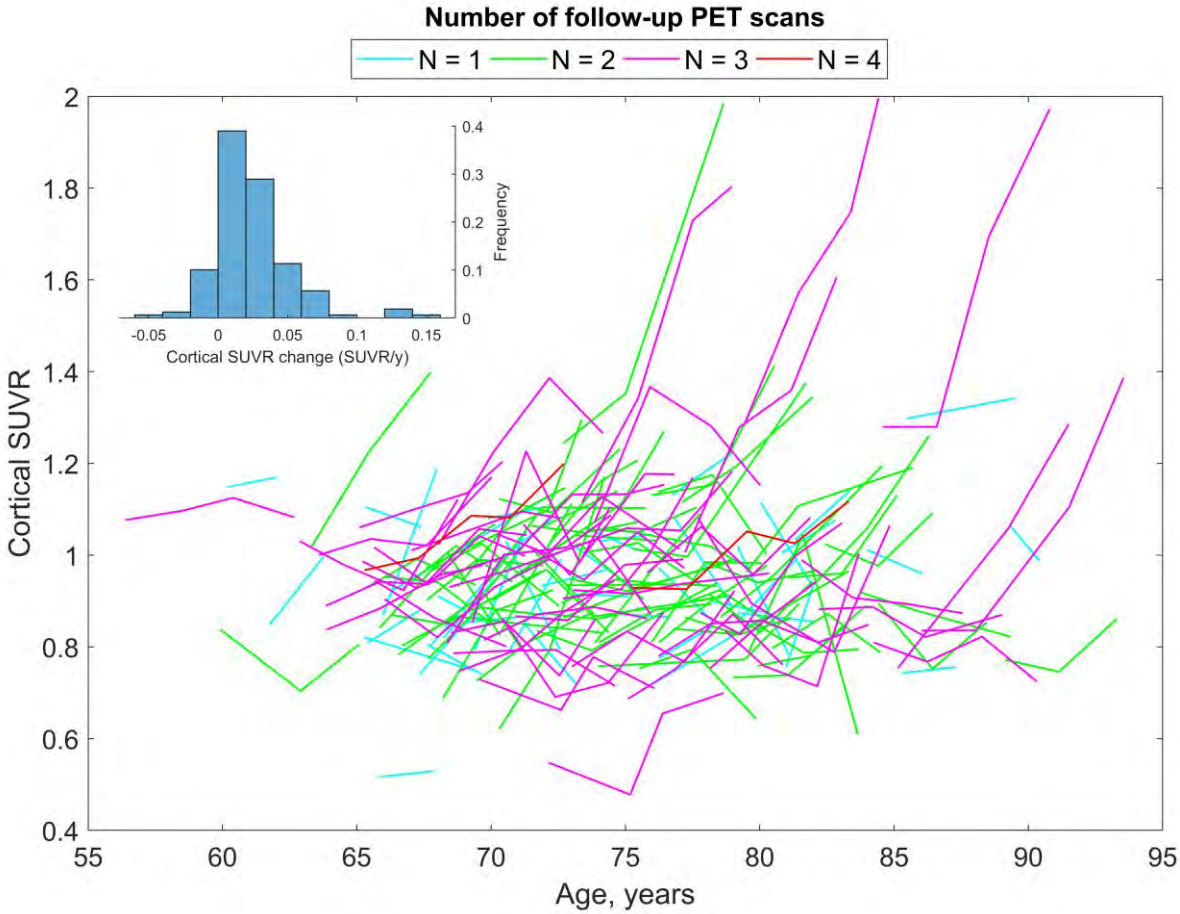

Figure 11 - Longitudinal trajectories of amyloid accumulation, as a function of age. The different colors are used to represent the number of follow-up amyloid PET scans. The embedded histogram represents annual rates of cortical SUVR change, as estimated using both fixed and random effects of a linear mixed model with time as the only fixed effect and random intercepts and slopes per subject. Abbreviations: SUVR: Standardized Uptake Value Ratio.

4.1.2.2 Baseline WMH predict amyloid accumulation

First, we studied the cross-sectional association between baseline cortical SUVR and baseline normalized WMH by running separate linear regressions for both global and each regional WMH, adjusting by age, sex, and APOE. Although all the WMH coefficients were positively associated with baseline cortical SUVR, none of them reached statistical significance (Global WMH: $\beta = 0.13$, $p = 0.08$; Frontal WMH: $\beta = 0.24$, $p = 0.07$; Parietal WMH: $\beta = 0.23$, $p = 0.23$; Temporal WMH: $\beta = 0.92$, $p = 0.44$; Occipital WMH: $\beta = 0.69$, $p = 0.47$). Of note, males showed higher cortical SUVR ($\beta = 0.62$, $p < 0.001$ in a model with age, sex, and APOE as predictors).

In the longitudinal analysis, we assessed whether WMH were predictive of amyloid accumulation over time. The results of the mixed models are summarized in Table 2.

Table 2 - Linear mixed model results for the association between baseline WMH normalized volumes and **amyloid accumulation over time. Results are expressed as standardized ß's of the time interaction** coefficient of WMH and baseline SUVR. Model 1 included only adjustment by baseline cortical SUVR (SUVR ~ time*(baseline_SUVR + WMH) + (time|rid) in Wilkinson notation), while Model 2a included age, sex, and APOE as well (SUVR ~ time*(baseline_SUVR + WMH + age + sex + APOE) + (time|rid)). Model 2b was the same as 2a but was fitted in the subset of participants who were amyloid negative with the more restrictive cut-point of PVE uncorrected SUVR = 1.05, in order to perform a sensitivity analysis. Abbreviations: WMH: White matter hyperintensities; SUVR: Standardized uptake value ratio.

	Model 1		Model 2[a]		Model 2[b]	
WMH predictor	ß (95% CI)	*p* value	ß (95% CI)	*p* value	ß (95% CI)	*p* value
Global						
Global WMH × time	0.19 (0.09 to 0.29)	< 0.001	0.15 (0.04 to 0.26)	0.006	0.19 (0.09 to 0.28)	< 0.001
Baseline SUVR × time	0.10 (0.04 to 0.16)	0.002	0.12 (0.05 to 0.18)	< 0.001	0.03 (-0.04 to 0.10)	0.40
Frontal						
Frontal WMH × time	0.17 (0.08 to 0.26)	< 0.001	0.13 (0.04 to 0.23)	0.006	0.14 (0.05 to 0.22)	0.001
Baseline SUVR × time	0.11 (0.05 to 0.17)	< 0.001	0.12 (0.06 to 0.19)	< 0.001	0.03 (-0.05 to 0.10)	0.48
Parietal						
Parietal WMH × time	0.23 (0.10 to 0.37)	< 0.001	0.20 (0.07 to 0.33)	0.003	0.24 (0.10 to 0.37)	< 0.001
Baseline SUVR × time	0.08 (0.02 to 0.14)	0.01	0.11 (0.04 to 0.17)	0.001	0.03 (-0.04 to 0.10)	0.40
Occipital						
Occipital WMH × time	0.03 (-0.06 to 0.11)	0.54	-0.004 (-0.08 to 0.07)	0.92	0.01(-0.07 to 0.09)	0.78
Baseline SUVR × time	0.10 (0.03 to 0.17)	0.003	0.12 (0.06 to 0.19)	< 0.001	0.04 (-0.04 to 0.11)	0.36
Temporal						
Temporal WMH × time	0.008 (-0.09 to 0.10)	0.88	-0.03 (-0.13 to 0.06)	0.49	0.08 (-0.05 to 0.22)	0.21
Baseline SUVR × time	0.10 (0.03 to 0.17)	0.003	0.13 (0.06 to 0.19)	< 0.001	0.04 (-0.04 to 0.11)	0.32

Apart from the significant effect of baseline cortical SUVR, higher global, frontal, and parietal WMH burden was significantly associated with faster rates of global amyloid accumulation, with and without adjustment by demographic covariates (Table 2, Model 1 and 2a). These significant relationships can be further visualized in Figure 12. Remarkably, after repeating the adjusted analysis with a more restrictive cut-point (n = 120), the association with baseline cortical SUVR disappeared but the association with WMH remained almost unchanged (Table 2, Model 2b).

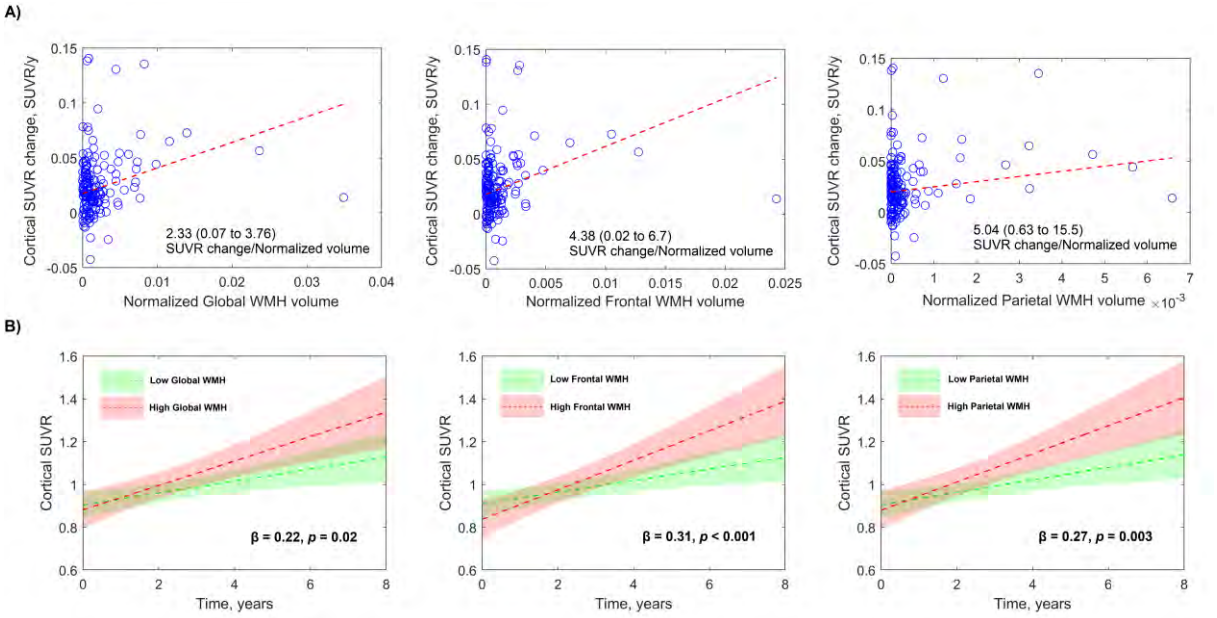

Figure 12 - A) Relationship between change in cortical SUVR and baseline WMH. Change in cortical SUVR was estimated using both fixed and random effects of a linear mixed model with time and baseline SUVR as fixed effects, and random intercepts and slopes per subject. Dashed lines represent robust bisquare linear regression fits. 95% CI for the slopes of these fits were computed using 5000-iteration bootstrap. B) Amyloid accumulation trajectories over time for subjects with high and low WMH burden. High (Low) WMH burden participants were defined as those above (below) the 85th percentile normalized WMH volume. Trajectories were estimated with linear mixed models adjusted by age, sex, APOE, and baseline SUVR, evaluated for a 75-year-**old male without APOE ε4 allele and at mean covariate values.**

4.1.2.3 Spatial patterns of WMH associated to amyloid accumulation

Here, we aimed at looking with better detail the WMH spatial patterns related to amyloid accumulation. We conducted linear mixed models at the WMH voxel level, as detailed in Sections 4.1.2.5.1 and 4.1.2.6, adjusted by age, sex, and APOE. Figure 13 shows both the frequency of WMH lesions (Figure 3 A)) and the spatial pattern of WMH associated with amyloid accumulation (Figure 3 B)). These WMH clusters spanned parietal and frontal lobes, confirming the analyses at the ROI level. Compared to the areas of maximum WMH frequency (Figure 3 A)), amyloid accumulation related-WMH displayed a more superior pattern of accumulation in frontal and parietal lobes (Figure 3 B), top row).

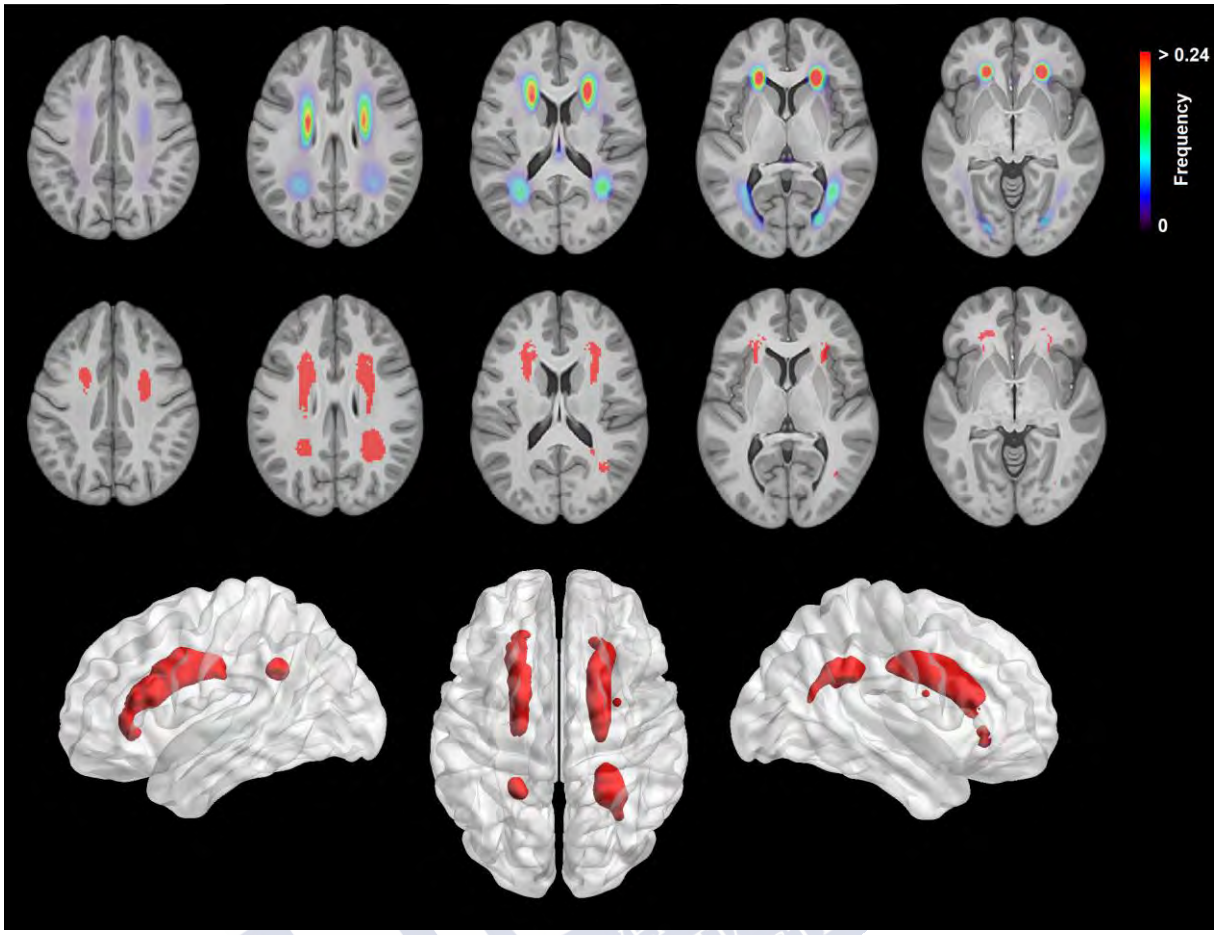

Figure 13 - Top Row: Spatial frequency of WMH in the study participants. Middle Row: Spatial distribution of WMH (in red) associated with faster amyloid accumulation, for the same axial slices as on top row. Bottom Row: 3D rendering of the spatial WMH pattern (in red) of middle row. WMH maps associated with amyloid accumulation were obtained using linear mixed models at the WMH-voxel level. Because for a significant proportion of voxels data was not enough to estimate random slopes, the model included only a random intercept per subject.

4.1.2.4 Regional distribution of WMH-related amyloid accumulation

Here, we explored which cortical areas within the ADNI cortical aggregate [58] drive the previously observed faster accumulation. For this, we fit separate linear mixed models with for each regional SUVR (response variable) and each of the previously found significant regional WMH (global, frontal, and parietal, independent variable) adjusted by baseline regional SUVR and demographics as described in Section 4.1.2.6. Figure 14 shows the cortical areas in which a faster accumulation was significantly associated with higher WMH burden. Global and parietal WMH displayed a similar pattern of accumulation, involving mainly frontal, parietal, and, to a lesser extent, cingulate areas. Fewer regions survived multiple comparisons correction for frontal WMH, that also involve frontal, parietal, and cingulate regions. Figure 15 shows the effect size of each WMH predictor on each cortical ROI.

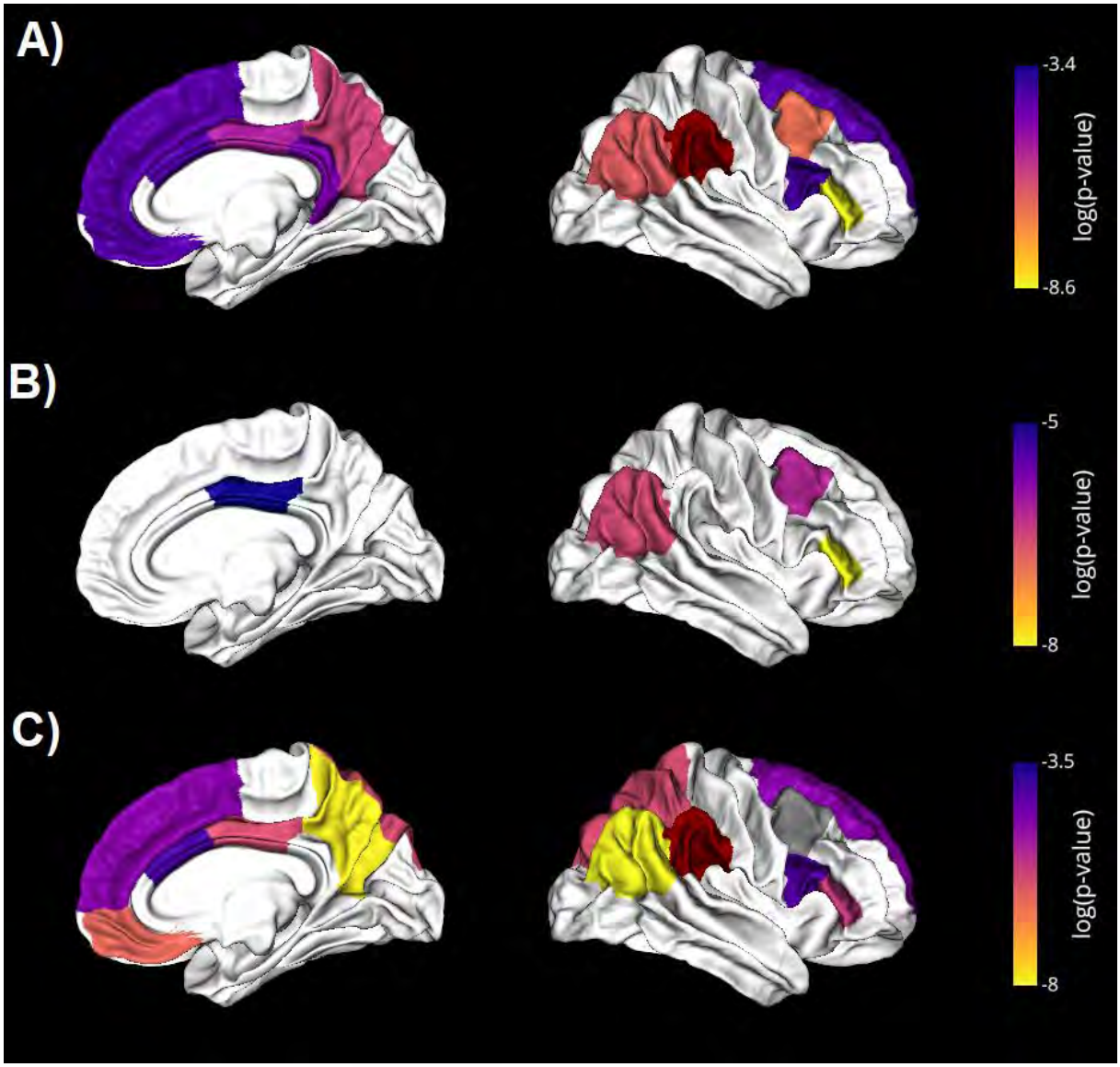

Figure 14 - Cortical regions in which amyloid accumulation is significantly (after FDR correction) associated to higher A) global WMH, B) frontal WMH, and C) parietal WMH. Linear mixed models with regional cortical SUVR as response variable, adjusted by demographics and baseline SUVR, were used. p-values (uncorrected) are expressed as natural log(p-value). Regions: A) Pars Triangularis, Caudal Middle Frontal, Inferior Parietal, Precuneus, Posterior Cingulate, Isthmus Cingulate, Superior Frontal, Medial Orbitofrontal, Caudal Anterior Cingulate, Pars Opercularis, Supramarginal. B) Pars Triangularis, Inferior Parietal, Caudal Middle Frontal, Posterior Cingulate. C) Caudal Middle Frontal, Inferior Parietal, Precuneus, Medial Orbitofrontal, Posterior Cingulate, Superior Parietal, Pars Triangularis, Superior Frontal, Pars Opercularis, Caudal Anterior Cingulate, Supramarginal.

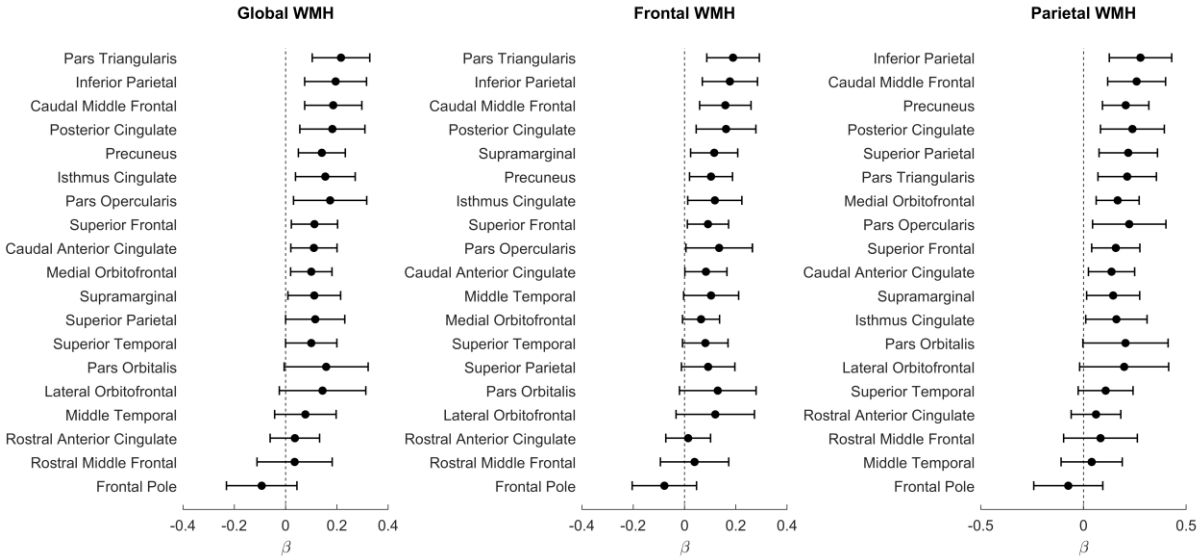

Figure 15 - Effect size (standardized ß) of each WMH predictor on each of the 19 regions comprising the **cortical aggregate used in this study. Standardized ß's represent the number of** SD that vary in the SUVR of each region of interest with 1 SD variation in WMH, per year. Abbreviations: WMH: White matter hyperintensities.

4.1.3 Discussion

The present study investigated whether WM lesions, assessed as WMH with FLAIR MRI, were associated with faster rates of amyloid accumulation, as measured with amyloid PET, among cognitively normal elderly with low baseline cortical amyloid. Our findings suggest that a characteristic spatial pattern of WMH, spanning superior areas of the frontal and parietal lobes, is predictive of future amyloid accrual, independently of continuous levels of subthreshold cortical pathology. This accumulation occurred in cortical regions previously identified as regions of early accumulation in AD [59,151-153], suggesting that the observed faster accumulation is not driven by processes other than early AD pathology. To the best of our knowledge, this is the first study in which an imaging biomarker is identified as a predictor of amyloid accumulation in amyloid-negative cognitively normal individuals.

Our findings are consistent with prior reports analyzing simultaneously the role of amyloid and tau in the emergence of WM lesions. The tau-independent relationship between WMH and amyloid, particularly with parietal WMH, was found in cross-sectional studies of asymptomatic familial AD [76] and in two recent reports in cognitively unimpaired elderly [82-83]. Here, we add to these previous findings by observing that a similar pattern of WMH is detectable at subclinical levels of amyloid pathology, partially supporting the hypothesis that WM lesions are secondary to amyloid deposition. Although the link between early amyloid deposition and WM damage is still not clear, several potential mechanisms such as oligodendrocyte disfunction and demyelination induced by amyloid oligomers [103], as well as axonal degeneration secondary to amyloid-related microglial activation [84,155], might explain this relationship. However, the findings of the present study do not exclude the possibility that the observed WMH patterns had a vascular disease etiology, with a causal or interactive link between cerebrovascular pathology and amyloid deposition, as suggested in a previous study [85]. More neuropathological and imaging studies are warranted to fully understand the relationship between early amyloid accumulation, WM disease, and vascular pathology.

The relationship between amyloid and WMH burden in preclinical AD has been explored before, but findings were often conflicting. Apart from the three large studies mentioned above that controlled for the influence of tau [76,82-83], other previous smaller studies have investigated how WMH relate to amyloid using both amyloid PET and CSF. Apparently, the rate of positive findings is significantly higher in CSF studies than when using amyloid PET. According to a review paper [156], only 2 out of 13 studies reported a positive correlation between amyloid and WMH burden, in contrast to the multiple CSF studies that found a positive association [157-161]. Potential explanations include the non-regional assessment of WMH, small sample sizes, the higher sensitivity of CSF to early amyloid pathology [162], and the fact that, as we have shown, amyloid-related WMH might be elevated at subthreshold levels. In this regard, our results also emphasize the need of redefining current amyloid PET cut-points to capture early amyloid pathology, as other studies have pointed out [59].

Apart from WMH measured with FLAIR, other studies using diffusion tensor imaging (DTI) in WM reported changes associated with amyloid burden on different DTI metrics [163]. As with WMH, results are conflicting [163-164], probably for the reasons previously discussed. Particularly interesting is a study in which a DTI measure of myelin integrity was found to be related to levels of CSF Aβ-42 [104], supporting the hypothesis of amyloid-related oligodendrocyte disfunction. Future studies will assess how white matter integrity and myelin relate with longitudinal amyloid accumulation in amyloid-negative elderly.

The fact that a regional distribution of WMH might be predictive of amyloid deposition among amyloid-negative elderly has important implications for anti-amyloid clinical trials, since the majority of efforts shift now towards the prevention of amyloid pathology, even in subjects on the AD pathway but with very mild amyloid burden, the so-called amyloid "accumulators" [137]. Recent evidence suggests that "accumulators" experience faster rates of cognitive decline [165-166] and disrupted brain connectivity [151], highlighting the clinical relevance of early amyloid accumulation. Beyond the scope of this study is the relative importance of WMH and amyloid accumulation in cognitive decline among these participants, which might be informative for the identification of novel therapeutic targets on WM. Further studies with longer follow-up times are needed to assess how useful are these WMH patterns to identify "accumulators" and to predict clinically relevant outcomes.

This study has several strengths. First, our cohort of cognitively normal elderly with low baseline amyloid was relatively large. Second, the number of repeated amyloid PET scans, with most of the participants having 2 or more follow-up scans, and the length of the follow-up, with a median time of 4.4 years and examinations up to 8 years. Third, the use of partial volume correction, which improved the sensitivity to detect changes without the use of WM reference regions, whose uptake varies with WM pathology [148-149]. This work also had some limitations: 1) ADNI inclusion criteria requires participants relatively free of cerebrovascular pathology and therefore WMH burden, which might compromise the generalizability of our findings in a community cohort. However, similar WMH patterns to those found in this study were also detected in the community cohort of the Mayo Clinic Study of Aging [82], suggesting that despite confounding pathology the patterns may be detectable. 2) We could not assess how the longitudinal change in WMH relate to amyloid accumulation since the FLAIR protocol changed at the end of ADNI2, from 2D axial FLAIR to high-resolution 3D FLAIR. Without a harmonization method, mixing these two protocols, particularly in a longitudinal study, might lead to incorrect inferences. 3) The prespecified cut-point we used to select amyloid-negative participants was derived without PVE correction and might be too high [59], which might lead to an important number of false amyloid-

negative individuals. However, the sensitivity analyses we conducted and the adjustment by baseline uptake levels suggests that our findings are robust against these limitations.

In conclusion, we provided further evidence supporting WMH as one of the earliest pathological features in AD progression. A specific spatial pattern of WMH was found to be predictive of future amyloid accumulation among cognitively normal older individuals with no evidence of amyloid pathology in amyloid PET. The spatial assessment of WMH may potentially allow the identification of subjects with amyloid burden levels beyond PET detectability limits.

4.2 ASSOCIATION BETWEEN AMYLOID PET TRACER UPTAKE IN WHITE MATTER AND ALZHEIMER DISEASE PROGRESSION

Over the past decades, AD has been conceptualized as a grey matter pathology defined by the abnormal accumulation of neuritic plaques and neurofibrillary tangles [17]. Nevertheless, accumulating evidence suggests that WM abnormalities may play an important role in the pathogenesis and progression of AD [74,76,102-103,132,167-170], although the putative effects with AD pathological hallmarks, particularly amyloid, remain unclear [156,164,171]. The fact that both normal aging and vascular disease independently contribute to WM lesion burden [172] complicates the measurement of AD-related WM changes in the elderly, exposing the need for novel, more specific, markers of WM degeneration.

Supported by recent investigations in Multiple Sclerosis, amyloid PET imaging has been postulated as a potential marker of WM degeneration [94,96-97,99-100,173]. Although the binding mechanism is not fully understood, it has been suggested that amyloid tracers might bind to the beta-sheet structure of the myelin protein, thus reflecting myelin integrity [53] even in normal appearing WM [98, 148]. Despite the aforementioned evidence, the association of demyelination reflected by amyloid PET with AD progression has yet to be investigated.

In this study, we hypothesized that low amyloid PET uptake in the WM reflects demyelination and that this pathologic change is associated with AD progression. To test our hypotheses, we examined the associations of Florbetapir uptake in cerebral WM with AD biomarkers and cognition, as well as with their longitudinal change. Additionally, we also explored the associations of brainstem uptake with the aforementioned AD markers to explore whether WM pathology extends to regions far from the cerebral cortex.

4.2.1 Specific Methods

4.2.1.1 Study Design:

Only ADNI participants who underwent concurrent clinical, MRI T1-weighted and FLAIR, amyloid PET, and CSF examinations were considered in this study. ADNI diagnostic cohorts included CN, MCI, and mild AD dementia subjects aged 55 to 95. Detailed information about the eligibility criteria for the different diagnostic cohorts can be found at http://adni.loni.usc.edu/methods/documents/.

4.2.1.2 Standard protocol approvals, registrations, and patient consents:

All participants provided written informed consent approved by the institutional review board of each ADNI participating institution.

4.2.1.3 MRI:

All subjects were scanned in 3T devices and had T1-weighted and FLAIR sequences. Quality-controlled Freesurfer [126] volumetric measurements of the hippocampus were made publicly available by researchers at the University of California, San Francisco (UCSF). UCSF researchers also provided FLAIR-derived volumetric measurements of total WMH burden. All the participants are scheduled to undergo at least one annual MRI follow-up visit. Further details can be found at http://adni.loni.usc.edu/data-samples/access-data/.

4.2.1.4 Amyloid PET

18F-Florbetapir PET scans were acquired 50 to 70 minutes post-injection and post-processed following the ADNI pipeline (http://adni.loni.usc.edu/methods/pet-analysis-method/pet-analysis/). Regional quantification of Florbetapir uptake was performed by investigators at the University of California, Berkeley. Cortical amyloid status (A+ or A-) was determined using the ADNI cortical aggregate [58] and a previously published cut-point of SUVR = 1.11 using the whole cerebellum as the reference region [174]. For the analyses carried out here, we used the SUVR normalized to cerebellar grey matter of the ADNI cortical aggregate. To evaluate Florbetapir uptake in cerebral WM, we used the SUVR normalized to cerebellar grey matter in an ADNI-defined volume of interest encoded as eroded WM (ErWM) [175], in which border regions were removed to avoid partial volume effects. In addition to the ErWM, we also evaluated the SUVR in the brainstem (again, normalized to cerebellar grey matter). To exclude any potential partial volume effect due to the size of the brainstem, a partial volume corrected version of all the analyses involving the brainstem was provided in Appendix 1.

4.2.1.5 CSF:

CSF levels of Aβ1-42 (Aβ-42) and phosphorylated tau181 (p-tau) were provided by the Center of Neurodegenerative Disease Research, University of Pennsylvania, for ADNI. We downloaded the measurements from the fully automated Roche Elecsys electrochemiluminescence immunoassay batch. Aβ-42 levels above precision limits (1700 pg/cc) were estimated using extrapolation and included in all the analyses. Total tau was not included due to its high correlation with p-tau, leading to almost identical results. A detailed description of the CSF procedures can be found at http://adni.loni.usc.edu/methods/.

4.2.1.6 Clinical assessments:

Global cognitive performance was assessed with the MMSE at baseline and with the Alzheimer's Disease Assessment Scale—Cognitive 13-Item (ADAS-Cog-13) [176] and the Clinical Dementia Rating—Sum of Boxes (CDR-SB) [123] at baseline and in subsequent follow-up visits. Changes in clinical diagnosis at follow-up were determined by a consensus Committee. All the participants are scheduled to undergo annual follow-up cognitive evaluations. Further details can be found at http://adni.loni.usc.edu/methods/.

4.2.1.7 Cut-point definition for ErWM and brainstem SUVRs

In order to operationalize the use of the ErWM and brainstem uptake as biomarkers, we defined binary categories of Normal/Abnormal WM or brainstem. Cut-points were established using the 10th percentile (90% sensitivity) of the distribution of the cortical SUVR-adjusted ErWM or brainstem SUVRs among A+ AD dementia patients [177]. To adjust by cortical SUVR, we fitted a linear regression between Eroded WM or brainstem SUVR, and cortical SUVR in A+ AD patients. Adjusted measures were obtained by subtracting ErWM or brainstem SUVR to the outputs of the linear regression. We adjusted by cortical SUVR because of its known positive correlation with WM uptake [178]. This approach was only operationalized in A+ subjects due to the low number of A- AD dementia participants.

4.2.1.8 Statistical Analysis

Kruskal-Wallis tests were used to evaluate differences in demographic continuous variables among the different diagnostic cohorts and amyloid status. Binary variables were compared using the $\chi 2$ test. Correlations were assessed using age-adjusted partial correlations.

To evaluate how demographic factors, cortical SUVR, and WMH influence ErWM and brainstem SUVRs, we fit separate general linear models for the latter variables (ErWM and brainstem SUVRs), inputted as continuous dependent variables, while the former factors are included as independent predictors.

Linear models were also fit for each diagnostic cohort and amyloid status (A- and A+) to evaluate cross-sectional associations of ErWM and brainstem SUVRs with CSF biomarkers, hippocampal volume, and cognition. Here, AD biomarkers and cognition act as dependent variables, while ErWM and brainstem SUVRs are inputted as continuous independent predictors in separate models. We adjusted by demographic factors, cortical SUVR, and WMH (and baseline MMSE and years of education for cognition). We included cortical SUVR and WMH as covariates because of their potential associations with AD progression [73,178-180] and WM SUVR [148-149]. CSF levels were log-transformed to reduce skewness of residuals. A- AD dementia was not evaluated due to the low number of subjects (13).

To evaluate the associations between baseline ErWM and brainstem SUVRs, and subsequent disease progression, we fitted separate linear-mixed effects models with a subject-specific random intercept. All the models were adjusted by the same factors used in the cross-sectional analysis, as well as by their interaction with time.

We explored a potential interaction effect with amyloid by merging A- and A+ subjects for each diagnostic cohort and evaluating a Cortical SUVR×ErWM SUVR or a Cortical SUVR×brainstem SUVR (and interaction with time in linear mixed models) interaction term for all the above linear models.

Cox regression, adjusted by the same covariates included in cognition models, was used to test the relation between ErWM and brainstem SUVRs with risk of progression from MCI to dementia.

Longitudinal and time-to-event relationships in A+ subjects were further demonstrated by replacing continuous WM and brainstem SUVRs by Normal/Abnormal WM or brainstem markers, as defined in Section 4.2.1.7.

A 2-tailed $P < .05$ was considered significant. The Statistics and Machine Learning Toolbox™ from MATLAB (R2017a) (https://es.mathworks.com/help/pdf_doc/stats/stats.pdf) was used for all the analyses.

4.2.2 Findings

4.2.2.1 Cohort Characteristics

Demographic characteristics and biomarker levels of the study participants are summarized in Table 3, according to diagnostic category and amyloid status. A- MCI subjects were significantly younger than the remaining cohorts ($P < .01$), except for A- CN. A- CN were more educated than A+ MCI and A+ AD dementia patients ($P < .05$). The percentage of APOE ε4 carriers was higher for A+ ($P < .01$ in all the diagnostic cohorts) and higher for increasing cognitive impairment ($P < .05$). The proportion of women in the A+CN cohort was

significantly higher than in the rest of the cohorts (P < .01). Cognition and AD biomarkers followed the expected trends. WMH volume was significantly lower in A- CN and A- MCI than in A+ participants (P < .05). Median follow-up times for each longitudinal outcome are reported in Table 4.

Table 3 - Demographic and biomarker characteristics of study participants, according to clinical diagnosis and amyloid status. Abbreviations: CN, cognitively normal; MCI, mild cognitive impairment; AD, **Alzheimer's disease; A+, positive cortical amyloid status (SUVR > 1.11); A-**, negative cortical amyloid status (SUVR < 1.11); MMSE, mini mental state examination; ADAS-Cog-**13, Alzheimer's Disease Assessment** Scale - Cognitive 13-Item; CDR-SB, clinical dementia rating sum of boxes; CSF, cerebrospinal fluid; Aβ42, amyloid beta 42 peptide; p-tau, hyperphosphorylated tau 181; WMH, white matter hyperintensity.

	Clinical Diagnosis	CN		MCI		AD dementia	
		A- (n = 143)	A+ (n = 73)	A- (n = 182)	A+ (n = 230)	A- (n = 13)	A+ (n = 104)
Characteristic							
Age,y		72 (6)	75 (6)	70 (8)	73 (7)	78 (8)	74 (8)
Women, %		45	68	46	43	8	44
ε4 carriers, %		19	47	26	66	8	76
Education, y		17 (2)	16 (3)	16 (2)	16 (3)	16 (2)	16 (3)
MMSE		29.0 (1.3)	29.0 (1.0)	28.6 (1.4)	27.6 (1.8)	23.4 (2.1)	23.0 (2.0)
ADAS-Cog-13		8.5 (4.3)	9.4 (4.2)	12.3 (5.4) (missing = 1)	17.1 (6.9)	26.7 (7.0)	31.4 (8.3) (missing = 3)
CDR-SB		0.0 (0.1)	0.1 (0.2)	1.2 (0.7)	1.6 (1.0)	4.3 (2.0)	4.6 (1.6)
CSF Aβ42, pg/cc		1612 (566)	999 (581)	1477 (572)	763 (309)	1532 (922)	608 (212)
CSF p-tau, pg/cc		19 (6)	27 (11)	18 (7)	33 (15)	30 (18)	39 (16)
Hippocampal Volume, cm^3		3.8 (0.5)	3.6 (0.4)	3.6 (0.6)	3.4 (0.5)	2.9 (0.6)	3.0 (0.5)
WMH volume, cm^3		5.0 (6.5)	9.4 (15.1)	5.6 (7.3)	8.7 (10.9)	5.2 (3.7)	9.4 (10.5)

Table 4 - Follow-up times of the outcomes considered in this study. Results are presented as mean months (standard deviation).

	Clinical Diagnosis	CN		MCI	
		A-	A+	A-	A+
Outcome					
Adas-Cog-13 follow-up time		53.5 (21.1)	49.6 (24.0)	52.8 (26.1)	44.3 (24.0)
CDR-SB follow-up time		55.0 (21.0)	49.9 (24.6)	52.9 (26.1)	46.5 (24.6)
WMH follow-up time		28.4 (18.0)	25.3 (18.0)	29.9 (19.3)	25.6 (19.9)
Hippocampus follow-up time		25.5 (13.0)	23.2 (13.8)	28.1 (13.8)	25.7 (12.5)

4.2.2.2 Associations of ErWM and brainstem SUVRs with demographic factors, cortical SUVR, and WMH

Figure 16 A) shows that both the relation of ErWM and brainstem SUVRs with cortical SUVR was dependent on cortical SUVR and on amyloid status. On the one hand, partial correlations adjusted by age showed that both ErWM and brainstem SUVRs were positively correlated with cortical SUVR in A- and A+ subjects (Figure 16 A), $P < .001$ for all the correlations). On the other hand, in order to assess the effect of amyloid status, we fit a multivariable model including age, sex, APOE ε4 carriage, WMH, cortical SUVR, amyloid status, and an interaction between amyloid status and cortical SUVR. Both the interaction ($\beta = -1.43$ for ErWM and $\beta = -1.78$ for brainstem, $P < .001$) and the amyloid status (A+ had lower SUVRs, $\beta = -1.9$ and $\beta = -2.4$, $P < .001$) terms were significantly associated with ErWM and brainstem SUVRs, indicating that the presence of cortical plaques results in a global reduction of uptake in the WM and the brainstem, independent of the increase driven by the severity of these plaques.

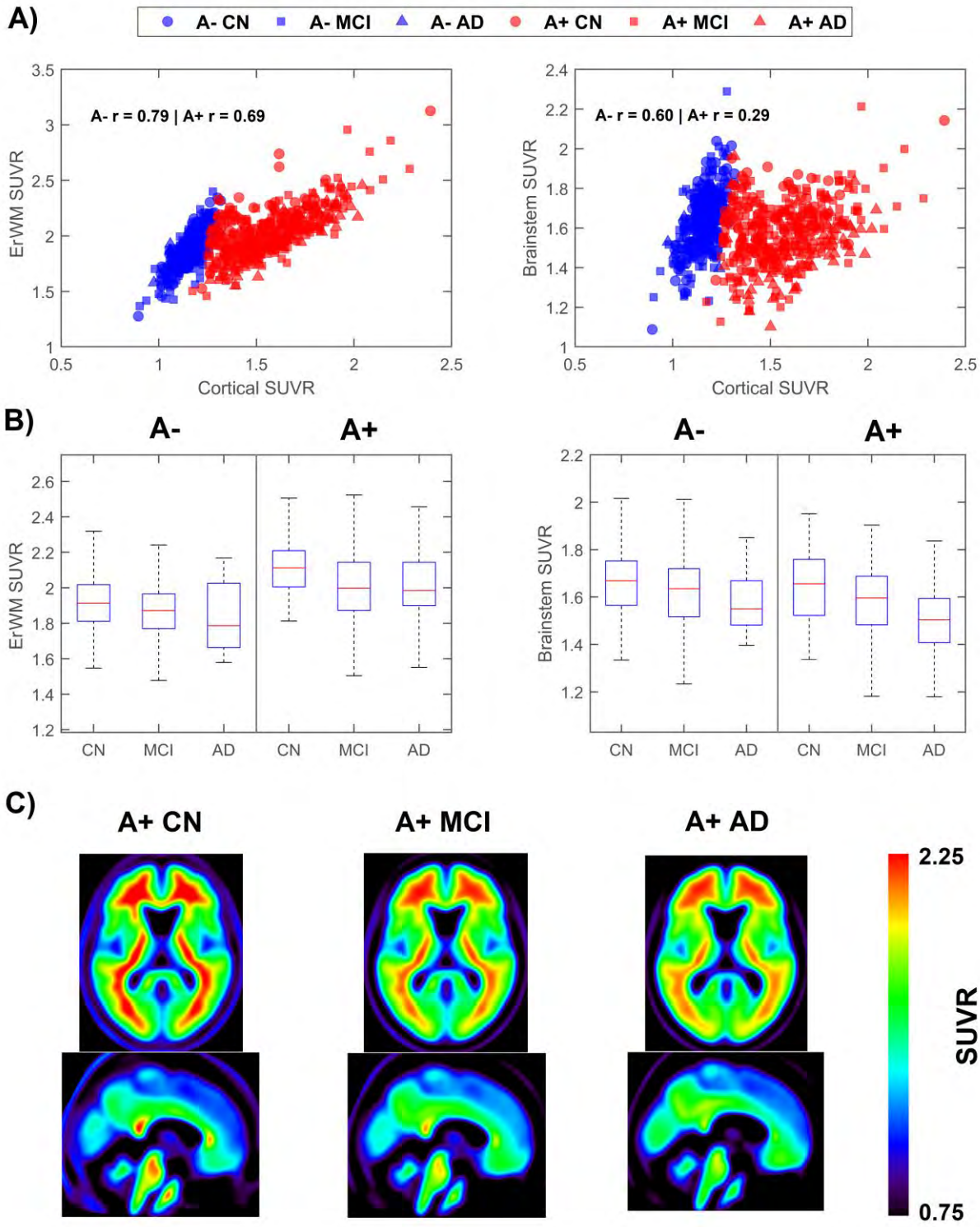

Figure 16 - Dependence of ErWM and brainstem SUVR with cortical SUVR and clinical symptoms. A) Dependence of ErWM and brainstem SUVRs with cortical SUVR. B) Boxplots of ErWM and brainstem SUVRs, for each diagnostic cohort and amyloid status. C) Mean image in MNI space of A+ CN, A+ MCI, and A+ AD dementia participants, depicting WM and brainstem uptake. Abbreviations: A, amyloid status; CN, **cognitively normal; MCI, mild cognitive impairment; AD, Alzheimer's Disease dementia; WM, white matter;** SUVR, standardized uptake value ratio; r, age-adjusted Pearson correlation coefficient.

Significant associations were also found for age ($\beta = 0.05$ and $\beta = 0.08$, $P < .05$), WMH ($\beta = -0.13$ and $\beta = -0.14$, $P < .001$), and APOE carriage (APOE carriers showed lower

SUVR, β = -0.24 and β = -0.24, P < .001). Sex was also associated with brainstem SUVR (males had higher SUVR, β = 0.33, P < .001), but not with ErWM SUVR (P = .59). The correlation between ErWM and brainstem SUVRs was high for both A- (r = 0.78, P < .001) and A+ (r = 0.75, P < .001).

4.2.2.3 Associations of ErWM and brainstem SUVRs with clinical diagnosis

Given the steep dependence of ErWM and brainstem SUVRs on amyloid status, we investigated the associations between these variables and clinical diagnosis for A- and A+ participants separately. Figures 16 B) and 16 C) show ErWM and brainstem SUVRs across diagnostic cohorts and amyloid status. For A+ participants, MCI had lower ErWM and brainstem SUVRs than CN (β = -0.62 for ErWM and β = -0.63 for brainstem, P < .001) and higher than AD dementia subjects (β = 0.30 and β = 0.55, P < .001). No significant differences were found across A- participants.

4.2.2.4 Associations of ErWM and brainstem SUVRs with AD biomarkers and cognition

Figure 17 A) shows that both low ErWM and brainstem SUVRs were significantly associated with low CSF Aβ-42 levels for all the diagnostic cohorts and amyloid statuses. Additional linear models including an interaction between cortical SUVR and WM or brainstem SUVRs revealed a significant interaction in CN (β = 0.08, P = .004 for WM and β = 0.07, P = .06 for brainstem), indicating that decreases in WM and brainstem uptake were associated with stronger decreases in CSF Aβ-42 if cortical SUVR is high.

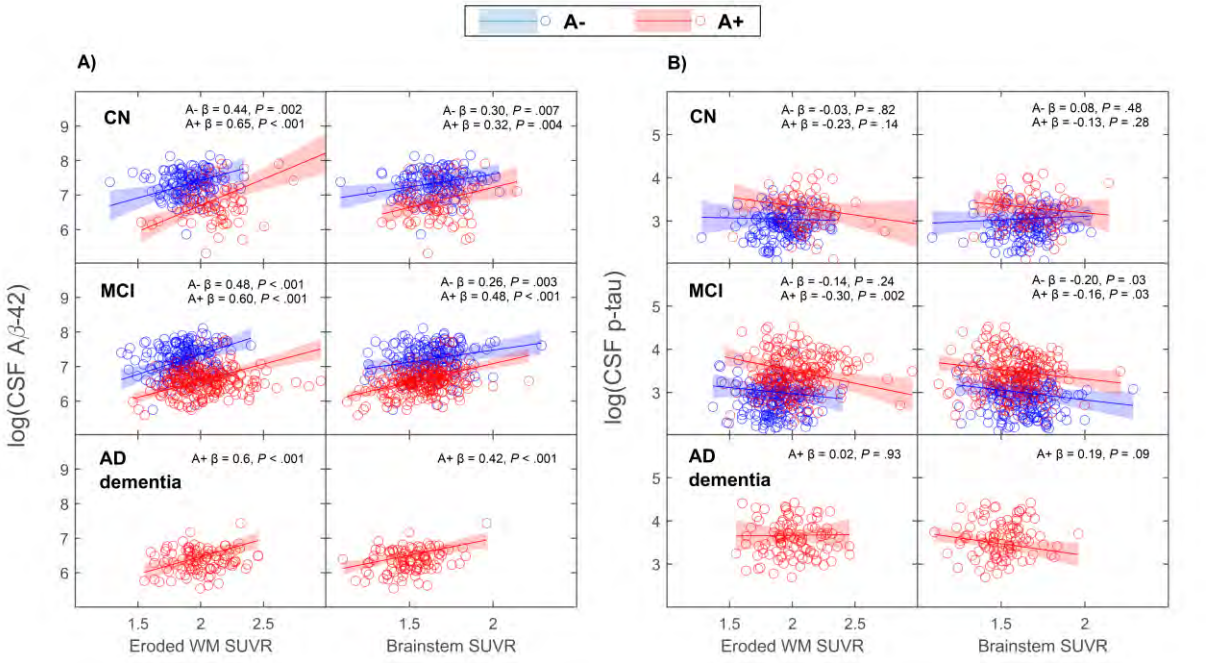

Figure 17 - Linear models relating ErWM and brainstem SUVRs with CSF biomarkers. A) CSF Aβ-42 and B) with CSF p-tau. Results are presented for each diagnostic cohort and amyloid status. Linear models are represented assuming a 75 years old female with one APOE ε4 allele, at mean covariate values. Shaded areas represent 95% confidence intervals. Abbreviations: A, amyloid status; CN, cognitively normal; MCI, **mild cognitive impairment; AD, Alzheimer's Disease; WM, white matter; CSF, cerebrospinal fluid; SUVR,** standardized uptake value ratio; β, standardized coefficient for the white matter or the brainstem.

Figure 17 B) shows that low ErWM SUVR was associated with high CSF p-tau only in A+ MCI; low brainstem SUVR correlated with high CSF p-tau in A- and A+ MCI. Interaction analysis showed that, in MCI, ErWM decreases were associated with stronger increases in p-tau levels if cortical SUVR is high (β = -0.08, P = .005). Low brainstem SUVR was associated with low Hippocampus volume only in A+ MCI (β = 0.15, P = .03).

Regarding cognition, only A+ MCI subjects showed a significant association between low ErWM and brainstem SUVRs, and high ADAS-Cog-13 (β = -0.22, P = .02 for ErWM and β = -0.19, P = .004 for brainstem) and CDR-SB (β = -0.33, P = .002 and β = -0.25, P < .001). No further significant associations with AD biomarkers or cognition were found.

4.2.2.5 Associations of ErWM and brainstem SUVRs with longitudinal change in cognition, WMH, and hippocampus volume

Table 5 summarizes the longitudinal associations of ErWM and brainstem SUVRs with longitudinal change in cognition, WMH, and hippocampus volume. Low baseline ErWM and brainstem SUVRs were significantly associated with faster cognitive decline in A+ CN and A+ MCI, but not among A- individuals. Interaction analyses showed that the effects of both low ErWM and low brainstem SUVRs on longitudinal cognition were stronger if cortical SUVR was high in CN (ADAS-Cog-13: unstandardized β, b = -2.8 pts/y/SUVR², P < .001 for ErWM and b = -4 pts/y/SUVR², P = .006 for brainstem; CDR-SB: b = -0.24, pts/y/SUVR², P = .04 and b = -0.48 pts/ y/SUVR², P = .04) and MCI (ADAS-Cog-13: b = -2.2 pts/y/SUVR², P = .004 and b = -5.4 pts/y/SUVR², P < .001; CDR-SB: b = -0.66, pts/y/SUVR², P = .001 and b = -2.04 pts/ y/SUVR², P < .001). Similarly, low baseline ErWM SUVR predicted increased WMH burden in A+ CN, A+ MCI, and A- MCI, while low brainstem SUVR did only in A+ CN and A+ MCI. Rates of WMH change were higher for A+ CN compared to A+ MCI. The effect of low WM or brainstem SUVRs in longitudinal WMH burden was higher for high cortical SUVR, as demonstrated by interaction analysis in CN (b = -1.3 cm³/y/SUVR², P = .01 and b = -2.4 cm³/y/SUVR², P = .03, respectively) and MCI (b = -1.9 cm³/y/SUVR², P = .006 and b = -3.3 cm³/y/SUVR², P = .003). Low longitudinal hippocampus volumes were associated with low baseline ErWM SUVR in A+ CN, A+ MCI, and A- MCI, and with low brainstem SUVR in A+ MCI. Interaction terms were not significant.

Table 5 - Longitudinal associations of ErWM and brainstem SUVRs, for different outcomes. ADAS-Cog-13 and CDR-SB Unstandardized **ß** were reported in pts/y/SUVR, WMH in cm^3/y/SUVR, and Hippocampus Volume in mm^3/y/SUVR. To avoid circularity, only follow-up visits were included in the WMH models. Abbreviations: WM, white matter; Unstandardized **ß**, non-standardized coefficient of the interaction term with time; CI, confidence interval; ADAS-Cog-**13, Alzheimer's Disease Assessment Scale -** Cognitive 13-Item; CDR-SB, clinical dementia rating sum of boxes; WMH, white matter hyperintensity; A, amyloid status; CN, cognitively normal; MCI, mild cognitive impairment.

		ErWM		Brainstem	
Outcome	Cohort	**Unstandardized ß** (95% CI)	*P* value	**Unstandardized ß** (95% CI)	*P* value
ADAS-Cog-13	A- CN	-0.07 (-1.40 to 1.26)	.92	0.62 (-0.56 to 1.80)	.30
	A+ CN	-1.86 (-3.15 to -0.57)	.005	-2.10 (-3.97 to -0.23)	.03
	A - MCI	0.33 (-0.87 to 1.53)	.59	0.11 (-0.91 to 1.12)	.83
	A + MCI	-3.41 (-4.65 to -2.13)	< .001	-4.21 (-5.48 to -2.94)	< .001
CDR-SB	A- CN	-0.11 (-0.33 to 0.11)	.32	-0.14 (-0.34 to 0.06)	.17
	A+ CN	-0.40 (-0.59 to -0.21)	< .001	-0.36 (-0.64 to -0.09)	.01
	A - MCI	-0.18 (-0.47 to 0.10)	.20	0.20 (-0.04 to 0.44)	.10
	A + MCI	-1.55 (-1.90 to -1.20)	< .001	-1.81 (-2.16 to -1.46)	< .001
WMH volume	A- CN	-0.96 (-2.20 to 0.29)	.13	-1.16 (-2.36 to 0.05)	.06
	A+ CN	-1.84 (-3.09 to -0.59)	.004	-1.66 (-3.30 to -0.03)	.04
	A - MCI	-2.08 (-3.12 to -1.04)	< .001	-0.58 (-1.50 to 0.33)	.21
	A + MCI	-1.39 (-2.21 to -0.58)	< .001	-1.24 (-2.09 to -0.39)	.004
Hippocampus volume	A- CN	66 (-56 to 188)	.29	34 (-75 to 142)	.54
	A+ CN	99 (2 to 196)	.04	28 (-93 to 150)	.64
	A - MCI	103 (28 to 179)	.007	40 (-23 to 104)	.21
	A + MCI	61 (8 to 114)	.02	99 (45 to 153)	< .001

Figure 18 further demonstrates the previous longitudinal relations after replacing continuous ErWM and brainstem SUVRs by Normal/Abnormal WM and brainstem categories, as defined in Section 4.2.1.7. The proportion of subjects with abnormal WM or brainstem marker was significantly lower in A+ CN than in A+ MCI (30% vs. 66%, P < .001 for WM and 44% vs. 63%, P = .003 for brainstem).

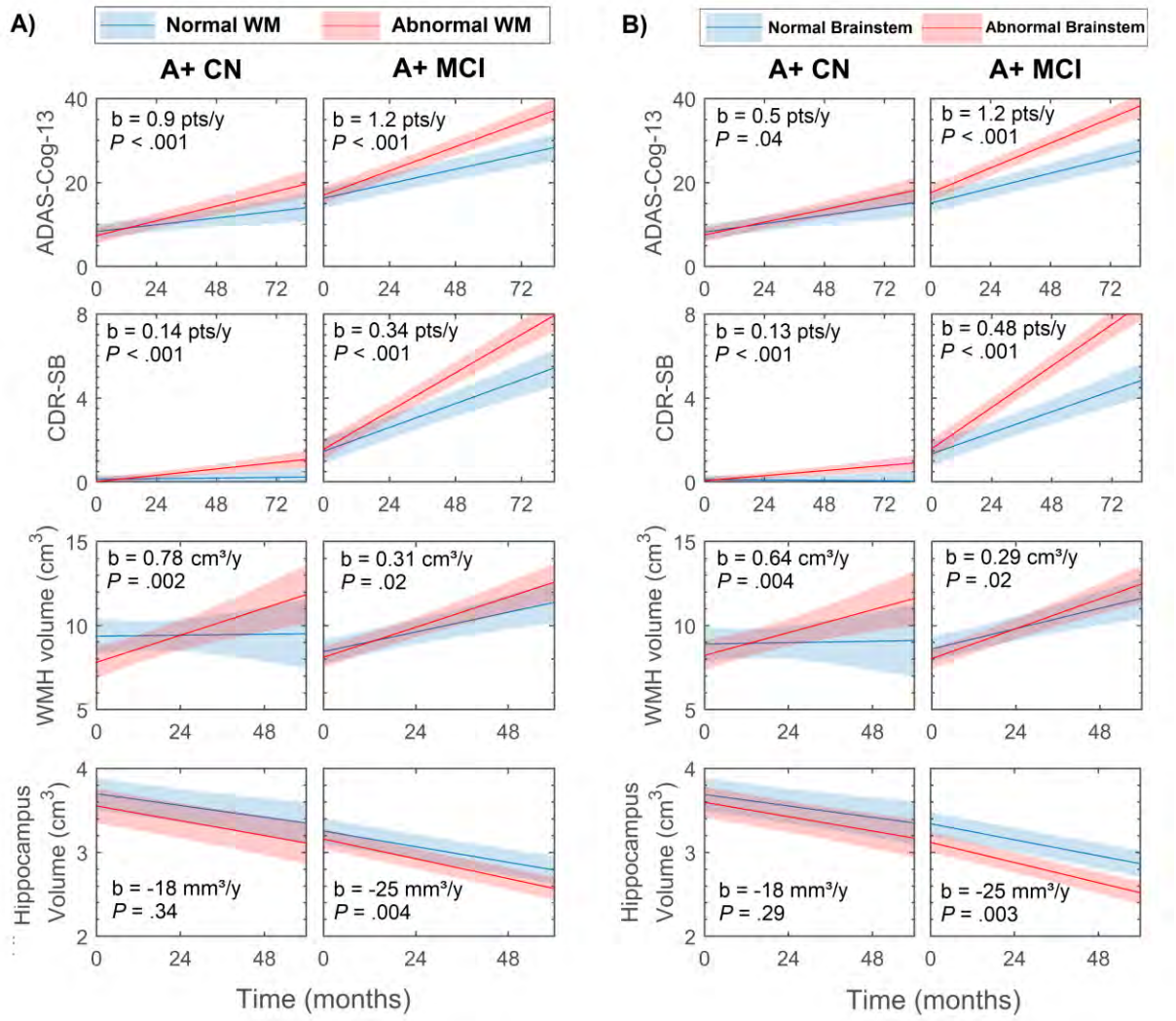

Figure 18 - Linear mixed models representing the longitudinal trajectories of A+ CN and A+ MCI. See text for the definition of normal/abnormal WM and brainstem uptake. To avoid circularity, only follow-up visits were included in the WMH models. Time represents the time from amyloid PET. Shaded areas represent 95% confidence intervals. Abbreviations: WM, white matter; A, amyloid status; CN, cognitively normal; MCI, mild cognitive impairment; ADAS-Cog-**13, Alzheimer's Disease Assessment Scale -** Cognitive 13-Item; CDR-SB, clinical dementia rating sum of boxes; WMH, white matter hyperintensity, b, unstandardized **β** coefficient of the interaction term between abnormal marker and time.

4.2.2.6 ErWM and brainstem SUVRs, and risk of progression from MCI to dementia

Cox regression analysis showed a significant association between lower ErWM and brainstem SUVRs, and higher risk of future dementia only in A+ MCI participants (unstandardized β, b = -2.92, P < .001 for ErWM and b = -3.11, P < .001 for brainstem). These associations were confirmed using the cut-points for Normal/Abnormal WM and brainstem (Figure 19).

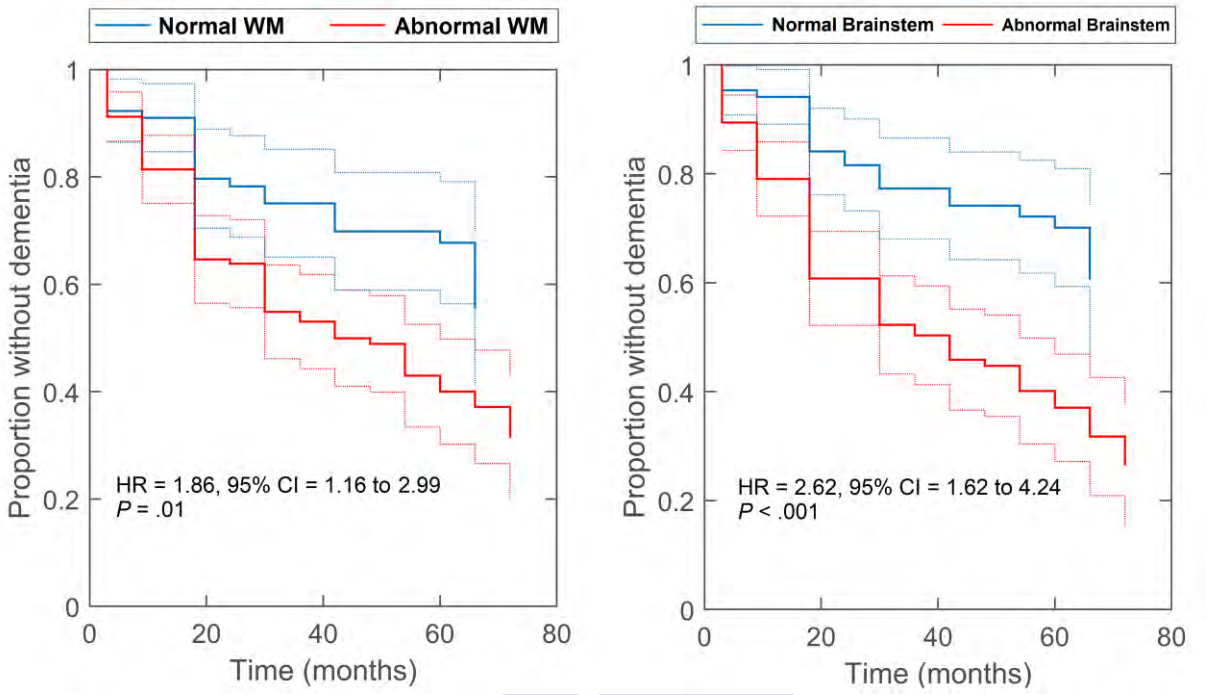

Figure 18 - Kaplan Meier survival curves for the risk of progression from A+ MCI to AD dementia. See text for the definition of normal/abnormal WM and brainstem uptake. Time represents the time from amyloid PET. Dashed lines represent 95% confidence intervals. Abbreviations: WM, white matter; HR, adjusted hazard ratio for abnormal markers, referenced to normal markers; CI, confidence interval.

4.2.3 Discussion

In this study, we investigated the relationship of Florbetapir uptake in cerebral WM and the brainstem with AD progression, under the assumption that low tracer retention in these areas reflects WM degeneration. We found that low tracer retention in WM and brainstem, independently of cortical SUVR and WMH, was associated with more abnormal CSF biomarkers and impaired cognition. These cross-sectional relations were further confirmed in longitudinal analyses, showing that reduced uptake in WM and the brainstem predicted future cognitive decline, higher WMH burden, and lower hippocampus volumes. Taken together, our findings add to recent studies linking WM lesions with reduced amyloid tracer uptake in normal aging and Multiple Sclerosis [97,99-100,148-149] and suggest that WM degeneration, as measured by amyloid PET, is relevant for the cognitive and pathological progression of preclinical and prodromal AD.

Consistent with a prior report [178], we found a significant positive association between WM uptake and age; however, the strength of this association was small compared to that of WMH and, specially, cortical SUVR. Despite of the strong positive association with cortical SUVR, we found that WM uptake is independently modulated by amyloid status as well: amyloid positive subjects showed a global decrease in WM and brainstem uptake compared to amyloid negative. The mechanism that leads to this complex behavior cannot be solely attributed to partial volume effects, as demonstrated by our PVE-corrected analysis (see Appendix 1). A potential explanation for the positive correlation with cortical SUVR might be the affinity of amyloid tracers for different Aβ fibrils [181] present in the WM and the brainstem [52,182], which are likely to increase in tandem with cortical pathology. The mechanisms behind the global decrease in WM uptake driven by amyloid positivity are, however, not nearly as clear. A recent study suggests that parietal WM lesions are specific for

AD [167], and proposed neuronal accumulation of tangles and subsequent Wallerian degeneration [88] as the mechanistic origin. Although this effect might explain our observations, particularly those related with tau and neurodegeneration, it is not clear how regions far from the cortex, such as deep WM and the brainstem, could be influenced by this process. Another possible mechanism of AD-related WM degeneration is the abnormal accumulation of soluble Aβ, the most toxic form of Aβ40, in these areas. Aβ oligomers, particularly Aβ-42, were found to be abnormally elevated in the WM of AD brains, independently of cortical plaque severity [103]. Demyelination associated to these oligomers [183] would thus explain the strong correlation between low CSF Aβ-42 levels and low WM and brainstem uptake, pursuant to the findings of a recent study [158]. Also, this observation might help to better understand why CSF Aβ-42 turns abnormal before amyloid PET [162], suggesting that abnormalities in WM might precede PET detectable cortical plaques. Whether this degeneration is the triggering effect leading to cortical deposition or simply an aging pathology that interacts with AD needs to be explored in future studies.

Longitudinal analyses confirmed that the observed cross-sectional associations had a relevant impact in the progression of preclinical and prodromal AD participants. These results might be of importance for prevention clinical trials since WM is not a common target of disease-modifying interventions [184]. Depending on the therapeutic target, clinical trials may prefer not to include participants with low WM or brainstem uptake in an attempt to anticipate the neurodegenerative cascade of AD.

Our longitudinal findings might also help to increase the positive predictive value of amyloid PET. It is estimated that 5 to 10 years separate detectable brain amyloidosis and atrophic changes [185], thus amyloid positivity is weakly linked with short-term decline and cognition. With the assessment of WM or brainstem uptake, amyloid PET might become an unexpected marker of AD-related neurodegeneration, and therefore be more closely associated with clinical symptoms and short-term progression. Investigations shall be carried out to see as how to best incorporate this new information together with other PET measures of amyloidosis in further studies [73].

The strengths of this study include 1) a relatively large sample of participants covering the spectrum of AD, with concurrent cognitive, amyloid PET, CSF, and MRI examinations, allowing the examination of multiple markers and 2) the separate analyses carried out for subjects in the Alzheimer's continuum (A+) at preclinical and prodromal stages. This work also had several limitations. First, the ADNI inclusion criteria requires participants relatively free of vascular pathology, which might compromise the generalizability of our findings in the community. Second, we studied white matter uptake globally rather than regionally, which might have blurred associations with markers at earlier stages in the disease. Third, we did not assess the longitudinal progression of WM and brainstem uptake due to the large number of patients needed to detect a significant decrease over the increase driven by cortical SUVR.

In conclusion, our findings suggest that amyloid PET can be used as an early marker of white matter degeneration that contributes to Alzheimer's Disease progression. Further studies are needed to fully understand 1) the role of white matter degeneration in Alzheimer's Disease, 2) the neuropathologic changes associated with low amyloid tracer retention in white matter, and 3) the dynamics of amyloid tracer retention in white matter.

4.3 STAGING THE COGNITIVE CONTINUUM IN PRODROMAL ALZHEIMER'S DISEASE WITH EPISODIC MEMORY

Recent research efforts shifted towards a biological description of AD in terms of in vivo biomarkers of brain amyloidosis (A), tauopathy (T) and neurodegeneration (N), all of them integrated in the purported AT(N) scheme [186]. This system plays a central role in the NIA-AA research framework [17], in which the definition of AD relies only on the presence of abnormal levels of both A and T (A+T+), while (N) biomarkers and cognitive symptoms, both non-specific for AD, provide complementary staging information [17].

Apart from the three classical syndromal cognitive stages, i.e., CN, MCI, and dementia, the NIA-AA research framework proposed a new 6-stage Numeric Clinical (NC) staging scheme for patients in the Alzheimer's continuum (patients with A+). Although this staging scheme is designed to monitor subtle changes in cognition in CN individuals, only a single stage (Stage 3) is used to describe the entire cognitive continuum of MCI [17].

In an attempt to stage cognitive symptoms in MCI, the ADNI and other studies defined the 'early' and 'late' stages of MCI on the basis of episodic memory performance [107-109]. Many studies demonstrated differences between these two groups, namely, slower progression rates to AD dementia [107-108], different prevalence in the community in comparison to the clinic [108-109], and different neuropathologic features [110-111,187-191], supporting the idea of a sequential evolution between these two groups. However, recent evidence has suggested that the observed differences might be caused by the high number of false positive MCI diagnoses in the early MCI group [112-113, 192-193], casting doubt on the effectiveness of this staging scheme to track the cognitive continuum in AD. Moreover, no previous study has investigated whether episodic memory provides independent information about severity and progression when applying the NIA-AA research framework criteria to define AD.

In this study, we investigated whether episodic memory staging describes the sequential evolution of cognitive symptoms in MCI patients with biomarker evidence of AD, as defined by the NIA-AA research framework, and whether it provides complementary prognostic information to the AT(N) profiles.

4.3.1 Specific Methods

4.3.1.1 Study Design:

Data were downloaded from the LONI website in November 2018. We examined all the patients in the ADNI1/GO/2 study with available clinical, MRI and CSF data at baseline. The diagnostic categories included, as defined in the ADNI study, were CN, Subjective Memory Complaints (SMC), early MCI (EMCI), late MCI (LMCI), and AD dementia. CN and SMC subjects had MMSE scores of 24 to 30, a CDR and Memory Box Score of 0, scores in the Logical Memory II Delayed Recall test from the Weschler Memory Scale-Revised [194] not below 1.5 standard deviations from normative scores, and absence of significant impairment in cognitive functions or activities of daily living. CN and SMC differed only in the presence of subjective memory concerns. EMCI and LMCI had the same MMSE range as CN and SMC, a Global CDR of 0.5, a Memory Box Score of at least 0.5, and functional performance sufficiently preserved to not being considered demented. The inclusion criteria for EMCI and LMCI differed only in the score obtained in the Logical Memory II Delayed Recall test from the Weschler Memory Scale-Revised [194], with LMCI patients scoring

below 1.5 standard deviations from normative data and EMCI scoring between 1 and 1.5 standard deviations below the standard. Finally, AD dementia patients had MMSE scores of 20 to 26, a Global CDR of 0.5 or 1, and met the NINCDS/ADRDA criteria for probable AD. Although MCI patients were the main focus of our case, the remaining cohorts were also included in a cross-sectional analysis to determine whether EMCI represents a transitional stage between SMC and LMCI in terms of biomarker abnormalities. Further details can be found at http://adni.loni.usc.edu/methods/documents/. Only MCI patients with clinically suspected MCI due to Alzheimer's disease at baseline, as reported by the ADNI investigators, were included. A total of 1147 patients, including 267 CN, 88 SMC, 252 EMCI, 324 LMCI, and 216 AD dementia had all available clinical, imaging, and CSF examinations.

4.3.1.2 CSF:

CSF measurements of Aβ42, p-tau, and t-tau were performed by the Center of Neurodegenerative Disease Research, University of Pennsylvania, for ADNI. We downloaded the measurements from the Roche Elecsys electrochemiluminescence immunoassay batch. Recent evidence indicates that this fully automated assay provides transferable cut-points between independent studies [30] which might result in a higher applicability of the findings of this study. A detailed description of the procedures used for CSF analysis can be found at http://adni.loni.usc.edu/methods/.

4.3.1.3 MRI:

All the examined patients had a T1-weighted MRI (1.5T or 3T) scan at baseline. A detailed MRI acquisition protocol of the different parts of the ADNI project can be found at http://adni.loni.usc.edu/methods/documents/. T1 scans were segmented with Freesurfer v5.1 [126]. The ADNI collaborators at the Center for Imaging of Neurodegenerative Diseases at University of California, San Francisco (UCSF), performed a thorough quality control of their own Freesurfer segmentations. We only included those patients with segmentations of the hippocampus that passed the ADNI quality control. Only non-accelerated MPRAGE or IR-SPGR sequences were used. We estimated TIV with SPM12 [129,195] since this measure demonstrated to be more accurate than the Freesurfer TIV [129] and because the Freesurfer TIV is biased by brain volume [196]. Given that the variability associated to different field strengths is small and comparable to within-scanner variability [197-198], we combined 1.5T and 3T volumetric measures and included a term to account for field strength in our linear analyses (see Section 4.3.1.5 below and Appendix 2 for more details).

4.3.1.4 Neuropsychology:

Cognition measures, as assessed by MMSE and the CDR-SB [199], were obtained at baseline and in subsequent follow-up visits for all the participants, although we restricted the analysis to patients with MCI given that the goal of this study is to investigate the prognostic added value of the proposed NC substages.

4.3.1.5 Implementation of the AT(N) framework:

We implemented the AT(N) framework using CSF Aβ42 and p-tau as markers of A and T, respectively, while hippocampal atrophy measured with MRI was used as a biomarker of (N). These measures are standard markers of A, T, and (N) in the NIA-AA research framework [17] and represent an accessible AT(N) implementation for most of the hospitals and memory clinics. CSF t-tau was not used here as (N) biomarker due to its tight correlation

with p-tau in AD [200] and because recent evidence suggests that CSF neurofilament light chain might be the most suitable CSF-based (N) marker [201].

Following recent recommendations, no adjustment for age was performed in CSF biomarkers [202]. To obtain an index for (N), we used the average between left and right hippocampal volumes normalized by TIV, and adjusted by age and field strength using linear regression in the subsample of CN with A-, as defined below. By including the field strength term (categorical), we account for the small bias introduced by the different field strengths [198]. A detailed description of this approach can be found in the Supplementary Material (Appendix 2). This index is referred to as adjusted Hippocampal Volume (aHV) and increases with atrophy severity.

The AT(N) framework requires the definition of cut-points that establish the separation between normal (negative) and abnormal (positive) levels of biomarkers. For our A marker, we established an externally derived cut-point of 1100 pg/cc based on agreement with amyloid PET imaging [30,203-204]. For T and (N), however, no externally derived cut-points that directly reflect tauopathy or neurodegeneration have been established for the Roche Elecsys assay and MRI under the ADNI protocol. In order to derive independent cut-points to be applied in our CN and MCI cohorts, we established cut-points using the 10th percentile (90% sensitivity) of the biomarker distribution among AD dementia patients with A+, as defined by the aforementioned A cut-point. We used this approach because it provided similar imaging cut-points to those obtained by maximizing the discrimination between cognitively impaired patients versus young controls [177], which arguably represents the most reliable alternative when no direct neuropathology measures are available.

4.3.1.6 NC staging:

Following the definition of the NC staging in the NIA-AA research framework [17], ADNI CN subjects with A+ can be regarded as Stage 1, SMC with A+ as Stage 2, and EMCI and LMCI with A+ as Stage 3. In order to keep a similar nomenclature, we defined a subdivision of Stage 3 patients into early and late substages (Early Stage 3 and Late Stage 3) following the same neuropsychological criteria used to define EMCI and LMCI [107]. A+ AD dementia patients are mildly demented and thus can be regarded as Stage 4.

4.3.1.7 Statistical Analysis:

We used Kruskal-Wallis tests to evaluate differences in demographic continuous variables among the different NC stages. The Tukey-Kramer method was applied for pairwise comparisons. Discrete demographic variables were compared using the $\chi 2$ test.

We used a one-tailed exact binomial test to assess the hypothesis that Stage 1 and Stage 2 patients progressed first to Early Stage 3.

Cross-sectional proportions of each biomarker profile across the NC stages were compared using a logistic regression for each AT(N) profile with profile status (absent or present) as the dependent variable and NC stage as the independent variable. The model was adjusted for age, sex, education years, number of APOE ε4 alleles, and baseline MMSE score.

Annual rates of change of MMSE and CDR-SB across the NC substages were compared by fitting a linear mixed effects model for each AT(N) profile. The model included a random intercept per subject, and fixed effect terms for NC substage, the interaction between NC substage and time, time, covariates, and the interaction between each covariate and time. The covariates included age, sex, education years, number of APOE ε4 alleles,

baseline cognitive score under consideration (MMSE or CDR-SB), and, as a sensitivity analysis, levels of CSF Aβ42, p-tau, t-tau, and age- and TIV-adjusted hippocampal volume. The adjusted mean rate of change, using Late Stage 3 as reference, was obtained from the coefficient of the interaction between NC substage and time.

We assessed the time of progression to AD dementia computing Kaplan Meier survival curves and fitting a cox proportional hazards model for each profile. The model was adjusted by the same covariates, including both baseline MMSE and CDR-SB, described above.

F tests were used to assess the significance of model coefficients. Post-hoc contrasts were conducted for pairwise comparisons. The significance level was set $\alpha = 0.05$. The Bonferroni correction was applied to correct for multiple inferences. We reported two-tailed p values, except for the binomial exact test. The Statistics and Machine Learning Toolbox™ from MATLAB (R2017a) (https://es.mathworks.com/help/pdf_doc/stats/stats.pdf) was used for all statistics.

4.3.2 Findings

4.3.2.1 Cohort characteristics:

The proportion of patients with A+ increased with symptomatology: 113 (42%) CN had A+, 32 (36%) in SMC, 132 (52%) in EMCI, 255 (79%) in LMCI, and 200 (93%) in AD dementia. Demographic information for A- participants is presented in Supplementary Table 1 (Appendix 2). Table 6 shows the characteristics of the A+ participants examined in this study, stratified by NC stages and the proposed substaging.

Table 6 - **Demographic Information for A+ (abnormal CSF Aβ42 levels) participants. Continuous variables** are reported as means ± standard deviation. P values were calculated using a Kruskal-Wallis test **(continuous variables) or a x2 test (categorica**l variables). Abbreviations: NC: Numeric Clinical. E. Stage 3: Early Stage 3. L. Stage 3: Late Stage 3. MMSE: Mini Mental State Examination score. CDR-SB: Clinical Dementia Rating—Sum of Boxes. APOE: Apolipoprotein E. N/A: Not assessed.

NC Stage	Stage 1	Stage 2	E. Stage 3	L. Stage 3	Stage 4	P Value
N =	113	32	132	255	200	
Demographics						
Age (years)	75±6	73±5	73±7	74±7	74±8	0.14
Female (%)	50	69	38	37	42	0.021
Education (years)	16±3	17±2	16±3	16±3	15±3	0.032
MMSE	29±1	29±1	28±2	27±2	23±2	<0.001
CDR-SB	0±0	0±0	1±1	2±1	4±2	<0.001
Follow-up (years)	5±3	3±2	4±2	4±2	N/A	<0.001
APOE ε4 carriers (%)	40	59	58	63	74	<0.001

Each stage had small differences in age, sex, and education. Cognitive measures worsened with increasing stage, with Early Stage 3 representing a trade-off between Stage 2

and Late Stage 3. APOE genotype followed the expected trend. Pairwise comparisons between Early and Late Stage 3 only showed that Early Stage 3 had significantly higher baseline MMSE score (median difference 1, 95% CI 1 to 2; $p < 0.001$). Post-hoc analyses can be found in the Appendix 2. Biomarker levels also had a higher rate of abnormality in the progression of NC Stages (Figure 20). Again, Early Stage 3 levels demonstrated to imbricate between Stage 2 and Late Stage 3, specially for T and (N) markers. Late Stage 3 displayed significantly more abnormal biomarker levels than Early Stage 3 ($p < 0.05$ for all the biomarkers). Biomarker levels for A- participants are presented in Supplementary Figure 1 (Appendix 2).

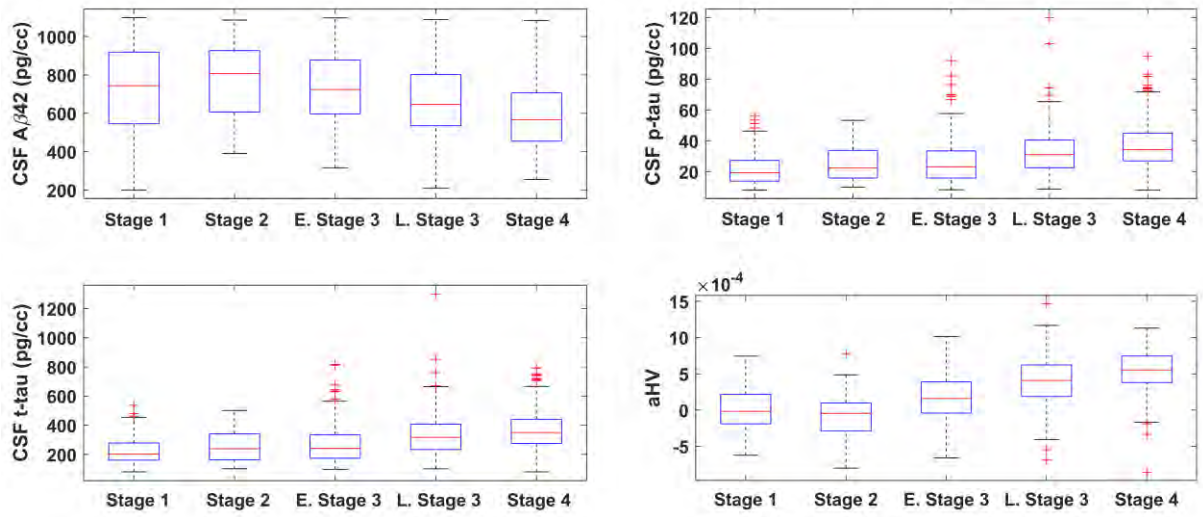

Figure 20 - Box plots showing biomarker levels across the different Numeric Clinical Stages and substages. aHV stands for intracanial volume-, field strength-, and age-adjusted hippocampal volume, and is higher and positive for higher atrophies. Abbreviations: CSF: Cerebrospinal Fluid. E. Stage 3: Early Stage 3. L. Stage 3: Late Stage 3.

4.3.2.2 AT(N) profiles across NC stages:

The 90% sensitivity approach used to derive biomarker cut-points yielded the following results: p-tau cut-point = 19.39 pg/cc and aHV cut-point = 1.82×10^{-4}. Figure 21 shows the prevalence of the AT(N) profiles for each stage. Demographic information for each profile in Early and Late Stage 3 can be found in Supplementary Table 2 (Appendix 2). The proportion of A+T+(N)+ increased at every NC stage (Stage 1 < Early Stage 3 < Late Stage 3, $p < 0.01$ for each comparison), while in A+T+(N)- and A+T-(N)- decreased (for A+T+(N)-, Early Stage 3 > Late Stage 3, $p < 0.05$; for A+T-(N)-, Stage 1 > Early Stage 3 > Late Stage 3, $p < 0.01$ for each comparison). No significant differences in prevalence were observed for A+T-(N)+.

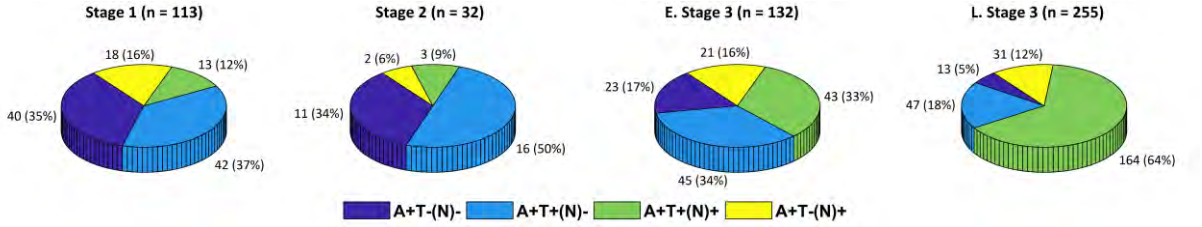

Figure 21 - Sample sizes and **prevalence of each AT(N) profile for patients in the Alzheimer's continuum,** across each Numeric Clinical Stage. Abbreviations: E. Stage 3: Early Stage 3. L. Stage 3: Late Stage 3.

4.3.2.3 Longitudinal Progression of Stage 1 and 2 patients:

During follow-up, 28 Stage 1 and 7 Stage 2 patients progressed to other stages on an average of 4.1±2.6 and 2.6±1.2 years, respectively. Nineteen Stage 1 and 3 Stage 2 progressed to Early Stage 3, while the rest progressed to Late Stage 3. No direct transitions to Stages 4-6 were observed. We regarded Early Stage 3 as those who progressed to a clinical diagnosis of MCI but had neuropsychological scores above (more normal) the limits specified in the ADNI inclusion criteria. The proportion of Stage 1 and 2 patients who transitioned to Early Stage 3 was higher than that of Late Stage 3 (65%, $p = 0.043$).

4.3.2.4 Cognitive decline:

To ascertain whether the new NC stages provided prognostic information to the AT(N) profiles we conducted linear mixed effects models for longitudinal measures of MMSE and CDR-SB. Table 7 shows the mean difference in annual rates of change for Early Stage 3 compared to Late Stage 3 patients. Overall, Early Stage 3 patients showed a slower decline on both MMSE and CDR-SB than patients in Late Stage 3 (Figure 22), with significant differences in A+T+(N)- and A+T+(N)+ profiles. Additional sensitivity analyses for varying p-tau and aHV cut-points (±15% around the values derived here) can be found in Supplementary Figure 2 (Appendix 2), showing the stability of the results.

Table 7 - Difference in annual change of cognitive measures in Early Stage 3 compared to Late Stage 3. A positive (negative) difference in annual change of MMSE (CDR-SB) means that the decline of Early Stage 3 is slower than in Late Stage 3. Quantities between parentheses are 95% CI. Abbreviations: L. Stage 3: Late Stage 3. E. Stage 3: Early Stage 3. MMSE: Mini Mental State Examination score. CDR-SB: Clinical Dementia Rating—Sum of Boxes.

Variable		Difference in annual change (pts/y)	P Value
MMSE			
	AT(N)		
	A+T-(N)-	0.16 (-0.08 to 0.40)	0.20
	A+T+(N)-	0.35 (0.17 to 0.53)	< 0.001
	A+T+(N)+	0.42 (0.19 to 0.64)	< 0.001
	A+T-(N)+	0.20 (-0.02 to 0.41)	0.07
CDR-SB			
	AT(N)		
	A+T-(N)-	-0.19 (-0.34 to -0.03)	0.02
	A+T+(N)-	-0.27 (-0.40 to -0.15)	< 0.001
	A+T+(N)+	-0.50 (-0.64 to -0.35)	< 0.001
	A+T-(N)+	-0.05 (-0.21 to 0.10)	0.50

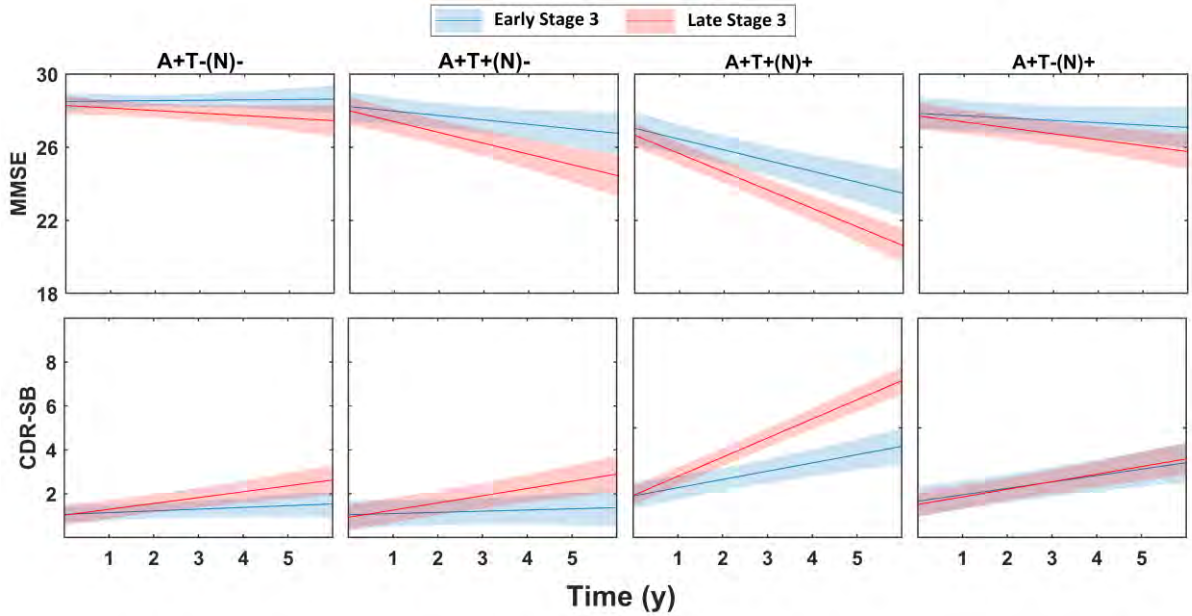

Figure 22 - Longitudinal progression of Mini Mental State Examination and Clinical Dementia Rating—Sum of Boxes for each biomarker profile and substage, as predicted by the fitted linear mixed models evaluated at mean **values of continuous covariates and reference categorical covariates (males and APOE ε4 non-**carriers). Shaded areas represent 95% confidence intervals. Abbreviations: MMSE: Mini Mental State Examination. CDR-SB: Clinical Dementia Rating—Sum of Boxes.

4.3.2.5 Progression to AD dementia:

At follow-up, 41 Early Stage 3 and 147 Late Stage 3 progressed to AD dementia (see Supplementary Table 3 (Appendix 2) for details). Figure 23 shows Kaplan Meier survival curves and hazard ratios for three of the four profiles (A+T-(N)- had only 6 progressions to AD dementia and was excluded from the analysis). Late Stage 3 patients had higher risk of progression to AD dementia than Early Stage 3, this risk being significantly higher for A+T+(N)+ patients but not for those with A+T+(N)- (Figure 23). Patients with an A+T-(N)+ profile showed a similar risk of progression to AD dementia. Sensitivity analyses for varying p-tau and aHV cut-points, presented in Supplementary Figure 2 (Appendix 2), showed that these results were robust under slight variations in cut-points.

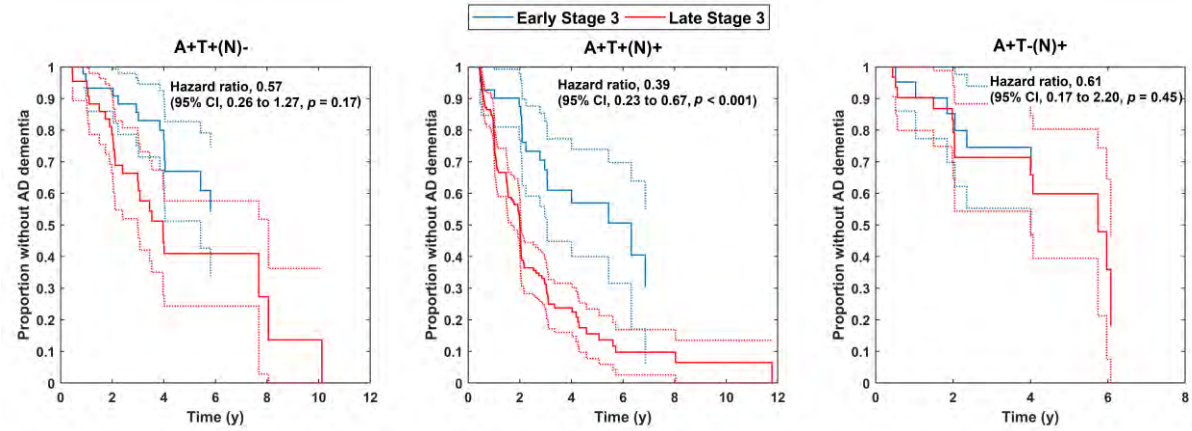

Figure 23 - Survival curves for the progression to AD dementia, according to AT(N) profiles and substages. Hazard ratios are defined as Early versus Late Stage 3. We did not include the A+T-(N)- because only 3 conversions to AD were observed for each substage. Dashed lines represent 95% confidence intervals.

4.3.3 Discussion

In the study presented here, we investigated the effectiveness of episodic memory as a descriptor of the cognitive continuum in MCI patients with biomarker evidence of AD. Although prior work had already drawn comparisons between the early and late stages of MCI in terms of progression and pathologic features [107-109,110-111,187-191], this is, to our knowledge, the first study in which the comparison has been performed among subjects with biomarker confirmation of AD, as defined by the NIA-AA research framework [17]. This is extremely important since recent studies have suggested that the high number of false positive MCI diagnoses in the EMCI group might have influenced previous results [112-113, 192-193], leaving the efficacy of the episodic memory staging to track cognition in prodromal AD unclear.

In contribution to solving for the aforementioned problem, our cross-sectional results suggest that Early Stage 3 represents a transitional stage between Stage 2 and Late Stage 3 in the pathophysiological progression of the disease (Figure 20 and 21). Moreover, Figure 21 indicates that biomarker abnormalities evolve according to a A+T-(N)- → A+T+(N)- → A+T+(N)+ temporal progression [31,138,205], in which Early Stage 3 fits in the expected way, i.e., with more (fewer) A+T+(N)+ (A+T-(N)-) profiles than in Stages 1 and 2 but fewer (more) than in Late Stage 3. The longitudinal tracking of Stage 1 and 2 patients showed that the most probable transition was to Early Stage 3, supporting our hypothesis that this stage represents not only a transitional phase in terms of biomarker profiles but also accurately describes the cognitive continuum of AD.

We also investigated whether episodic memory staging of Stage 3 patients was indicative of patient progression for a given AT(N) profile. We found that cognitive decline and progression to AD dementia were faster in Late Stage 3 than in Early Stage 3 patients only for AD-type profiles (profiles with A+T+) (Table 7 and Figures 3 and 4). This finding was independent of intra-profile levels of Aβ42, p-tau, t-tau and hippocampal atrophy, suggesting that episodic memory actually provides complementary information about the severity of the disease. It is not clear, however, to what extent these differences in progression can be attributed to a more fine-grained staging system rather than to differences in cognitive reserve [206] or concomitant pathology burden. Under the cognitive reserve scenario, some subjects would exhibit less impaired cognition than expected for a given burden of AD neuropathologic changes. In this context, our Early Stage 3 patients might represent subjects with high cognitive reserve, although it is also possible that the higher impairment of Late Stage 3 patients might be due to the presence of concomitant pathologies. For instance, vascular pathology is known to accelerate cognitive deterioration [208-209] and recent evidence suggest that vascular pathology might be a core AD feature [76].

Regardless of the origin of cognitive differences between Early and Late Stage 3 patients, the significantly divergent outcomes observed in this study indicate that proper accounting for these substages might result in a better prediction of cognitive decline and, thus, in increased power for interventional trials using profile-based participant selection. Also, the rapid progression to AD dementia observed in A+T+ LMCI suggests that these patients might be appropriate candidates for symptomatic treatment, allowing to treat symptoms earlier in the disease course.

Episodic memory staging may also help to harmonize prognosis results obtained across different Stage 3 cohorts. Since current guidelines for the definition of Stage 3 or MCI leave the definition of abnormality cut points in cognitive scores to the discretion of the researcher

[17-18,209-210], the proportion of patients in the early stage might vary dramatically from cohort to cohort, resulting in a wide range of estimates of prognostic accuracy for the different biomarkers of AD [211-212]. This variability was one of the main factors that hampered the development of recommendations regarding the use of CSF and imaging biomarkers in predicting short-term decline [202]. Differences might be even more disparate in community cohorts, in which EMCI prevalence is much higher than in the clinic [108-109]. In this regard, accounting for substages seems to be a promising approach to reduce variability across different Stage 3 cohorts, improving the quality of the evidence for the development of new guidelines.

Our analysis has also revealed the heterogeneous nature of the A+T-(N)+ profile. Regarded as a combination of early AD pathologic changes and other non-AD conditions [17], this profile has proven to be equally likely across the different stages (Figure 21) and, therefore, seems to lie outside the biomarker progression observed in the other 3 profiles of the Alzheimer's continuum. Not to mention, rates of progression were similar in Early and Late Stage 3, suggesting that episodic memory is not useful in predicting progression when the impairment is caused by other non-AD conditions. Furthermore, Figures 22 and 23 show that cognitive decline and conversion to AD dementia was faster for A+T+(N)+ profiles in comparison to A+T-(N)+, confirming that the addition of the T biomarker predicts faster progression [17,213] compared to previous amyloid-neurodegeneration schemes [18,209].

This study has strengths. First, by comparing early and late MCI subjects with biomarker evidence of AD we excluded false positive MCI diagnoses that potentially contaminated the findings of previous studies, increasing the reliability of our findings. Second, by performing an analysis based on the AT(N) framework we provided first-time evidence indicating that episodic memory is an accurate descriptor of the AD cognitive pathway only in patients with the NIA-AA research framework definition of AD (A+T+). Third, our findings might help to refine the NC staging scheme, describing symptom progression more accurately at the MCI stage.

Our study was not without its limitations. Given the lack of autopsy-validated cut-points reflecting tauopathy or neurodegeneration in published literature, we used an alternative method which does not reflect brain pathology directly, but that provides similar imaging cut-points to those obtained when discriminating between cognitively normal young and A+ cognitively impaired subjects [177]. Biomarker values close to the cut-point were commonly found, which might limit the applicability of our results for subjects with borderline biomarker levels. We combined 1.5T and 3T data in our analyses, which, despite the statistical corrections we used, might have influenced our results. Although many cognitive tests can be used to objectively assess a memory deficit, only the Logical Memory II Delayed Recall test from the Weschler Memory Scale-Revised was used in this study. It is not clear whether the categorization into Early and Late Stage 3 might vary using different tests, leading to better or worse staging and prognostic information. Another limitation is that ADNI MCI cohorts represent only a highly preselected fraction of patients with MCI and, therefore, conclusions made here regarding different MCI cohorts and community MCI samples are plausible but need future confirmation. Further investigations are needed to confirm the observed differences in Early Stage 3 versus Stage 2, given the low number of the latter studied here.

In conclusion, our findings might help to describe the symptomatic progression in AD more accurately, leading to a potential refinement of the NC staging scheme that will result in power increases for profile-based clinical trials.

USC
UNIVERSIDADE
DE SANTIAGO
DE COMPOSTELA

CONCLUSIONS

5 CONCLUSIONS

Overall, the main findings of this thesis support the hypothesis that biomarkers other than the conventional markers of amyloid, tau, and neurodegeneration are associated with the pathogenesis and progression of AD. Specifically, this thesis provides the following conclusions:

- WMH are associated with a faster accumulation of amyloid pathology in CN subjects without elevated cortical amyloid burden, as measured with amyloid PET.
- Amyloid PET tracer retention in the WM is sensitive to demyelinating pathology in these areas. This demyelination predicts progression in preclinical and prodromal AD.
- Episodic memory is useful to track the prodromal cognitive continuum and provides complementary prognostic information to amyloid, tau, and neurodegeneration biomarkers.

BIBLIOGRAPHY

6 BIBLIOGRAPHY

1.- Masters CL, Bateman R, Blennow K, et al. Alzheimer's disease. Nat Rev Dis Primers. 2015 Oct 15;1:15056.
2.- Brookmeyer R, Johnson E, Ziegler-Graham K, et al. Forecasting the global burden of Alzheimer's disease. Alzheimers Dement. 2007 Jul;3(3):186-91.
3.- Alzheimer's Association. 2017 Alzheimer's disease facts and figures. Alzheimers Dement. 2017;13(4):325–73.
4.- Hurd MD, Martorell P, Langa KM. Monetary costs of dementia in the United States. N Engl J Med. 2013;369(5):489–90.
5.- Brookmeyer R, Corrada MM, Curriero FC, et al. Survival following a diagnosis of Alzheimer disease. Arch Neurol. 2002 Nov;59(11):1764-7.
6.- Perl DP. Neuropathology of Alzheimer's disease. Mt Sinai J Med. 2010 Jan-Feb;77(1):32-42.
7.- Braak H, Braak E. Evolution of the neuropathology of Alzheimer's disease. Acta Neurol Scand Suppl. 1996;165:3-12.
8.- Leuzy A, Heurling K, Ashton NJ, et al. In vivo Detection of Alzheimer's Disease. Yale J Biol Med. 2018 Sep 21;91(3):291-300.
9.- McKhann G, Drachman D, Folstein M, et al. Clinical diagnosis of Alzheimer's disease: report of the NINCDS-ADRDA Work Group under the auspices of Department of Health and Human Services Task Force on Alzheimer's disease. Neurology 1984;34:939–44.
10.- Petersen R C, Doody R, Kurz A. et al. Current concepts in mild cognitive impairment. Arch Neurol 2001581985–1992.
11.- Nelson PT, Head E, Schmitt FA, et al. Alzheimer's disease is not "brain aging": neuropathological, genetic, and epidemiological human studies. Acta Neuropathol. 2011 May;121(5):571-87.
12.- Barnes LL, Leurgans S, Aggarwal NT, et al. Mixed pathology is more likely in black than white decedents with Alzheimer dementia. Neurology. 2015 Aug 11;85(6):528-34.
13.- Bennett DA, Schneider JA, Arvanitakis Z, et al. Neuropathology of older persons without cognitive impairment from two community-based studies. Neurology. 2006 Jun 27;66(12):1837-44.
14.- Knopman DS, Parisi JE, Salviati A, Neuropathology of cognitively normal elderly. J Neuropathol Exp Neurol. 2003 Nov;62(11):1087-95.
15.- Dubois B, Hampel H, Feldman HH, et al. Preclinical Alzheimer's disease: Definition, natural history, and diagnostic criteria. Alzheimers Dement. 2016 Mar;12(3):292-323.
16.- Jack CR Jr, Wiste HJ, Therneau TM. Associations of Amyloid, Tau, and Neurodegeneration Biomarker Profiles With Rates of Memory Decline Among Individuals Without Dementia. JAMA. 2019 Jun 18;321(23):2316-2325.
17.- Jack CR Jr, Bennett DA, Blennow K, et al. NIA-AA Research Framework: Toward a biological definition of Alzheimer's disease. Alzheimers Dement. 2018 Apr;14(4):535-562.
18.- Dubois B, Feldman HH, Jacova C, et al. Advancing research diagnostic criteria for Alzheimer's disease: the IWG-2 criteria. Lancet Neurol. 2014 Jun;13(6):614-29.
19.- Biomarkers Definitions Working Group. Biomarkers and surrogate endpoints: preferred definitions and conceptual framework. Clin Pharmacol Ther. 2001 Mar;69(3):89-95.

20.- Donohue MC, Sperling RA, Petersen R, et al. Association Between Elevated Brain Amyloid and Subsequent Cognitive Decline Among Cognitively Normal Persons. JAMA. 2017 Jun 13;317(22):2305-2316.
21.- Hansson O, Zetterberg H, Buchhave P, et al. Association between CSF biomarkers and incipient Alzheimer's disease in patients with mild cognitive impairment: a follow-up study.
22.- Kesslak JP, Nalcioglu O, Cotman CW. Quantification of magnetic resonance scans for hippocampal and parahippocampal atrophy in Alzheimer's disease. Neurology. 1991 Jan;41(1):51-4.
23.- Bohnen NI, Djang DS, Herholz K, et al. Effectiveness and safety of 18F-FDG PET in the evaluation of dementia: a review of the recent literature. J Nucl Med. 2012 Jan;53(1):59-71.
24.- Saint-Aubert L, Lemoine L, Chiotis K, et al. Tau PET imaging: present and future directions. Mol Neurodegener. 2017 Feb 20;12(1):19.
25.- Peskind ER, Riekse R, Quinn JF, et al. Safety and acceptability of the research lumbar puncture. Alzheimer Dis Assoc Disord. 2005 Oct-Dec;19(4):220-5.
26.- Blennow K, Hampel H. CSF markers for incipient Alzheimer's disease. Lancet Neurol. 2003 Oct;2(10):605-13.
27.- Andreasen N, Blennow K. CSF biomarkers for mild cognitive impairment and early Alzheimer's disease. Clin Neurol Neurosurg. 2005 Apr;107(3):165-73.
28.- Sutphen CL, Jasielec MS, Shah AR, et al. Longitudinal Cerebrospinal Fluid Biomarker Changes in Preclinical Alzheimer Disease During Middle Age. JAMA Neurol. 2015 Sep;72(9):1029-42.
29.- Mattsson N, Andreasson U, Persson S, The Alzheimer's Association external quality control program for cerebrospinal fluid biomarkers. Alzheimers Dement. 2011 Jul;7(4):386-395.e6.
30.- Hansson O, Seibyl J, Stomrud E, et al. CSF biomarkers of Alzheimer's disease concord with amyloid-β PET and predict clinical progression: A study of fully automated immunoassays in BioFINDER and ADNI cohorts. Alzheimers Dement. 2018 Nov;14(11):1470-1481.
31.- Jack CR Jr, Holtzman DM. Biomarker modeling of Alzheimer's disease. Neuron. 2013 Dec 18;80(6):1347-58.
32.- Tolar M, Abushakra S, Sabbagh M. The path forward in Alzheimer's disease therapeutics: Reevaluating the amyloid cascade hypothesis. Alzheimers Dement. 2019 Nov 4. pii: S1552-5260(19)35450-0.
33.- Apostolova LG, Dutton RA, Dinov ID, et al. Conversion of mild cognitive impairment to Alzheimer disease predicted by hippocampal atrophy maps. Arch Neurol. 2006 May;63(5):693-9.
34.- Fox NC, Scahill RI, Crum WR, et al. Correlation between rates of brain atrophy and cognitive decline in AD. Neurology. 1999 May 12;52(8):1687-9.
35.- Whitwell JL, Josephs KA, Murray ME, et al. MRI correlates of neurofibrillary tangle pathology at autopsy: a voxel-based morphometry study. Neurology. 2008 Sep 2;71(10):743-9.
36.- Scahill RI, Schott JM, Stevens JM, et al. Mapping the evolution of regional atrophy in Alzheimer's disease: unbiased analysis of fluid-registered serial MRI. Proc Natl Acad Sci U S A. 2002 Apr 2;99(7):4703-7.
37.- McDonald CR, McEvoy LK, Gharapetian L, et al. Regional rates of neocortical atrophy from normal aging to early Alzheimer disease. Neurology. 2009 Aug 11;73(6):457-65.

38.- Sluimer JD, van der Flier WM, Karas GB, et al. Whole-brain atrophy rate and cognitive decline: longitudinal MR study of memory clinic patients. Radiology. 2008 Aug;248(2):590-8.
39.- Cardenas VA, Chao LL, Studholme C, et al. Brain atrophy associated with baseline and longitudinal measures of cognition. Neurobiol Aging. 2011 Apr;32(4):572-80.
40.- Jack CR Jr, Shiung MM, Gunter JL, et al. Comparison of different MRI brain atrophy rate measures with clinical disease progression in AD. Neurology. 2004 Feb 24;62(4):591-600.
41.- Thompson PM, Hayashi KM, De Zubicaray GI, et al. Mapping hippocampal and ventricular change in Alzheimer disease. Neuroimage. 2004 Aug;22(4):1754-66.
42.- Vemuri P, Jack CR Jr, et al. Role of structural MRI in Alzheimer's disease. Alzheimers Res Ther. 2010 Aug 31;2(4):23.
43.- Duara R, Loewenstein DA, Potter E, et al. Medial temporal lobe atrophy on MRI scans and the diagnosis of Alzheimer disease. Neurology. 2008 Dec 9;71(24):1986-92.
44.- Jack CR Jr, Petersen RC, O'Brien PC, et al. MR-based hippocampal volumetry in the diagnosis of Alzheimer's disease. Neurology. 1992 Jan;42(1):183-8.
45.- Ashburner J, Friston KJ, et al. Voxel-based morphometry--the methods. Neuroimage. 2000 Jun;11(6 Pt 1):805-21.
46.- Klõppel S, Stonnington CM, Chu C, et al. Automatic classification of MR scans in Alzheimer's disease. Brain. 2008 Mar;131(Pt 3):681-9.
47.- Bacskai BJ, Frosch MP, Freeman SH, et al. Molecular imaging with Pittsburgh Compound B confirmed at autopsy: a case report. Arch Neurol. 2007 Mar;64(3):431-4.
48.- Bacskai BJ, Hickey GA, Skoch J, et al. Four-dimensional multiphoton imaging of brain entry, amyloid binding, and clearance of an amyloid-beta ligand in transgenic mice. Proc Natl Acad Sci U S A. 2003 Oct 14;100(21):12462-7.
49.- Curtis C, Gamez JE, Singh U, et al. Phase 3 trial of flutemetamol labeled with radioactive fluorine 18 imaging and neuritic plaque density. JAMA Neurol. 2015 Mar;72(3):287-94.
50.- Clark CM, Schneider JA, Bedell BJ, et al. Use of florbetapir-PET for imaging beta-amyloid pathology. JAMA. 2011 Jan 19;305(3):275-83.
51.- Sabri O, Sabbagh MN, Seibyl J, et al. Florbetaben PET imaging to detect amyloid beta plaques in Alzheimer's disease: phase 3 study. Alzheimers Dement. 2015 Aug;11(8):964-74.
52.- Iseki E, Matsushita M, Kosaka K, et al. Distribution and morphology of brain stem plaques in Alzheimer's disease. Acta Neuropathol. 1989;78(2):131-6.
53.- Catafau AM, Bullich S. Amyloid PET imaging: applications beyond Alzheimer's disease. Clin Transl Imaging. 2015;3(1):39-55.
54.- Price JC, Klunk WE, Lopresti BJ, et al. Kinetic modeling of amyloid binding in humans using PET imaging and Pittsburgh Compound-B. J Cereb Blood Flow Metab. 2005 Nov;25(11):1528-47.
55.- Tolboom N, Yaqub M, Boellaard R, et al. Test-retest variability of quantitative [11C]PIB studies in Alzheimer's disease. Eur J Nucl Med Mol Imaging. 2009 Oct;36(10):1629-38.
56.- Lopresti BJ, Klunk WE, Mathis CA, et al. Simplified quantification of Pittsburgh Compound B amyloid imaging PET studies: a comparative analysis. J Nucl Med. 2005 Dec;46(12):1959-72.
57.- Jack CR Jr, Wiste HJ, Lesnick TG, et al. Brain β-amyloid load approaches a plateau. Neurology. 2013 Mar 5;80(10):890-6.
58.- Landau SM, Breault C, Joshi AD, et al. Amyloid-β imaging with Pittsburgh compound B and florbetapir: comparing radiotracers and quantification methods. J Nucl Med. 2013 Jan;54(1):70-7.

59.- Villeneuve S, Rabinovici GD, Cohn-Sheehy BI, et al. Existing Pittsburgh Compound-B positron emission tomography thresholds are too high: statistical and pathological evaluation. Brain. 2015 Jul;138(Pt 7):2020-33.
60.- Klunk WE, Koeppe RA, Price JC, et al. The Centiloid Project: standardizing quantitative amyloid plaque estimation by PET. Alzheimers Dement. 2015 Jan;11(1):1-15.e1-4.
61.- Wolk DA, Klunk W. Update on amyloid imaging: from healthy aging to Alzheimer's disease. Curr Neurol Neurosci Rep. 2009 Sep;9(5):345-52.
62.- Forsberg A, Engler H, Almkvist O, et al. PET imaging of amyloid deposition in patients with mild cognitive impairment. Neurobiol Aging. 2008 Oct;29(10):1456-65.
63.- Jicha GA, Parisi JE, Dickson DW, et al. Neuropathologic outcome of mild cognitive impairment following progression to clinical dementia. Arch Neurol. 2006 May;63(5):674-81.
64.- Rabinovici GD, Furst AJ, O'Neil JP, et al. 11C-PIB PET imaging in Alzheimer disease and frontotemporal lobar degeneration. Neurology. 2007 Apr 10;68(15):1205-12.
65.- Drzezga A, Grimmer T, Henriksen G, et al. Effect of APOE genotype on amyloid plaque load and gray matter volume in Alzheimer disease. Neurology. 2009 Apr 28;72(17):1487-94.
66.- Chételat G, Villemagne VL, Pike KE, et al. Relationship between memory performance and β-amyloid deposition at different stages of Alzheimer's disease. Neurodegener Dis. 2012;10(1-4):141-4.
67.- Jagust WJ, Bandy D, Chen K, et al. The Alzheimer's Disease Neuroimaging Initiative positron emission tomography core. Alzheimers Dement. 2010 May;6(3):221-9.
68.- Chételat G, Villemagne VL, Villain N, et al. Accelerated cortical atrophy in cognitively normal elderly with high β-amyloid deposition. Neurology. 2012 Feb 14;78(7):477-84.
69.- Knopman DS, Jack CR Jr, Wiste HJ, et al. Selective worsening of brain injury biomarker abnormalities in cognitively normal elderly persons with β-amyloidosis. JAMA Neurol. 2013 Aug;70(8):1030-8.
70.- Ceccaldi M, Jonveaux T, Verger A, et al. Added value of 18F-florbetaben amyloid PET in the diagnostic workup of most complex patients with dementia in France: A naturalistic study. Alzheimers Dement. 2018 Mar;14(3):293-305.
71.- Rabinovici GD, Gatsonis C, Apgar C, et al. Association of Amyloid Positron Emission Tomography With Subsequent Change in Clinical Management Among Medicare Beneficiaries With Mild Cognitive Impairment or Dementia. JAMA. 2019 Apr 2;321(13):1286-1294.
72.- Johnson KA, Minoshima S, Bohnen NI, et al. Appropriate use criteria for amyloid PET: a report of the Amyloid Imaging Task Force, the Society of Nuclear Medicine and Molecular Imaging, and the Alzheimer's Association. Alzheimers Dement. 2013 Jan;9(1):e-1-16.
73.- Hanseeuw BJ, Betensky RA, Mormino EC, et al. PET staging of amyloidosis using striatum. Alzheimers Dement. 2018 Oct;14(10):1281-1292.
74.- Nasrabady SE, Rizvi B, Goldman JE, et al. White matter changes in Alzheimer's disease: a focus on myelin and oligodendrocytes. Acta Neuropathol Commun. 2018 Mar 2;6(1):22.
75.- Braak H, Thal DR, Ghebremedhin E, et al. Stages of the pathologic process in Alzheimer disease: age categories from 1 to 100 years. J Neuropathol Exp Neurol. 2011 Nov;70(11):960-9.
76.- Lee S, Viqar F, Zimmerman ME, et al. White matter hyperintensities are a core feature of Alzheimer's disease: Evidence from the dominantly inherited Alzheimer network. Ann Neurol. 2016 Jun;79(6):929-39.
77.- Fazekas F, Kleinert R, Offenbacher H, et al. Pathologic correlates of incidental MRI white matter signal hyperintensities. Neurology. 1993 Sep;43(9):1683-9.

78.- Debette S, Markus HS. The clinical importance of white matter hyperintensities on brain magnetic resonance imaging: systematic review and meta-analysis. BMJ. 2010 Jul 26;341:c3666.
79.- Brickman AM. Contemplating Alzheimer's disease and the contribution of white matter hyperintensities. Curr Neurol Neurosci Rep. 2013 Dec;13(12):415.
80.- Puzo C, Labriola C, Sugarman MA, et al. Independent effects of white matter hyperintensities on cognitive, neuropsychiatric, and functional decline: a longitudinal investigation using the National Alzheimer's Coordinating Center Uniform Data Set. Alzheimers Res Ther. 2019 Jul 27;11(1):64.
81.- Longstreth WT Jr, Manolio TA, Arnold A, et al. Clinical correlates of white matter findings on cranial magnetic resonance imaging of 3301 elderly people. The Cardiovascular Health Study. Stroke. 1996 Aug;27(8):1274-82.
82.- Graff-Radford J, Arenaza-Urquijo EM, Knopman DS, et al. White matter hyperintensities: relationship to amyloid and tau burden. Brain. 2019 Aug 1;142(8):2483-2491.
83.- Weaver NA, Doeven T, Barkhof F, et al. Cerebral amyloid burden is associated with white matter hyperintensity location in specific posterior white matter regions. Neurobiol Aging. 2019 Aug 9. pii: S0197-4580(19)30279-9.
84.- Liddelow SA, Guttenplan KA, Clarke LE, et al. Neurotoxic reactive astrocytes are induced by activated microglia. Nature. 2017 Jan 26;541(7638):481-487.
85.- Hughes TM, Wagenknecht LE, Craft S, et al. Arterial stiffness and dementia pathology: Atherosclerosis Risk in Communities (ARIC)-PET Study. Neurology. 2018 Apr 3;90(14):e1248-e1256.
86.- Erten-Lyons D, Woltjer R, Kaye J, et al. Neuropathologic basis of white matter hyperintensity accumulation with advanced age. Neurology. 2013 Sep 10;81(11):977-83.
87.- McAleese KE, Firbank M, Dey M, et al. Cortical tau load is associated with white matter hyperintensities. Acta Neuropathol Commun 2015;3:60.
88.- Rotshenker S. Wallerian degeneration: the innate-immune response to traumatic nerve injury. J Neuroinflammation. 2011 Aug 30;8:109.
89.- Fazekas G, Fazekas F, Schmidt R, et al. Brain MRI findings and cognitive impairment in patients undergoing chronic hemodialysis treatment. J Neurol Sci. 1995 Dec;134(1-2):83-8.
90.- Scheltens P, Barkhof F, Leys D, et al. A semiquantative rating scale for the assessment of signal hyperintensities on magnetic resonance imaging. J Neurol Sci. 1993 Jan;114(1):7-12.
91.- Kapeller P, Barber R, Vermeulen RJ, et al. Visual rating of age-related white matter changes on magnetic resonance imaging: scale comparison, interrater agreement, and correlations with quantitative measurements. Stroke. 2003 Feb;34(2):441-5.
92.- Prins ND, van Straaten EC, van Dijk EJ, et al. Measuring progression of cerebral white matter lesions on MRI: visual rating and volumetrics. Neurology. 2004 May 11;62(9):1533-9.
93.- Gouw AA, van der Flier WM, van Straaten EC, et al. Reliability and sensitivity of visual scales versus volumetry for evaluating white matter hyperintensity progression. Cerebrovasc Dis. 2008;25(3):247-53.
94.- Stankoff B, Freeman L, Aigrot MS, et al. Imaging central nervous system myelin by positron emission tomography in multiple sclerosis using [methyl-^{11}C]-2-(4'-methylaminophenyl)- 6-hydroxybenzothiazole. Ann Neurol. 2011 Apr;69(4):673-80.
95.- Landau SM. Optimizing Longitudinal Amyloid-β PET Measurement: The Challenges of Intensity Normalization. J Nucl Med. 2018 Oct;59(10):1581-1582.

96.- Faria Dde P, Copray S, Sijbesma JW, et al. PET imaging of focal demyelination and remyelination in a rat model of multiple sclerosis: comparison of [11C]MeDAS, [11C]CIC and [11C]PIB. Eur J Nucl Med Mol Imaging. 2014 May;41(5):995-1003.
97.- Zeydan B, Lowe VJ, Schwarz CG, et al. Pittsburgh compound-B PET white matter imaging and cognitive function in late multiple sclerosis. Mult Scler. 2018 May;24(6):739-749.
98.- Pietroboni AM, Carandini T, Colombi A, et al. Amyloid PET as a marker of normal-appearing white matter early damage in multiple sclerosis: correlation with CSF β-amyloid levels and brain volumes. Eur J Nucl Med Mol Imaging. 2019 Feb;46(2):280-287.
99.- Matías-Guiu JA, Cabrera-Martín MN, Matías-Guiu J, et al. Amyloid PET imaging in multiple sclerosis: an (18)F-florbetaben study. BMC Neurol. 2015 Nov 25;15:243.
100.- Bodini B, Veronese M, García-Lorenzo D, et al. Dynamic Imaging of Individual Remyelination Profiles in Multiple Sclerosis. Ann Neurol. 2016 May;79(5):726-738.
101.- Wallin A, Gottfries CG, Karlsson I, et al. Decreased myelin lipids in Alzheimer's disease and vascular dementia. Acta Neurol Scand. 1989 Oct;80(4):319-23.
102.- Lee DY, Fletcher E, Martinez O, et al. Regional pattern of white matter microstructural changes in normal aging, MCI, and AD. Neurology. 2009 Nov 24;73(21):1722-8.
103.- Collins-Praino LE, Francis YI, Griffith EY, et al. Soluble amyloid beta levels are elevated in the white matter of Alzheimer's patients, independent of cortical plaque severity. Acta Neuropathol Commun. 2014 Aug 17;2:83.
104.- Dean DC, Hurley SA, Kecskemeti SR, et al. Association of Amyloid Pathology With Myelin Alteration in Preclinical Alzheimer Disease. JAMA Neurol. 2017 Jan 1;74(1):41-49.
105.- Wechsler DA. Wechsler Memory Scale-Revised. Psychological Corporation; New York: 1987.
106.- Rey A. L'examen clinique en psychologie. Presses Universitaires de France; Paris: 1964.
107.- Aisen PS, Petersen RC, Donohue MC, et al. Alzheimer's Disease Neuroimaging Initiative. Clinical Core of the Alzheimer's Disease Neuroimaging Initiative: progress and plans. Alzheimers Dement 2010;6(3):239-46.
108.- Jessen F, Wolfsgruber S, Wiese B, et al. German Study on Aging, Cognition and Dementia in Primary Care Patients. AD dementia risk in late MCI, in early MCI, and in subjective memory impairment. Alzheimers Dement 2014;10(1);76-83.
109.- Petersen RC, Gill DP, Phillips LE, et al. Early MCI as an imaging target: Data from the National Alzheimer's Coordinating Center. Alzheimers Dement 2010;6(4):S58
110.- Lee P, Ryoo H, Park J, et al. Morphological and microstructural changes of the hippocampus in early MCI: a study utilizing the Alzheimer's Disease Neuroimaging Initiative database. J Clin Neurol 2017;13:144-54.
111.- Lee ES, Yoo K, Lee YB, et al. Default mode network functional connectivity in early and late mild cognitive impairment. Alzheimer Dis Assoc Disord 2016; 30:289-96.
112.- Edmonds EC, McDonald CR, Marshall A, et al. Early versus late MCI: Improved MCI staging using a neuropsychological approach. Alzheimers Dement 2019 May;15(5):699-708.
113.- Thomas KR, Eppig JS, Weigand AJ, et al. Artificially low mild cognitive impairment to normal reversion rate in the Alzheimer's Disease Neuroimaging Initiative. Alzheimers Dement 2019 Apr;15(4):561-569.
114.- Selkoe DJ, Hardy J. The amyloid hypothesis of Alzheimer's disease at 25 years. EMBO Mol Med 2016; 8: 595–608.

115.- Jack CR Jr, Knopman DS, Jagust WJ, et al. Tracking pathophysiological processes in Alzheimer's disease: an updated hypothetical model of dynamic biomarkers. Lancet Neurol. 2013;12(2):207–216. doi:10.1016/S1474-4422(12)70291-0.
116.- Bateman RJ, Aisen PS, De Strooper B, et al. Autosomal-dominant Alzheimer's disease: a review and proposal for the prevention of Alzheimer's disease. Alzheimers Res Ther. 2011 Jan 6;3(1):1.
117.- Hartley D, Blumenthal T, Carrillo M, et al. Down syndrome and Alzheimer's disease: Common pathways, common goals. Alzheimers Dement. 2015 Jun;11(6):700-9.
118.- Hardy J, De Strooper B. Alzheimer's disease: where next for anti-amyloid therapies? Brain. 2017 Apr 1;140(4):853-855.
119.- Heneka MT, Carson MJ, El Khoury J, et al. Neuroinflammation in Alzheimer's disease. Lancet Neurol. 2015 Apr;14(4):388-405.
120.- Hachinski VC, Iliff LD, Zilhka E, et al. Cerebral blood flow in dementia. Arch Neurol. 1975 Sep;32(9):632-7.
121.- Sheikh JYJ. Geriatric Depression Scale (GDS): recent evidence and development of a shorter version Clinical Gerontology: A Guide to Assessment and Intervention, The Haworth Press, New York (1986).
122.- Folstein MF, Folstein SE, McHugh PR. "Mini-mental state". A practical method for grading the cognitive state of patients for the clinician. J Psychiatr Res. 1975 Nov;12(3):189-98.
123.- Morris JC. The Clinical Dementia Rating (CDR): current version and scoring rules. Neurology. 1993 Nov;43(11):2412-4.
124.- Wechsler D. WMS-R: Wechsler Memory Scale-Revised: Manual. San Antonio, TX: Psychological Corporation; 1987.
125.- Bittner T, Zetterberg H, Teunissen CE, et al. Technical performance of a novel, fully automated electrochemiluminescence immunoassay for the quantitation of β-amyloid (1-42) in human cerebrospinal fluid. Alzheimers Dement. 2016 May;12(5):517-26.
126.- Bruce Fischl. FreeSurfer. Neuroimage. 2012 Aug 15; 62(2): 774–781.
127.- Friston KJ, Ashburner JT, Kiebel SJ, et al. Elsevier/Academic Press; 2007. Statistical Parametric Mapping: the Analysis of Functional Brain Images.
128.- Malone IB, Leung KK, Clegg S, et al. Accurate automatic estimation of total intracranial volume: a nuisance variable with less nuisance. Neuroimage. 2015 Jan 1;104:366-72.
129.- Schmidt P, Gaser C, Arsic M, et al. An automated tool for detection of FLAIR-hyperintense white-matter lesions in Multiple Sclerosis. Neuroimage. 2012 Feb 15;59(4):3774-83.
130.- Greve DN, Salat DH2, Bowen SL, et al. Different partial volume correction methods lead to different conclusions: An (18)F-FDG-PET study of aging. Neuroimage. 2016 May 15;132:334-343.
131.- Sattarivand M, Kusano M, Poon I, et al. Symmetric geometric transfer matrix partial volume correction for PET imaging: principle, validation and robustness. Phys Med Biol. 2012 Nov 7;57(21):7101-16.
132.- Prins ND, Scheltens P. White matter hyperintensities, cognitive impairment and dementia: an update. Nat Rev Neurol. 2015 Mar;11(3):157-65.
133.- Araque Caballero MÁ, Suárez-Calvet M, Duering M, et al. White matter diffusion alterations precede symptom onset in autosomal dominant Alzheimer's disease. Brain. 2018 Oct 1;141(10):3065-3080.

134.- Strain JF, Smith RX, Beaumont H, et al. Loss of white matter integrity reflects tau accumulation in Alzheimer disease defined regions. Neurology. 2018 Jul 24;91(4):e313-e318.
135.- Jacobs HIL, Hedden T, Schultz AP, et al. Structural tract alterations predict downstream tau accumulation in amyloid-positive older individuals. Nat Neurosci. 2018 Mar;21(3):424-431.
136.- Tosto G, Zimmerman ME, Hamilton JL, et al. The effect of white matter hyperintensities on neurodegeneration in mild cognitive impairment. Alzheimers Dement. 2015 Dec;11(12):1510-1519.
137.- McMillan CT, Chételat G. Amyloid "accumulators": The next generation of candidates for amyloid-targeted clinical trials? Neurology. 2018 Apr 24;90(17):759-760.
138.- Jack CR Jr, Vemuri P, Wiste HJ, et al. Evidence for ordering of Alzheimer disease biomarkers. Arch Neurol. 2011 Dec;68(12):1526-35.
139.- Schmidt P, Pongratz V, Küster P, et al. Automated segmentation of changes in FLAIR-hyperintense white matter lesions in multiple sclerosis on serial magnetic resonance imaging. Neuroimage Clin. 2019;23:101849.
140.- Sudre CH, Cardoso MJ, Ourselin S. Longitudinal segmentation of age-related white matter hyperintensities. Med Image Anal. 2017 May;38:50-64.
141.- Hammers A, Allom R, Koepp MJ, et al. Three-dimensional maximum probability atlas of the human brain, with particular reference to the temporal lobe. Hum Brain Mapp. 2003 Aug;19(4):224-47.
142.- Sargolzaei S, Sargolzaei A, Cabrerizo M, et al. Estimating Intracranial Volume in Brain Research: An Evaluation of Methods. Neuroinformatics. 2015 Oct;13(4):427-41.
143.- Labbé C, Koepp M, Ashburner J, et al. Absolute PET Quantification with Correction for Partial Volume Effects with Cerebral Structures. Quantitative Functional Brain Imagaing with Positron Emission Tomography. 1998:59–66.
144.- Greve DN, Svarer C, Fisher PM, Feng L, et al. Cortical surface-based analysis reduces bias and variance in kinetic modeling of brain PET data. Neuroimage. 2014 May 15;92:225-36.
145.- Brendel M, Högenauer M, Delker A, et al. Improved longitudinal [(18)F]-AV45 amyloid PET by white matter reference and VOI-based partial volume effect correction. Neuroimage. 2015 Mar;108:450-9.
146.- López-González FJ, Moscoso A, Efthimiou N, et al. Spill-in counts in the quantification of 18F-florbetapir on Aβ-negative subjects: the effect of including white matter in the reference region. EJNMMI Physics. In press.
147.- Matsubara K, Ibaraki M, Shimada H, et al. Impact of spillover from white matter by partial volume effect on quantification of amyloid deposition with [11C]PiB PET.
148.- Zeydan B, Schwarz CG, Lowe VJ, et al. Investigation of white matter PiB uptake as a marker of white matter integrity. Ann Clin Transl Neurol. 2019 Mar 3;6(4):678-688.
149.- Glodzik L, Rusinek H, Li J, et al. Reduced retention of Pittsburgh compound B in white matter lesions. Eur J Nucl Med Mol Imaging. 2015 Jan;42(1):97-102.
150.- Genovese CR, Lazar NA, Nichols T. Thresholding of statistical maps in functional neuroimaging using the false discovery rate. Neuroimage. 2002 Apr;15(4):870-8.
151.- Palmqvist S, Schöll M, Strandberg O, et al. Earliest accumulation of β-amyloid occurs within the default-mode network and concurrently affects brain connectivity. Nat Commun. 2017 Oct 31;8(1):1214.
152.- Cho H, Choi JY, Hwang MS, et al. In vivo cortical spreading pattern of tau and amyloid in the Alzheimer disease spectrum. Ann Neurol. 2016 Aug;80(2):247-58.

153.- Mattsson N, Palmqvist S, Stomrud E, et al. Staging β-Amyloid Pathology With Amyloid Positron Emission Tomography. JAMA Neurol. 2019 Jul 17.
154.- Suárez-Calvet M, Kleinberger G, Araque Caballero MÁ, et al. sTREM2 cerebrospinal fluid levels are a potential biomarker for microglia activity in early-stage Alzheimer's disease and associate with neuronal injury markers. EMBO Mol Med. 2016 May 2;8(5):466-76.
155.- Al-Mashhadi S, Simpson JE, Heath PR, et al. Oxidative Glial Cell Damage Associated with White Matter Lesions in the Aging Human Brain. Brain Pathol. 2015 Sep;25(5):565-74.
156.- Roseborough A, Ramirez J, Black SE, Edwards JD. Associations between amyloid β and white matter hyperintensities: A systematic review. Alzheimers Dement. 2017 Oct;13(10):1154-1167.
157.- Kandel BM, Avants BB, Gee JC, et al. White matter hyperintensities are more highly associated with preclinical Alzheimer's disease than imaging and cognitive markers of neurodegeneration. Alzheimers Dement (Amst). 2016 Apr 7;4:18-27.
158.- Pietroboni AM, Scarioni M, Carandini T, et al. CSF β-amyloid and white matter damage: a new perspective on Alzheimer's disease. J Neurol Neurosurg Psychiatry. 2018 Apr;89(4):352-357.
159.- Scott JA, Braskie MN, Tosun D, et al. Cerebral amyloid is associated with greater white-matter hyperintensity accrual in cognitively normal older adults. Neurobiol Aging. 2016 Dec;48:48-52.
160.- Marnane M, Al-Jawadi OO, Mortazavi S, et al. Periventricular hyperintensities are associated with elevated cerebral amyloid. Neurology. 2016 Feb 9;86(6):535-43
161.- Scott JA, Braskie MN, Tosun D, et al. Cerebral Amyloid and Hypertension are Independently Associated with White Matter Lesions in Elderly. Front Aging Neurosci. 2015 Dec 1;7:221.
162.- Palmqvist S, Mattsson N, Hansson O. Cerebrospinal fluid analysis detects cerebral amyloid-β accumulation earlier than positron emission tomography. Brain. 2016 Apr;139(Pt 4):1226-36.
163.- Molinuevo JL, Ripolles P, Simó M, et al. White matter changes in preclinical Alzheimer's disease: a magnetic resonance imaging-diffusion tensor imaging study on cognitively normal older people with positive amyloid β protein 42 levels. Neurobiol Aging. 2014 Dec;35(12):2671-2680.
164.- Racine AM, Adluru N, Alexander AL, et al. Associations between white matter microstructure and amyloid burden in preclinical Alzheimer's disease: A multimodal imaging investigation. Neuroimage Clin. 2014 Feb 19;4:604-14.
165.- Landau SM, Horng A, Jagust WJ. Memory decline accompanies subthreshold amyloid accumulation. Neurology. 2018 Apr 24;90(17):e1452-e1460.
166.- Farrell ME, Chen X, Rundle MM, et al. Regional amyloid accumulation and cognitive decline in initially amyloid-negative adults. Neurology. 2018 Nov 6;91(19):e1809-e1821.
167.- McAleese KE, Walker L, Graham S, et al. Parietal white matter lesions in Alzheimer's disease are associated with cortical neurodegenerative pathology, but not with small vessel disease. Acta Neuropathol 2017;134(3):459-473.
168.- Mito R, Raffelt D, Dhollander T, et al. Fibre-specific white matter reductions in Alzheimer's disease and mild cognitive impairment. Brain 2018;141(3):888-902.
169.- Yoshita M, Fletcher E, Harvey D, et al. Extent and distribution of white matter hyperintensities in normal aging, MCI, and AD. Neurology 2006;67(12):2192-2198.
170.- Rabin JS, Perea RD, Buckley RF, et al. Global white matter diffusion characteristics predict longitudinal cognitive change independently of amyloid status in clinically normal older adults. Cereb Cortex 2019;29(3):1251-1262.

171.- Kantarci K, Schwarz CG, Reid RI, et al. White matter integrity determined with diffusion tensor imaging in older adults without dementia: Influence of amyloid load and neurodegeneration. JAMA Neurol 2014;71(12):1547-1554.
172.- Schmidt R, Lechner H, Fazekas F, et al. Assessment of cerebrovascular risk profiles in healthy persons: Definition of research goals and the austrian stroke prevention study (ASPS). Neuroepidemiology 1994;13(6):308-313.
173.- Wang Y, Wu C, Caprariello A V., et al. In Vivo Quantification of Myelin Changes in the Vertebrate Nervous System. J Neurosci 2009;29(46):14663-14669.
174.- Joshi AD, Pontecorvo MJ, Clark CM, et al. Performance Characteristics of Amyloid PET with Florbetapir F 18 in Patients with Alzheimer's Disease and Cognitively Normal Subjects. J Nucl Med 2012;53(3):378-384.
175.- Landau SM, Fero A, Baker SL, et al. Measurement of Longitudinal Amyloid Change with 18F-Florbetapir PET and Standardized Uptake Value Ratios. J Nucl Med 2015;56(4):567-574.
176.- Mohs RC, Knopman D, Petersen RC, et al. Development of cognitive instruments for use in clinical trials of antidementia drugs: Additions to the Alzheimer's Disease Assessment Scale that broaden its scope. Alzheimer Dis Assoc Disor 1997;11 Suppl 2:S13-21.
177.- Jack CR, Wiste HJ, Weigand SD, et al. Defining imaging biomarker cut points for brain aging and Alzheimer's disease. Alzheimer's Dement 2017;13(3):205-216.
178.- Lowe VJ, Lundt ES, Senjem ML, et al. White Matter Reference Region in PET Studies of 11 C-Pittsburgh Compound B Uptake: Effects of Age and Amyloid-β Deposition. J Nucl Med 2018;59(10):1583-1589.
179.- Boyle PA, Yu L, Fleischman DA, et al. White matter hyperintensities, incident mild cognitive impairment, and cognitive decline in old age. Ann Clin Transl Neurol 2016;3(10):791-800.
180.- Stenset V, Johnsen L, Kocot D, et al. Associations between white matter lesions, cerebrovascular risk factors, and low CSF Aβ42. Neurology 2006;12;67(5):830-833.
181.- Lockhart A, Lamb JR, Osredkar T, et al. PIB is a non-specific imaging marker of amyloid-beta (Aβ) peptide-related cerebral amyloidosis. Brain 2007;130(Pt 10):2607-2615.
182.- Wisniewski HM, Wegiel J, Wang KC, et al. Ultrastructural studies of the cells forming amyloid in the cortical vessel wall in Alzheimer's disease. Acta Neuropathol 1992;84(2):117-127.
183.- Horiuchi M, Maezawa I, Itoh A, et al. Amyloid β1-42 oligomer inhibits myelin sheet formation in vitro. Neurobiol Aging 2012;33(3):499-509.
184.- Cummings J, Lee G, Ritter A, et al. Alzheimer's disease drug development pipeline: 2018. Alzheimer's Dement Transl Res Clin Interv 2018;4:195-214.
185.- Jack CR, Therneau TM, Wiste HJ, et al. Transition rates between amyloid and neurodegeneration biomarker states and to dementia: a population-based, longitudinal cohort study. Lancet Neurol 2016;15(1):56-64.
186.- Jack CR Jr, Bennett DA, Blennow K, et al. A/T/N: An unbiased descriptive classification scheme for Alzheimer disease biomarkers. Neurology 2016;87(5):539-47.
187.- Cai S, Huang L, Zou J, et al. Changes in thalamic connectivity in the early and late stages of amnestic mild cognitive impairment: a resting-state functional magnetic resonance study from ADNI. PLoS One 2015;10:e0115573.
188.- Risacher SL, Kim S, Shen L, et al. The role of apolipoprotein E (APOE) genotype in early mild cognitive impairment (E-MCI). Front Aging Neurosci 2013;5:11.

189.- Wolfsgruber S, Wagner M, Jessen F, et al. CSF beta-amyloid 42, CSF tau, hippocampal volume and verbal episodic memory performance in early versus late mild cognitive impairment, Alzheimers Dement 2013;9(4):S218.
190.- Wu L, Rowley J, Mohades S, et al. Dissociation between brain amyloid deposition and metabolism in early mild cognitive impairment. PLoS One 2012;7:e47905.
191.- Ye BS, Seo SW, Yang JJ, et al. Comparison of cortical thickness in patients with early-stage versus late-stage amnestic mild cognitive impairment. Eur J Neurol 2014;21:86-92.
192.- Edmonds EC, Delano-Wood L, Clark LR, et al. Susceptibility of the conventional criteria for mild cognitive impairment to false-positive diagnostic errors. Alzheimers Dement 2015 Apr;11(4):415-24.
193.- Edmonds EC, Delano-Wood L, Galasko DR, et al. Subjective cognitive complaints contribute to misdiagnosis of mild cognitive impairment. J Int Neuropsychol Soc 2014 Sep;20(8):836-47.
194.- Weschler D, Wechsler Memory Scale–Revised manual, San Antonio, TX: Psychological Corporation (2008).
195.- Penny W, Friston K, Ashburner J, et al. Statistical Parametric Mapping: The Analysis of Functional Brain Images, Academic Press (2007).
196.- Klasson N, Olsson E, Eckerstrõm C, et al. Estimated intracranial volume from FreeSurfer is biased by total brain volume. Eur Radiol Exp. 2018 Dec; 2: 24.
197.- Jack CR Jr, Barnes J, Bernstein MA, et al. Magnetic resonance imaging in Alzheimer's Disease Neuroimaging Initiative 2. Alzheimers Dement 2015 Jul;11(7):740-56.
198.- Jovicich J, Czanner S, Han X, et al. MRI-derived measurements of human subcortical, ventricular and intracranial brain volumes: Reliability effects of scan sessions, acquisition sequences, data analyses, scanner upgrade, scanner vendors and field strengths. Neuroimage 2009 May 15;46(1):177-92.
199.- O'Bryant SE, Waring SC, Cullum CM, et al. Staging Dementia Using Clinical Dementia Rating Scale Sum of Boxes Scores: A Texas Alzheimer's Research Consortium Study. Arch Neurol 2008;65(8):1091-95.
200.- Blennow K, Wallin A, Agren H, et al. Tau protein in cerebrospinal fluid: a biochemical marker for axonal degeneration in Alzheimer disease? Mol Chem Neuropathol 1995;26:231-45.
201.- Kern S, Syrjanen JA, Blennow K, et al. Association of Cerebrospinal Fluid Neurofilament Light Protein With Risk of Mild Cognitive Impairment Among Individuals Without Cognitive Impairment. JAMA Neurol 2018 Nov 12.
202.- Herukka SK, Simonsen AH, Andreasen N, et al. Recommendations for cerebrospinal fluid Alzheimer's disease biomarkers in the diagnostic evaluation of mild cognitive impairment. Alzheimers Dement 2017;13(3):285-95.
203.- Schindler SE, Gray JD, Gordon BA, et al. Cerebrospinal fluid biomarkers measured by Elecsys assays compared to amyloid imaging. Alzheimers Dement 2018;14(11):1460-69.
204.- Shaw LM, Waligorska T, Fields L, et al. Derivation of cutoffs for the Elecsys® amyloid β (1–42) assay in Alzheimer's disease. Alzheimers Dement (Amst) 2018 11;10:698-705.
205.- Bateman RJ, Xiong C, Benzinger TL, et al. Clinical and Biomarker Changes in Dominantly Inherited Alzheimer's Disease. N Engl J Med 2012 Aug 30;367(9):795-804.
206.- Stern Y. Cognitive reserve in ageing and Alzheimer's disease. Lancet Neurol 2012 Nov;11(11):1006-12.
207.- Helzner EP, Luchsinger JA, Scarmeas N, et al. Contribution of vascular risk factors to the progression in Alzheimer disease. Arch Neurol 2009 Mar;66(3):343-8.

208.- Li J, Wang YJ, Zhang M, et al. Vascular risk factors promote conversion from mild cognitive impairment to Alzheimer disease. Neurology 2011 Apr 26;76(17):1485-91.
209.- Albert MS, DeKosky ST, Dickson D, et al. The diagnosis of mild cognitive impairment due to Alzheimer's disease: recommendations from the National Institute on Aging-Alzheimer's Association workgroups on diagnostic guidelines for Alzheimer's disease. Alzheimers Dement 2011;7(3):270-79.
210.- Dunn B. Early Alzheimer's Disease: Developing Drugs for Treatment. Draft Guidance for Industry. in: Services USDoHaH, Administration FaD, (CDER) CfDEaR, (CBER) CfBEaR (Eds.) Office of the Federal Register, National Archives and Records Administration, Silver Spring, MD; 2018: 7060-61.
211.- Prestia A, Caroli A, Wade SK, et al. Prediction of AD dementia by biomarkers following the NIA-AA and IWG diagnostic criteria in MCI patients from three European memory clinics. Alzheimers Dement 2015;11(10):1191-201.
212.- Prestia A, Caroli A, Herholz K, et al. Diagnostic accuracy of markers for prodromal Alzheimer's disease in independent clinical series. Alzheimers Dement 2013;9(6):677-86.
213.- Cummings J, The National Institute on Aging-Alzheimer's Association Framework on Alzheimer's disease: Application to clinical trials. Alzheimers Dement. 2019 Jan;15(1):172-78.

USC
UNIVERSIDADE
DE SANTIAGO
DE COMPOSTELA

APPENDICES

APPENDIX 1

Supplementary Analysis: Partial volume correction

Although the Eroded WM volume of interest is, by definition, robust against partial volume effects (PVE) (borders are removed), the brainstem could be affected. Thus, we repeated all the analyses after applying partial volume correction (PVC) to confirm that these effects have not influenced our main findings.

T1 structural scans were segmented using Freesurfer 6.0. Amyloid PET scans, at the maximum preprocessing level in the ADNI pipeline, were coregistered to the T1 scan using Freesurfer (mri_coreg). Then, the PETSurfer implementation of the Symmetric Geometric Transfer Matrix [1,2], a ROI-based correction [3], was run on each individual. The FWHM of the point spread function was assumed to be 8 mm, as done in previous studies using ADNI data [4].

Section 4.2.2.2 with PVC

Supplementary Fig. 1 shows that the relation of brainstem SUVR with cortical SUVR was

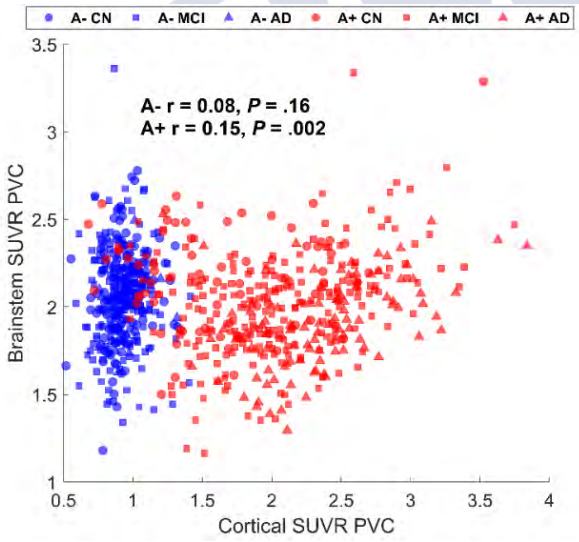

Supplementary Figure 1: Relation between brainstem SUVR and cortical SUVR, according to diagnosis and amyloid status.

dependent on cortical SUVR and on amyloid status. On the one hand, partial correlations adjusted by age showed that brainstem SUVR was positively correlated with cortical SUVR only in A+ subjects (Fig. 1, P = .002). On the other hand, in order to assess the effect of amyloid status, we fit a multivariable model including age, sex, APOE ε4 carriage, WMH, cortical SUVR, and amyloid status. No interaction term was included due the non-significant correlation in A- subjects. The amyloid status term was significantly associated with brainstem SUVR (A+ had lower SUVR, β = -0.37, P = .002), indicating that cortical amyloidosis results in a global reduction of uptake in the brainstem, independent of the increase driven by cortical SUVR.

Significant associations were also found for WMH (β = -0.14, P < .001) and APOE status (APOE carriers showed lower SUVR, β = -0.26, P = .002).

Section 4.2.2.3 with PVC

Supplementary Fig. 2 shows brainstem SUVR across diagnostic cohorts and amyloid status. For A+ participants, MCI had lower brainstem SUVR than CN (β = -0.71, P < .001) and higher than AD dementia subjects (β = 0.49, P < .001). No significant differences were found across A- participants.

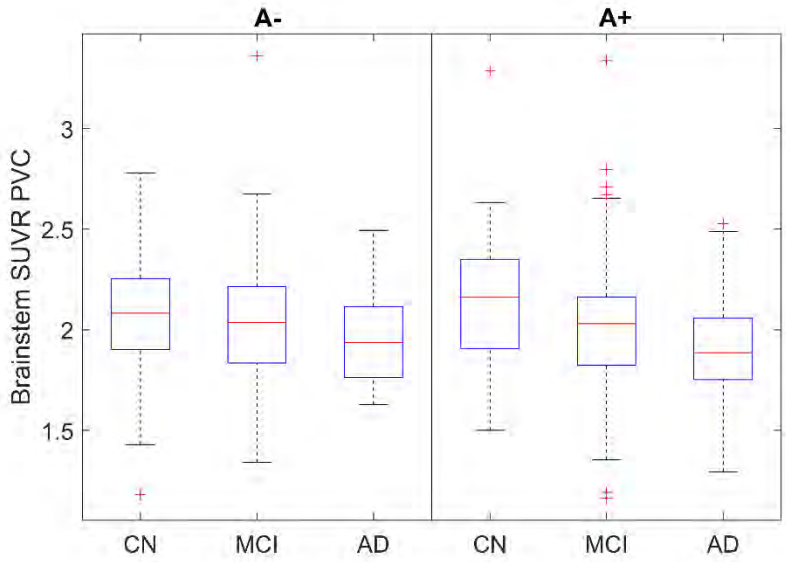

Supplementary Figure 2: Brainstem SUVR for each diagnostic cohort and amyloid status.

Section 4.2.2.4 with PVC

Supplementary Fig. 3 shows that low brainstem SUVR was significantly associated with low CSF Aβ-42 levels for all the diagnostic cohorts and amyloid statuses, except for A- CN. Additional linear models including an interaction between cortical SUVR and brainstem SUVR revealed a significant interaction in CN (β = 0.09, P = .006) and MCI (β = 0.07, P = .02), indicating that decreases in brainstem uptake were associated with stronger decreases in CSF Aβ-42 if cortical SUVR is high.

Supplementary Fig. 3 shows that low brainstem SUVR correlated with high CSF p-tau in A- and A+ MCI, and A+ CN, although did not reach statistical significance. Low brainstem SUVR was associated with low Hippocampus volume only in A+ MCI (β = 0.11, P = .06). Regarding cognition, only A+ MCI subjects showed a significant association between low brainstem SUVR and high ADAS-Cog-13 (β = -0.15, P = .02) and CDR-SB (β = -0.19, P = .007). No further significant associations with AD biomarkers or cognition were found.

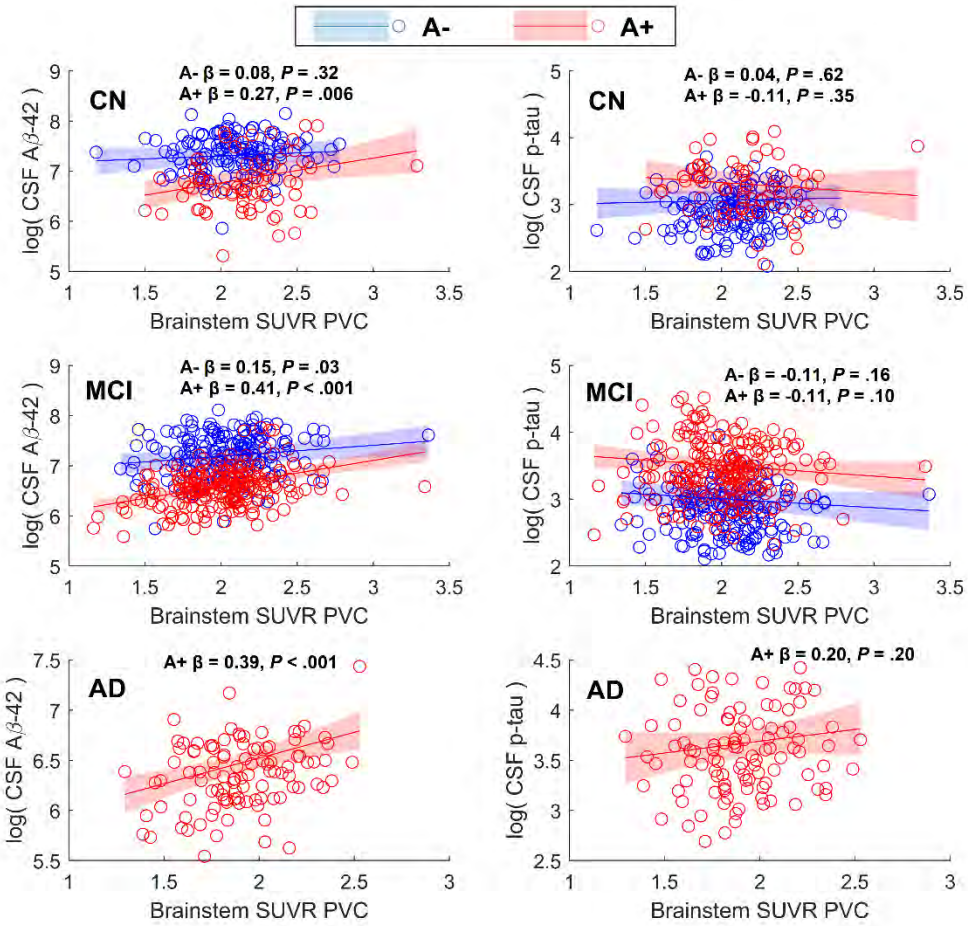

Supplementary Figure 3: Linear models relating brainstem SUVR with CSF Aβ-42 and with CSF p-tau, for each diagnostic cohort and amyloid status.

Section 4.2.2.5 with PVC

Supplementary Table 1 summarizes the longitudinal associations of brainstem SUVR with longitudinal change in cognition, WMH, and hippocampus volume. Low baseline brainstem SUVR was significantly associated with faster cognitive decline in A+ CN and A+ MCI, but not among A- individuals (only a significant decline in A- CN individuals for CDR-SB). Interaction analyses showed that the effects of low brainstem SUVR on longitudinal cognition were stronger if cortical SUVR was high in CN (ADAS-Cog-13: unstandardized β, b = -1.2 pts/y/SUVR², P < .001; CDR-SB: b = -0.10, pts/y/SUVR², P = .04) and MCI (ADAS-Cog-13: b = -1.9 pts/y/SUVR², P < .001; CDR-SB: b = -0.45, pts/y/SUVR², P < .001). Similarly, low baseline brainstem SUVR predicted increased WMH burden in A+ CN and A+ MCI. The rate of WMH change was higher for A+ CN compared to A+ MCI. The effect of low brainstem SUVR in longitudinal WMH burden was higher for high cortical SUVR, as demonstrated by interaction analysis in CN (b = -0.42 cm³/y/SUVR², P = .06) and MCI (b = -0.63 cm³/y/SUVR², P = .006). Low longitudinal hippocampus volumes were associated with low brainstem SUVR in A+ MCI. Interaction terms were not significant.

		Brainstem	
Outcome	Cohort	**Unstandardized ß (95% CI)**	*P* value
ADAS-Cog-13	A- CN	0.24 (-0.12 to 0.72)	.20
	A+ CN	-1.32 (-2.28 to -0.48)	.002
	A - MCI	0.24 (-0.24 to 0.72)	.30
	A + MCI	-1.56 (-2.28 to -0.96)	< .001
CDR-SB	A- CN	-0.11 (-0.19 to -0.04)	.003
	A+ CN	-0.24 (-0.37 to -0.11)	< .001
	A - MCI	0.04 (-0.06 to 0.15)	.42
	A + MCI	-0.69 (-0.86 to -0.52)	< .001
WMH volume	A- CN	0.28 (-0.23 to 0.80)	.28
	A+ CN	-0.85 (-1.55 to -0.15)	.02
	A - MCI	0.00 (-0.43 to 0.44)	.98
	A + MCI	-0.5 (-0.94 to -0.06)	.03
Hippocampus volume	A- CN	9 (-38 to 56)	.72
	A+ CN	33 (-17 to 83)	.20
	A - MCI	8 (-20 to 37)	.56
	A + MCI	36 (8 to 64)	.01

Supplementary Table 1: Longitudinal associations of Eroded WM and brainstem SUVR, for different outcomes.

Supplementary Fig. 4 further demonstrates the previous longitudinal relations after replacing continuous brainstem SUVR by Normal/Abnormal brainstem categories, as defined in Section 4.2.1.7. The proportion of subjects with abnormal brainstem marker was significantly lower in A+ CN than in A+ MCI (37% vs. 66%, P < .001).

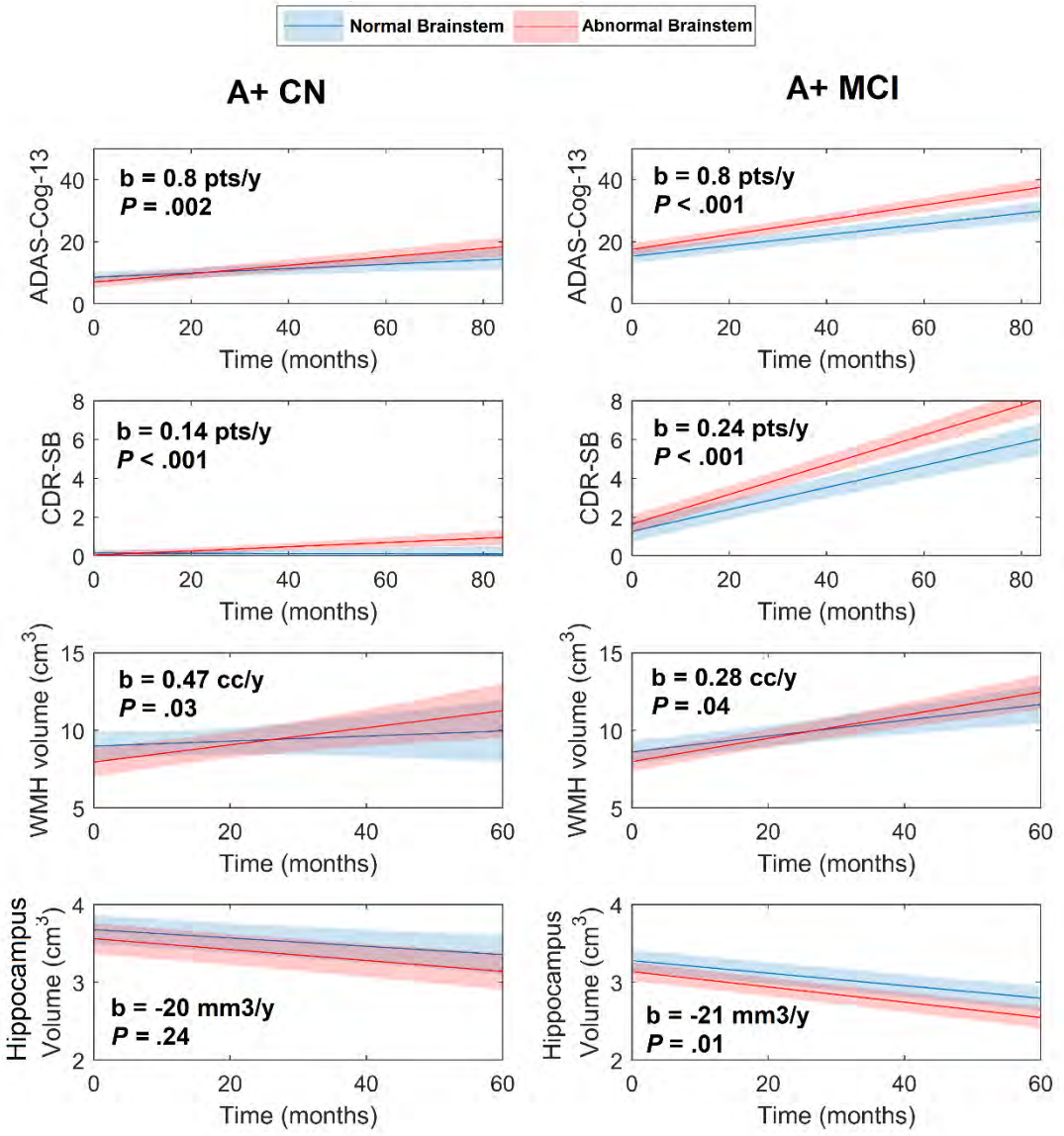

Supplementary Figure 4: Linear mixed models representing the longitudinal trajectories of A+ CN and A+ MCI, for normal and abnormal brainstem uptake categories.

Section 3.6 with PVC

Cox regression analysis showed a significant association between lower brainstem SUVR and higher risk of future dementia only in A+ MCI participants (unstandardized β, b = -1.52, P < .001). These associations were confirmed using the cut-points for Normal/Abnormal brainstem (Supplementary Fig. 5).

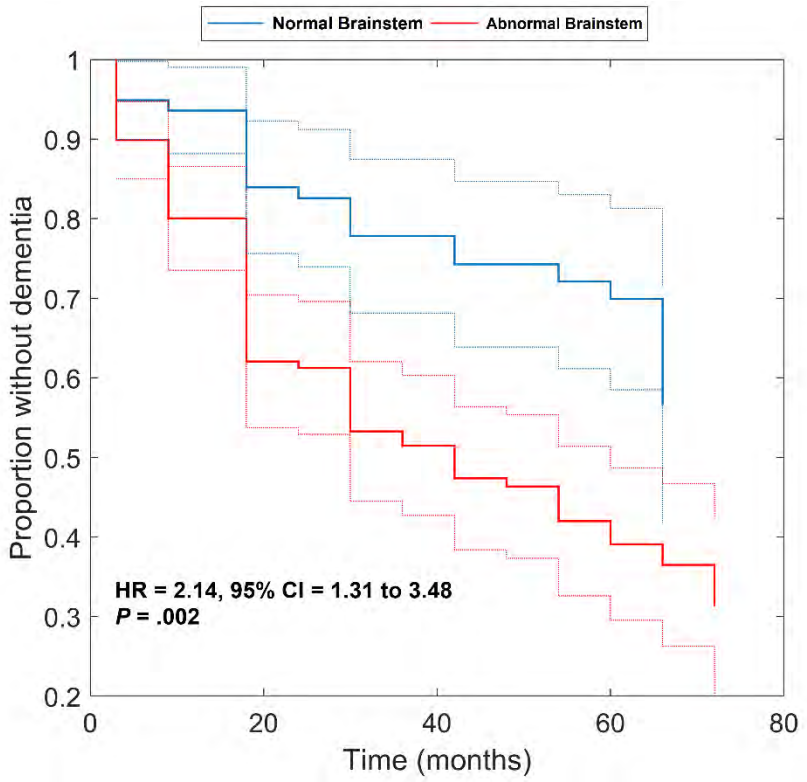

Supplementary Figure 5: Kaplan Meier survival curves for the risk of progression from A+ MCI to AD dementia, according to normal and abnormal categories of brainstem uptake.

References

[1] Greve, D. N., Salat, D. H., Bowen, S. L., Izquierdo-Garcia, D., Schultz, A. P., Catana, C., ... & Johnson, K. A. (2016). Different partial volume correction methods lead to different conclusions: An 18 F-FDG-PET study of aging. NeuroImage, 132, 334-343.

[2] Greve, D. N., Svarer, C., Fisher, P. M., Feng, L., Hansen, A. E., Baare, W., ... & Knudsen, G. M. (2014). Cortical surface-based analysis reduces bias and variance in kinetic modeling of brain PET data. Neuroimage, 92, 225-236.

[3] Correction for partial volume effects in PET: principle and validation. Rousset OG, Ma Y, Evans AC, J Nucl Med. 1998 May; 39(5):904-11.

[4] Gonzalez-Escamilla G, et al., PETPVE12: an SPM toolbox for Partial Volume Effects correction in brain PET - Application to amyloid imaging with AV45-PET, Neuroimage. 2017 Feb 15;147:669-677.

APPENDIX 2

Supplementary Table 1 - Demographic information for A- participants.

Cohort	CN	SMC	EMCI	LMCI	AD
N =	154	56	120	69	16
Demographics					
Age (years)	74±6	72±6	69±7	73±9	79±8
Female (%)	51	54	48	41	31
Education (years)	16±3	17±3	16±3	16±3	15±3
MMSE	29±1	29±1	29±1	28±2	24±2
CDR-SB	0±0	0±0	1±1	1±1	5±2
APOE ε4 carriers (%)	14	21	23	23	19

Supplementary Table 2 - Demographic information for Early and Late Stage 3 patients according to AT(N) profile.

AT(N)	A+T-(N)-	A+T+(N)-	A+T+(N)+	A+T-(N)+
N (Early/ Late Stage 3) =	23/13	45/47	43/164	21/31
Demographics		Early/Late Stage 3		
Age (years)	70±7/74±8	72±6/74±8	74±6/74±7	74±7/73±8
Female (%)	35/23	49/60	35/34	24/26
Education (years)	15±2/17±3	15±3/16±3	16±3/16±3	17±3/17±2
MMSE	29±1/27±2	28±2/28±2	28±2/27±2	28±2/27±2
CDR-SB	1±1/1±1	1±1/1±1	2±1/2±1	1±1/2±1
APOE ε4 carriers (%)	35/23	76/53	60/73	43/42

Supplementary Table 3 - Demographic information of Stage 3 patients who remained stable during follow-up or progressed to AD dementia, according to AT(N) profile. Only patients with at least one follow-up visit are presented.

AT(N)	A+T-(N)-	A+T+(N)-	A+T+(N)+	A+T-(N)+
N (Stable/ Progressive) =	29/6	51/39	70/131	33/19
Demographics	Stable/Progressive Stage 3			
Age (years)	72±8/72±6	72±7/73±8	75±6/74±7	75±7/72±8
Female (%)	31/33	47/64	33/34	24/26
Education (years)	16±2/16±3	16±3/15±3	16±3/16±3	17±3/17±2
MMSE	28±2/29±2	28±2/28±2	27±2/27±2	28±2/27±2
CDR-SB	1±1/1±1	1±1/2±1	2±1/2±1	2±1/2±1
APOE ε4 carriers (%)	31/33	73/56	67/73	30/63
Number of Early Stage 3	20/3	31/14	24/18	15/6
Number of Late Stage 3	9/3	20/25	46/113	18/13

Supplementary Figure 1 - Biomarker levels in A- participants.

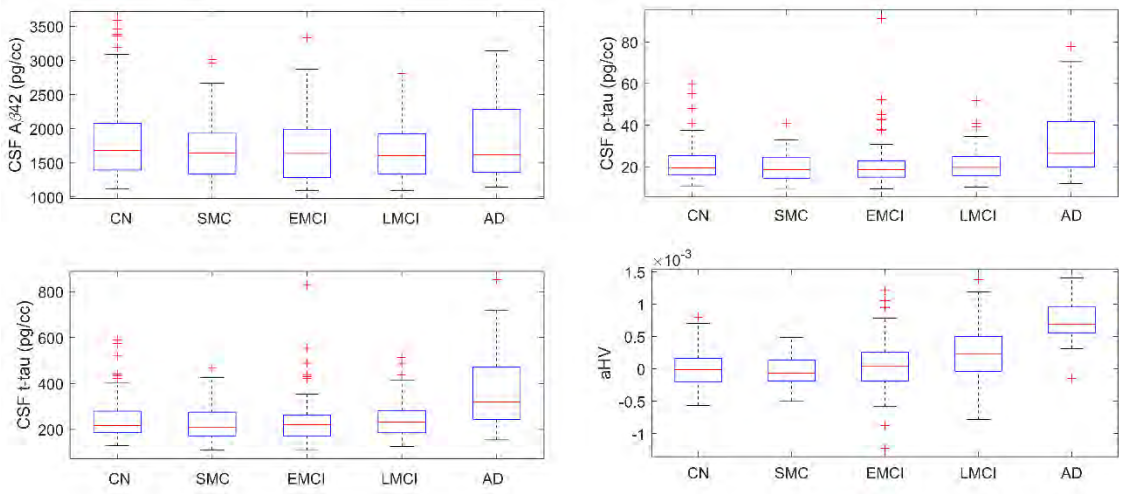

Supplementary Figure 2 - Sensitivity analysis in Difference in annual change of MMSE and CDR-SB, and Hazard Ratios for AD dementia, for changes up to ±15% in p-tau and aHV cut-points.

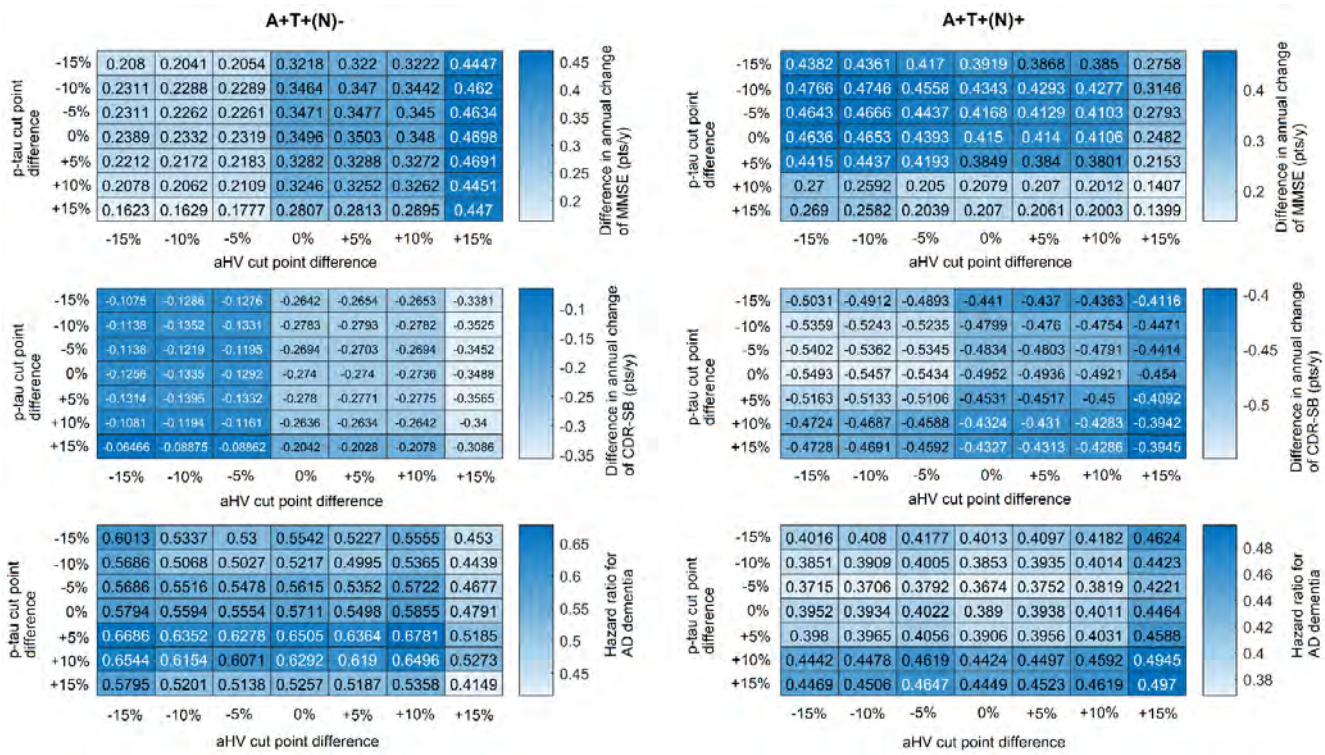

Supplementary Methods:

Derivation of the adjusted Hippocampal volume.

In order to account for the effects of age and field strength on hippocampus volumes, we performed linear regression in the sample of A- cognitively normal participants.

$$\frac{HV}{TIV} = \beta_0 + \beta_1 \times age + \beta_2 \times Field$$

Where HV stands for hippocampus volume (average between left and right), TIV for total intracranial volume, and Field is a binary variable representing field strength (1.5T and 3T). β's are regression parameters.

aHV is therefore calculated in the following way:

$$aHV = \beta_0 + \beta_1 \times age + \beta_2 \times Field - HV'/TIV'$$

Where HV' and TIV' stand for the hippocampus and total intracranial volumes of the subject under consideration.